Osseointegration of Complex Scaffolds

A Dissertation Presented for the

Doctor of Philosophy

Degree

The University of Tennessee, Knoxville

Rebecca Elaine Rifkin
May 2020

Copyright © 2020 by Rebecca Elaine Rifkin.
All rights reserved.

DEDICATION

To my mother, father, brother and husband who have believed in me, and pushed me to keep going even when I was terrified that I wasn't good enough. To my friends who kept encouraging me. To my mentors, without whom I'm sure I wouldn't be able to write a scientific sentence let alone finish this.

ACKNOWLEDGEMENTS

There are not enough complimentary words I can think, and I need all of them, to thank David Anderson. Without his support and guidance this work would not have been possible. Similarly, the support from my committee during the goat surgeries was crucial in carrying out this research. The support from my lab mates, specifically Austin Bow, and Remiguisz Grzeskowiak made all the goat work possible. It would be insane not to mention the unbelievable help from Carolyn Wilson. Additionally the Comparative and Experimental Medicine program staff, specifically Dr. Stephen Kania and Kim Rutherford who's help has been invaluable. Finally, our research technician, Elizabeth Croy and the countless number of veterinary and undergraduate research assistants who helped take care of the extensive goat herd.

I would like to thank the Department of Defense via the U.S. Army Medical Research and Material Command (MRMC) for funding my position as a graduate research assistant in the CEM program and detailed much of the research. For the portions of the work that have been published, I would like to thank my co-authors, editors, reviewers and publishers for their time and patience. I would like to thank the material design and development team, specifically Bailey Jackson based in the Center for Integrative Nanotech. The University of Arkansas at Little Rock characterized and provided the materials utilized in this research. I would like to thank Mohamed A. Aboulkhair and Dr. Kania's lab for helping me with the whole genomic sequencing of the Staphylococcal isolates. I would be remiss if I did not thank G-d, who guided me even when I almost screwed this whole thing up, advised and watched over me and saw me to the end of this project.

ABSTRACT

Regenerative therapies, or bone substitutes, for long bone fractures are on the verge of becoming standard practice. Development of a wide variety of synthetic materials has been undertaken in effort to improve healing of debilitating fractures. An ideal bone substitutes would mimic natural bone physiology. The form and function of long bones must first be understood in order to create the ideal regenerative material. From there, basic fracture healing provides key insights as to where and how fractures may advance to stages of non-healing. The ideal bone substitute would be both osteo-inductive and osteo-conductive. An effective material to promote bone healing in large defects has yet to be developed, and large animal preclinical models are lacking. Few large animal studies looking at bone regeneration exceed ninety days making long-term osseointegration of the bone substitute difficult. One of the most studied platforms for synthetic bone substitutes are nanohydroxyapatite and polyurethane composites due to their biocompatibility and bioresorbability. The studies detailed here focus on the biological assessment of a bone substitute that contains polyurethane, nanohydroxyapatite, and decellularized bone particles. A multitude of in vivo assessments were carried out to assess the impact of the bone substitute on a novel preclinical large animal model of long term bone healing. Baseline gait assessment characteristics were able to be determined for goat models relating to apparently healthy goats prior to the start of the bone healing model. Positive results were associated with long term integration of the bone substitute when the material was impregnated with the growth factor bone morphogenetic protein-2. The most catastrophic complication of any bone substitute used for long bone fractures, infection was encountered. Phenotypic and whole genomic characterization of the *Staphylococcal* associated infections, and subsequent osteomyelitis, were performed. It was recognized that there was an initial bone proliferation associated with *Staphylococcus aureus* associated osteomyelitis cases. The successful large animal preclinical model may provide an alternative to study bone substitutes. Conventional fixation methodologies may be removed, after sufficient healing time, to allow for further investigation into the integration and rehabilitation of the bone substitute with the native bone.

TABLE OF CONTENTS

Chapter 1. Bone Physiology: Structure, repair, and altered states of healing 1
Abstract 2
Introduction 3
Long Bone: Function, Anatomy, Composition, Cellularity 3
Function 3
Gross Anatomy (Organ Level) 3
Blood and Nerve Supply 4
Microscopic Anatomy (Tissue Level) 5
Composition of Bone 5
Fracture Repair 8
Stage I- Inflammation 8
Stage II- Soft callus formation 9
Stage III- Hard callus formation 9
Stage IV- Bone remodeling 9
Bone Morphogenetic Protein-2 9
Abnormal Fracture Healing (Delayed and Non-unions) 10
Osteoconductive Scaffolds 12
Osteomyelitis 14
Conclusion 15
References 16
Appendices 24
Chapter 2. Use of a pressure-sensing walkway system for biometric assessment of goats 31
Abstract 32
Introduction 33
Materials and Methods 34
Goats 34
Data Collection 34
Gait Variables 35
Force Variables 36
Statistical Analysis 36
Results 36
Discussion 38
References 41
Appendices 46
Chapter 3. Assessment of osseointegration of a novel synthetic bone scaffold in a tibia segmental defect model 54
Abstract 55
Introduction 56
Materials and Methods 58

Scaffold Fabrication 58
Study Design 58
Surgical procedure and scaffold implantation in caprine tibias 58
Lameness evaluation post-operatively 59
Imaging assessment of ostectomy gaps and scaffold integration 60
High definition thermal imaging 60
Radiographic assessment 60
Dual energy x-ray absorptiometry (DEXA) 60
Computed tomography 60
Biomechanical testing 60
Microscopic assessment of ostectomy gap and scaffold integration 61
Statistical analysis 62
Results 62
Clinical observations 62
Lameness evaluation 63
Imaging assessment of ostectomy gap and scaffold osseointegration 63
High definition thermal imaging 63
Radiographs 63
Bone mineral density (BMD) 63
Computed tomography 64
Biomechanical testing 64
Microscopic assessment of ostectomy gap and scaffold integration 64
Discussion 65
Conclusions 68
References 69
Appendices 75
Chapter 4. Characterization of post-operative hypertrophic osteomyelitis induced by *Staphylococcus aureus* 87
Abstract 88
Introduction 89
Materials and Methods 90
Case Population 90
Bacterial Isolates and Culture Methods 91
Isolation and Phenotypic Identification of Staphylococcus aureus 91
Genomic analysis 92
Statistical analysis 92
Results 92
Radiographic Analysis 92
Histomorphometric Analysis 93
Genomic Analysis 93
Discussion 93
References 95
Appendices 99

Chapter 5. Conclusions and future research 105
Conclusions 106
Future Research 106
References 108
VITA……...111

LIST OF TABLES

Table 1-1. Major cytokines, growth factors, non-collagenous proteins and their proposed roles. 28

Table 2-1. Working definitions used for gait variables. 48

Table 2-2. Descriptive statistics for the stance gait parameters. 49

Table 2-3. Descriptive statistics for the stride gait parameters. 50

Table 2-4.Student's t-test evaluating day 1 versus day 3. 51

Table 3-1. Radiographic scoring for assessment of ostectomy gap filling. 77

Table 3-2. Final group break down showing the number of defects in each group that healed (formed a bridging callus) versus those showing insufficient healing (lack of bridging callus). 78

Table 3-3. Group x Month interactions for bone mineral density as measured by DEXA (P=0.057). 81

Table 3-4. Group x Time point interactions for average osteoclast count per mm of bone surface. 86

Table 4-1. Radiographic scoring for assessment of ostectomy gap filling. 100

Table 4-2. Descriptive data of each strain of osteomyelitis subjected to whole genomic sequencing. 101

Table 4-3. Bioinformatic data from *S. aureus* isolates subjected to whole genomic sequencing. 104

LIST OF FIGURES

Figure 1-1. Endochondral ossification and long bone blood supply. 25

Figure 1-2. Anatomy of a long bone. 26

Figure 1-3. Haversian systems. 27

Figure 1-4. Commitment of a mesenchymal stem cell to an osteocyte with important proteins. 29

Figure 1-5. An accelerated overview of the four stages of bone healing (inflammation, soft callus formation, hard callus formation, remodeling) as seen in a mouse model of long bone fracture healing. 30

Figure 2-1. Examples of halter-lead training and sample gait analysis. 47

Figure 2-2. Box plots for Maximum Force (%BW), Maximum Force (Kg), and Maximum Peak Pressure (KPa). 52

Figure 2-3. Box plots for Impulse (%BW*sec) and Impulse (Kg*sec). 53

Figure 3-1. Multi-layered nHA-PU-DBP based scaffolds implanted into 2.5 cm segmental defects in the goat tibia. 76

Figure 3-2. Radiographs were acquired monthly. 79

Figure 3-3. DEXA Imaging and Analysis. 80

Figure 3-4. Computed tomography (CT). 82

Figure 3-5. Von Kossa (percent mineralization) staining. 83

Figure 3-6. Goldner's Trichrome (percent osteoid) staining. 84

Figure 3-7. The average osteoclast count per mm of bone surface. 85

Figure 4-1. Radiographic ostectomy gap filling of an *S. aureus* goat and a case comparsion. 102

Figure 4-2. Tetracycline labelling of an *S. aureus* goat and a case comparsion. 103

ABBREVIATIONS

BMP. ..... bone morphogenetic protein
BMD…… .....bone mineral density
BW.. ..... body weight
cm……..... centimeter
CT…… ..... computed tomography
DBP…….....decellularized bone particles
FGF. ..... fibroblast growth factor
IGF... ..... insulin-like growth factor
IL…..... interluekin
ISO……..... international organization for standardization
g…….....grams
HU…….....hounsfield units
Kgs. kilograms
kPa. kilopascals
kgf…… ..... kilograms force
MLTS. .....multilocus sequence typing
MMSCRAMM……..……..... microbial surface components recognizing adhesive matrix molecules
nHA. .....nanohydroxyapatite
OR……..... odds ratio
PDGF. .....platelet derived growth factor
PU... ..... polyurethane
rh…… ..... recombinant human
S. aureus.....*Staphylococcus aureus*
sec... .....seconds
ST...sequence type
std…….....standard deviation
VLS. .....visual lameness score
TNF- IX . ..... tumor necrosis factor- alpha
TBF-B. ..... transforming growth factor beta
TRAP…… .....tartate resistant acid phosphatase

CHAPTER 1.
BONE PHYSIOLOGY: STRUCTURE, REPAIR, AND ALTERED STATES OF HEALING

Abstract

The purpose of this review is to understand the need for bone substitutes in clinical applications of long bone fractures. Knowledge of long bone anatomy is the basic first essential step towards understanding the form and function of long bones. From there, basic fracture healing can be understood so as to understand where and how fractures may advance to stages of non-healing. This gives rise to understanding when bone substitutes may be used and what are the most common substitutes available. Finally, a devastating complication of long bone fractures and the use of bone substitutes is infection. The use of bone substitutes, fracture healing, delayed fracture healing and infection are vast subjects and far from fully understood. The presented article is a knowledge update with more specific information given to fracture healing regarding growth factors, bone substitutes regarding polyurethane-nanohydroxyapatite based platforms, and infection with specific interest of *Staphylococcus aureus*.

Introduction

Long bone fractures in a healthy adult are the result of major trauma, or high energy injury [1]. In military personnel, extremity injuries, and associated fractures, are the most common body region injured during combat [2, 3]. The tibia is the most commonly fractured long bone [2, 3]. In civilian population this it typically the result of falls, sporting, or motor vehicle accidents [1]. In military personnel, tibial injuries associated with combat are typically the result of gunshots, explosion, and improves explosive devices [2, 3].

The use of regenerative therapies for human musculoskeletal defect injuries is on the verge of becoming standard practice. [4] Traditionally, catastrophic fractures have required the use of bone substitutes (grafting) when a decision has been made to salvage a limb [5, 6]. The gold standard for bone grafting materials has been the autograft (bone taken from the patient's own body) or the allograft (cadaveric bone from a bone bank) [7, 8]. The procedure is not without complication. Approximately 30-60% of grafting procedures result in one or more complications, ranging from infection to incomplete integration, to donor site pain [9]. In humans, the incidence of non-union fractures is approximately 5-10% [10]. The consensus for the definition of delayed healing or fracture non-union is inconsistent and subjective [11]. Musculoskeletal injuries have been reported to now compromise approximately 50% of all combat wounds and are becoming an orthopedic burden of disease highlighting the need for Food and Drug Administration approval of new regenerative therapies to lower the incidence of these costly fractures [12-14].

This first section serves to understand typical long bone conduct as the gold standard for return to function after long bone fracture. The normal function, anatomy, and composition of long bones is reviewed first because to ensure bone substitutes perform suitably they must mimic the intrinsic nature of long bones. Normal fracture healing is then reviewed to understand gaps in which abnormal fracture healing may occur and the use bone substitutes are then needed. Abnormal fracture healing is reviewed to understand how bone substitutes have been used and when they are used in times that fracture healing has gone wrong. This is followed by available bone grafting materials both natural and synthetic. Finally, a short section is provided on the main complication of bone grafting, infection.

Long Bone: Function, Anatomy, Composition, Cellularity

Function

Bone serves primarily as the body's structural support, locomotion system, and adapts in response to alterations of mechanical environment [15, 16]. It provides maintenance for mineral homeostasis (primarily calcium and phosphorous), acid-base balance, and supports an environment for hematopoietic cell development and bone marrow production [15].

Gross Anatomy (Organ Level)

Regardless of mammalian species, long bones form by endochondral ossification, a process by which bones evolve from cartilaginous prototypes that are permeated by

vessels and undergo mineralization [**Fig 1-1**; 17, 18][1]. Therefore, long bones are divided anatomically starting with a hollow tube, also known as the diaphysis (primary center of ossification), which flares at either end into the cone shaped metaphyses followed by growth plates and ending in rounded epiphyses (secondary center of ossification) [15, 17]. The cylindrical diaphysis is formed by a covering of compact bone [15, 19]. The internal architecture of the diaphysis holds the medullary cavity [19]. Cortical bone is thick in the middle of the diaphysis and flares towards each metaphysis [19]. The cone shaped metaphysis at either end is again surrounded by compact bone, although thinner, while the internal structure is inhabited by cancellous (spongy) bone [19]. Both trabecular and cortical (compact) bone are composed of lamellae. Cortical lamellae, or Haversian systems, are cylindrical in shape and form a branching network [15]. Trabecular lamellae, or packets, are semilunar in shape and form a three- dimensional lattice of plates and rods with varying density [15, 19]. Metaphysis' are responsible for transferring load into the bone cortex [17]. The growth plates are regions of bone elongation just beyond the metaphysis [17]. Finally, the epiphysis refers to the ends of long bone and have an internal structure similar to the metaphysis [17]. The outer layer of the epiphysis is thinner compact bone except where these ends articulate with adjoining bones, at which point they are covered in hyaline cartilage [**Fig 1-2**; 19, 20].

Long bones are covered by a double layered membrane (periosteum) except at the hyaline cartilage ends and where it is pierced by interesting ligaments and tendons [17, 19]. The outer layer is fibrous, while the inner layer is cellular and retains bone- forming capacity beyond maturity that is reactivated during fracture healing [17, 18]. The medullary cavity, within the diaphysis, is filled with either predominately red (hematopoietic) or yellow (fat) marrow depending on the stage of life with red marrow being more dominate in younger age groups while yellow is more customary in older age groups [17]. Finally, a conceptual endosteal layer exists at the bone medullary cavity interface to explain functional modifications seen during adaptation events [**Fig 1-2**; 17].

Blood and Nerve Supply

The skeletal system itself receives an indulgent blood supply, estimating 5-10% of the overall cardiac output [19]. Arterial blood enteral through the largest nutrient artery via the diaphyseal cortex to divide into proximal and distal intramedullary branches which eventually branch into arterioles to permeate the Haversian or Volkmann's canals [17, 19]. Cortical bone receives up to one-third of its blood supply to its outer surface from the periosteal arteries. Venous drainage is accomplished by veins that follow accompanying arteries [**Fig 1-1**; 19]. There is no lymphatic system present within bone [19]. Both sensory and motor nerves are found within bone [19]. Periosteal nerves are sensory and contain pain receptors for tearing and tension [17].

[1] All figures and tables for this chapter are presented in the appendix.

Microscopic Anatomy (Tissue Level)

Long bones can be divided into four categories: woven bone, lamellar bone, cortical bone or trabecular bone. Woven, or immature bone, is seen in areas of rapid growth or states of high bone turn over [15, 19]. It is characterized by a collagen fibers that are laid down in a random pattern with an immense number or bone progenitor cells [17]. Lamellar bone is present on both cortical and trabecular bone. It is mature bone with systematic collagen fibers [19].

Lamellar bone, within the cortex or just beneath the articular cartilage, is arranged into Harversian systems (osteons) [17]. The boundary of each Haversian system is a cement line [19]. The lamellae are aligned into concentric cylinders that run lengthwise and hold nerves and vessels [20]. Volkmann's canals are horizontal canals connecting the Haversian systems to each other [21]. Between osteons, the lamellae are referred to as interstitial lamellae [17]. Circumferential lamellae exist when layers are oriented parallel to the circumference of the bone [17]. Cortical bone is almost non-porous (porosity of 5-10%) and extremely dense [22]. Within this dense system, small holes (lacuna) exist within the matrix that have been made during formation, or remodeling [22]. This system and density give cortical bone both strength and restricted flexibility [**Fig 1-3**, 22, 23].

In contrast, lamellae within the trabecular bone are arranged in parallel [17]. Anastomosing plates or rods orient themselves to reflect adaptation to mechanical stresses experienced by bone itself [17]. It is exceedingly porous (75-95%) with pores being interconnected and filled either marrow [22].

Composition of Bone

Long bones are composed of 20 to 40% organic bone matrix, 50 to 70% mineral, 5 to 10% water, and <3% lipids. Cells involved in the structural integrity of bone are osteoblasts, osteocytes, and osteoclasts [15, 17].

Organic bone matrix can be broken down into collagenous or non-collagenous proteins, proteoglycans, and lipids [17]. Up to 90% of the bone collagen is Type I collagen [22, 24]. Other collagen proteins (i.e. Types II or IX collagens) may be found in trace amounts as organization components or in pathologic conditions [15, 24].Type I collagen is a triple helical molecule composed of three amino acid chains which have extensive cross- linkages, both among themselves and between adjacent molecules [19, 22]. While it has been well described, recombinant forms of type I collagen are gaining popularity as platforms for bone regeneration [25]. Deposition of Type I collagen molecules occurs in rows with perforations between adjacent molecules in the horizontal direction of 35 to 40 nm [17, 22]. Rows are staggered so that molecules overlap and are offset by a stance of 64 to 70 nm [17, 22]. Collagen molecules are connected through immature enzymatic cross-linkages [22]. This packaging and enzymatic cross-linking provides the strength and insolubility to bone [17]. The collagen fibers arranged in parallel make up lamellae and are arranged either concentrically or parallel depending on if they are in cortical or trabecular bone [17].

Non-collagenous proteins are numerous with a wide range of functions from cytokines to enzymes to adhesion molecules [17, 19]. Important non-collagenous proteins and their proposed roles are summarized in **Table 1-1** [26, 27]. Proteoglycans and lipids are the final important components of bone. While the role of proteoglycans remains unclear, it is thought to potentially attract water. [17, 19]. This allows resistance to

compression due it's composition of hyaluronic acid, chondroitin and dermatan sulfates, heparin sulfate and heparin, and keratin suflate aggregated to a protein core [17, 19]. While lipids in bone may aid in promoting calcification by binding calcium to cell membranes [17]. Water may be freely mobile, bound to the surface in the mineral phase, or bound as a hydroxyl component of other molecules in bone [22]. An inverse relationship exists between the water content of bone and its mechanical properties with a lower water content significantly increasing bone stiffness while a higher water content reduces it [22]. Bound water is associated with bone strength and mobile water is correlated with the modulus of elasticity and the porosity of bone [22].

Bone mineral exists in a crystal form composed mainly of hydroxyapatite [19, 22]. The mineral crystal orientation giving bone anisotropic properties while providing significant hardness, stiffness and strength [17, 19]. The main minerals contributing to the hydroxyapatite crystal are calcium and phosphorous [22]. Other major minerals including calcium and phosphorous are carbonate, magnesium, sodium, manganese, zinc, copper and fluoride to make up 65% of bone by weight [17]. Osteoid, or unmineralized organic matrix, is originally laid down in woven bone and must undergo mineralization to become lamellar bone [17, 19, 22]. The process of mineralization may differ based on if bone is going from unwoven to lamellar bone (maturation) or if bone is going from lamellar bone to lamellar bone (remodeling) [17, 19]. With remodeling, mineralization may occur at nucleation sites within the collagen itself because specific proteins such as osteonectin or bone sialoprotein may act as a nidus or the mineralization process to occur [17, 19].

Alternatively, when bone undergoes maturation mineralization it is thought to occur through extracellular matrix vesicles in an orderly process [17, 19, 22]. An overview is one in which osteoid is produced, matures, and mineral is exchanged for water in the hole zones of collagen molecules to not disrupt spatial organization [17, 19]. The exact mechanism by which mineral comes to be concentrated within extracellular matrix vesicles is poorly understood with physiologic fluids perhaps becoming supersaturated with mineral, crystal inhibitors present, genetic control, hormonal control and Vitamin D all playing roles [17,19]. Once vesicles (cytoplasmic blebs) are formed from bone cells in woven bone and minerals are concentrated, they precipitate in the form of amorphous crystals with the vesicles thought to contain specific enzymes and phospholipids to bone mineralization [17]. After precipitation, a specified mass is reached and the amorphous crystals becomes crystalline hydroxyapatite and are deposited within the hole zones of collagen molecules [17, 19] Surfaces of collagen fibers must be mineralized as well and in order for the process of mineralization to continue, inhibitors of mineralization must be destroyed [17]. After this occurs, woven bone is no longer present and the new lamellar bone can undergo further remodeling to finish becoming mature bone.

Bone cells that affect structural integrity of bone are osteoblasts, osteocytes and osteoclasts [17]. Osteoprogenitor cells exist as undifferentiated mesenchymal cells that have the properties of stem cells in that they have the ability to differentiate in order to give rise to and maintain new bone cells (osteoblasts) which synthesize new bone matrix (osteoid) on bone surfaces [15, 17, 19]. They arise from self- renewing pluripotent stem cells in various tissues and commitment to the osteoblast lineage requires the canonical Runx2/Wnt/B-catenin pathway and associated proteins [15, 28]. In bone, these

committed yet undifferentiated mesenchymal stem cells are present on the endosteum, Haversian and Volkamann's canals, as well as the inner layer of the periosteum as bone-lining cells [19].

Osteoblasts arise from osteoprogenitor cells and their shape is dependent on their amount of activity [15, 17 19]. Inactive, or quiescent, osteoblasts resemble discs and are thought to form the endosteum [15, 17]. Active osteoblasts are plump with extensive organelles as they are responsible for bone matrix (osteoid) synthesis and secretion, mainly Type I collagen and glycosoaminoglycans [15, 17, 19]. Interaction occurs between osteoblasts and mature bone cells (osteocytes) in the regulation of calcium homeostasis and mineralization of bone [17, 19, 29]. Osteoblasts respond with osteocytes to mechanical stress to mediate changes in bone shape and size [15, 17, 19]. Osteoblasts then differentiate into primary bone cells (osteocytes) depending on a variety of growth factors and transcription factors. For our purposes, it is assumed that molecular and cellular signaling proceeds in a normal fashion. **Fig.1-4** provides a brief overview for commitment of a multipotent mesenchymal stem cell to a mature osteocyte with growth factors and signaling outlined in **Table 1-1** [30]. For simplicity, osteoblasts secrete osteoid or new mineralized bone, a key marker when evaluating bone formation.

Osteocytes lie within lacunae within mineralized bone and represent terminally differentiated osteoblasts [15]. They function within syncytial networks to support bone structure and metabolism [15]. They make contact with other osteocytes or osteoblasts by the use of long cytoplasmic processes (filopodia) that lie within the canaliculi in mineralized bone [15, 17]. Osteocytes themselves retain limited capacity to form new bone, and only under extreme stress seem to play a limited role in bone resorption [15, 17, 31].

Osteoclasts arise from hematopoietic stem cells of the granulocyte-monocyte origin [15, 17]. They are multinucleated, and are the only cells known to be capable of resorbing bone. Osteoclasts are able to bind to bone matrix via integrin receptors present in the osteoclast membrane [15]. Once bound, they are able to resorb bone. Briefly, the mineral present in bone is dissolved by secretion of hydrogen ions [17]. Next, the collagen present in bone matrix is cleaved into polypeptide fragments [17. This action creates a concavity in the bone called Howships lacuna [17].

Bone remodeling occurs in four sequential phases; activation, resorption, reversal, and formation [15]. It is the process by which bone maintains strength and mineral homeostasis [15]. It occurs by three mechanisms; apposition and resorption at the endosteal surface, apposition and resorption at the periosteal surface, and activation, resorption and formation at the Haversian system [19]. Remodeling is first activated by an interaction between osteoclasts and osteoblasts through a "coupling" mechanism that is poorly understood [19]. Resorption is carried out by osteoclasts in the form of a "cutting cone" [19]. The defect then becomes filled with fibrovascular tissue [19]. The outer edge of where resorption ends and bone formation begins is known as the "cement" or "reversal" line [19]. Finally, bone formation is carried out by osteoblasts. This remodeling process may provide the key insights into specific cytokines or cell signaling that allow the process of fracture repair to be more closely understood. Attention will be paid to bone morphogenetic protein-2 later on as it is a prominent cytokine upregulated during fracture repair [32].

Fracture Repair

In this section, the normal fracture repair sequence is reviewed as the gold standard for a bone healing. Fractures are the most common traumatic injuries and approximately 10% of them do not heal properly in humans [33]. Fractures themselves are the result of structural failure of bone [34]. They are the result of loading factors on bone itself and the intrinsic nature of bone [34]. The magnitude, rate and direction of load influence the likelihood of fracture because bone is viscoelastic, constantly under strain, and allows stress reduction to occur in a time-dependent manner [34]. Cortical bone has different mechanical properties dependent on the direction it is loaded in (anisotropy) [34]. Bone is strong but brittle due to its composition as described above and various in amounts of cancellous versus cortical bone dependent on the area of bone allowing bone to fracture differently dependent on the area that force is directed [34].

Fracture healing is regulated by the nature of the fracture itself, the stability of its fixation, and biological processes [33]. One of the most widely examined treatments for enhancing fracture healing is bone morphogenetic proteins [33]. In order to enhance the use of bone morphogenetic proteins, conditions for fracture healing must be optimized [33]. The sequential four-stage model is reviewed to describe the fundamental events that occur over a timeline of fracture healing [35]. There are often significant overlaps between the stages [35]. This will provide the ideal timeline for which bone substitutes, often loaded with bone morphogenetic proteins, should aim to mimic natural bone in terms of repair followed by integration or degradation of the substitute itself.

Fractures may heal as a result of direct (primary) or indirect healing (secondary) [36]. Direct fracture healing is the result of correct anatomical reduction of the fracture ends, without any gap formation, and a stable fixation [36]. In the tibia, and other associated long bones, the most common form of fractures healing is indirect [36]. Indirect healing involves both endochondral and intramembranous bone healing, but does not require perfect anatomical reduction or rigid stable conditions [36]. A four-stage model to describe the basic events that occur during indirect fracture healing has been developed from histological observations of healing fractures [35]. The stages consist of inflammation, soft callus formation, hard callus formation, and remodeling [35]. An accelerated overview is provided by **Fig 1-5** with a mouse model of fracture healing that occurs in 1 month [33].

Stage I- Inflammation

Immediately following a fracture, an acute inflammatory response begins and peaks within the first 24 hours [36]. Inflammation typically subsides by 7 days [36]. Initially there is disruption to soft tissue integrity, disruption to normal vascular function, and a hematoma is generated [35, 36]. The hematoma coagulates in, and around, the fracture ends and within the medulla to form the initial template for a fracture callus [36]. There is a secretion of numerous proinflammatory cytokines. The main inflammatory cytokines have previously been described in Table 1. Mesenchymal stem cells associated with bone formation and repair originate from the periosteum, bone marrow, circulation, and surrounding soft tissues play an initial role in this early stage of fracture healing [35, 36]. Finally, once the initial clot has formed, reorganization into granular tissue begins with phagocytic cells clearing degenerated cells and debris [35].

Stage II- Soft callus formation

Soft callus formation begins concurrently with the end stage of the immediate inflammatory phase [35]. It provides the cartilaginous template for hard callus formation. It forms as a result of the endochondral ossification process for bone healing [35]. Cells responsible for forming this semi-rigid, principally avascular, soft callus are chondrocytes and fibroblasts [35]. Cartilaginous regions grow and merge, forming a central fibrocartilaginous plug that splints the fracture [35]. Chondrocytes then undergo hypertrophy and mineralization before undergoing apoptosis. Exact growth factors that stimulate fibroblast and chondrocyte proliferation are numerous. For an up to date list, the reader is referred to a current article by Schindeler et al [35]. In response to the various factors, chondrocytes generate large amounts of extracellular matrix protein, mainly types II or X [35]. Vascularization of the soft callus is stimulated by numerous pro-angiogenic growth factors some of which are briefly mentioned in **Table 1-1**.

Stage III- Hard callus formation

This stage of bone repair is characterized by high levels of osteoblast activity. Vasculature plays a critical role in terms of increased oxygen tension being necessary for osteoblast differentiation. The formation of mineralized bone matrix occurs and arises directly from the peripheral callus in areas of stability [35]. Revascularization occurs along with removal of the soft callus [35]. This new initial woven bone is irregular, containing both proteinaceous and mineralized extraceullar matrix [35]. Mechanical stability, and the replacement of calcified cartilage by woven bone marks the end of hard callus formation with bone remodeling beginning to take place concurrently [36].

Stage IV- Bone remodeling

The initial step in bone remodeling involves converting irregular woven bone into lamellar bone and restoring the original cortical structure [35]. Osteoclasts become the key cell type as they become polarized to adhere to, and resorb, mineralized bone in areas that are irregular [35]. These irregular areas are known as “Howship’s lacuna” [35]. Once resorption is complete, osteoblasts lay down new bone on the irregular surface [35]. Molecular signaling is again complex and beyond this limited discussion.

Bone Morphogenetic Protein-2

Clearly there are numerous cytokines and growth factors responsible for initiation of fracture repair. The aim of this review is to highlight the bone morphogenetic proteins as they are known for osteoinductive capacity during fracture repair [37]. Bone morphogenetic proteins are members of the transforming growth factor beta superfamily with activity that was first identified in the 1960s [38, 37]. They are the most extensively reviewed candidates for fracture repair and are available in synthetic forms either derived from Chinese hamster ovary cells or E. coli [33, 37). Although there are numerous bone morphogenetic proteins, the most studied and FDA tested are BMP-2 and BMP-7 [33]. BMP-2 itself is an endogenous mediator of fracture repair [39]. It is necessary for fracture repair and in mice lacking BMP-2 spontaneous fractures do not resolve with time [39]. Unfortunately, Large amounts of BMP-2 are difficult to produce and extremely costly [40]. There is increasing evidence of deleterious side effects of associated with off-label use of BMP-2 products despite its ability to elicit an outstanding pro-osteogenic

effect [41]. This may associated with the large initial release of the protein from various BMP-2 containing products [42, 43]. While the majority of recombinant human BMP-2 (rhBMP-2) is traditionally derived from Chinese hamster ovary cells, *E. coli* derived rhBMP-2 has been shown to show compatible fusion rates [40, 44-46]. *E. coli* derived rhBMP-2 is more cost effective and has shown potential as a growth factor capable of elution from scaffolds with a pore size of 100-300 um [44]. In typical fractures, BMP-2 is upregulated for up to 4 weeks supporting the idea that an alternative strategy is to have a sustained release of BMP-2 allowing for enhanced osteogenic differentiation while potentially mitigating side effects [32, 42, 47, 48]. Currently recombinant human BMP-2 and -7 are available under various regulatory conditions; however, testing is still under way as it is still unknown how to use these potent proteins safely and effectively [33]. Newer studies have explored other various BMPs and their effects on fracture repair with particular attention to BMP-4 and 6 with promising results [50, 51].

These stages of fracture repair are not separate from one and another [35]. For example, cartilage mineralization, vascular invasion and woven bone formation occur concurrently with the replacement of the peripheral callus with lamellar bone [35]. It is important to remember that fracture repair is highly regulated and influenced by numerous factors such as cellular, molecular and genetic factors [35]. Further information regarding overlap of molecular signaling, interactions and phases is beyond the scope of this review and the reader is referred to other articles [35, 36].

Abnormal Fracture Healing (Delayed and Non-unions)

When a fracture is unable to heal or heals in a manner slower than expected it may be classified as a non-union or delayed union [52]. In human patients, the average risk of nonunion per fracture is near 2% with up to a 10% incidence in elderly patients or clavicular and tibial fractures [53]. The incidence of non-union is highly dependent on injury, host factors, and is site dependent [54]. Consensus for the definitions of delayed and non-unions currently do not exist, are inconsistent and subjective [55]. In 2007, Giannoudis et al came up with the diamond concept [56]. This concept required 4 key elements that every fracture must have to heal. They are the presence of osteogenic cells, growth factors, mechanical stability with the requirement of tissue vascularity, and a stable osteoconductive scaffold [55, 56].

With a delayed union, the fracture goes through the normal stages of healing clinically, but the radiographic appearance of fracture healing is delayed [52]. One definition may be “a fracture in which healing has not occurred in the expected time and the outcome remains uncertain” [55]. Factors that may induce a delayed fracture include a reduced blood supply, or infection at the fracture site [52]. These factors may be more prevalent in fractures where the skin surface has been disrupted and the bone is exposed to the environment (open) versus a fracture where the skin is intact (closed) [52]. Additionally, if the repair of the fracture has been too rigid, callus formation will be inhibited and a gap of greater than 1 mm will delay union in human patients [52].

A non-union occurs if the fracture has failed to progress to the stage of a bridging callus by 6 months [52]. However, the United States Food and Drug Administration defines non-union as a fracture that must be at least 9 months old and has not shown signs of progressive healing for 3 consecutive months [55]. Alternative definitions include a timeline of 6-8 months, or twice the time in which a fracture should heal [55].

Some authors feel that specifying a time for every fracture is not helpful [55]. One definition for a non-union, as described by one author, could be a symptomatic fracture with no potential to heal without intervention [55]. In humans, general factors on the patient side include age, corticosteroid therapy, and systemic disease, but these are uncommon in animals [54].

Non-unions may be classified into two broad categories based on the Weber and Czech classification system [55]. They may be either hypertrophic or atrophic (Harwood). With hypertrophic non-unions, the fracture site is typically hyper-vascular with potential for biological activity [55]. This is a fracture that typically can be resolved with improved mechanics [55]. Under atrophic conditions, the opposite is true, and the site is hypo-vascular and incapable of biological activity. These fractures require additional therapies as changing the mechanical environment alone will not solve the fractures inability to heal [55].

The first requirement for fracture healing is the presence of osteogenic cells [56]. Lack of these cells may arise from fractures that are open to the environment or those that have undergone extensive surgical exposures [55]. Additionally, systemic biology of the patient may affect the availability of osteogenic cells [55]. Finally, infection is detrimental to these cells leading both to injury and reduced ability of local tissue to support cellular healing [55].

The second key element leading to non-union is a lack of signaling molecules, or growth factors. These molecules may be more important in the initial stages of fracture healing as they are very active at the fracture hematoma site [55]. These growth factors are secreted from numerous cells as reviewed in **Table 1-1**. With open fractures or procedures that lead to a disturbance in the healing process during any time of fracture healing, the environment for callus formation becomes disrupted, predisposing healing towards a non-unions [55]. These signaling molecules are most detrimentally affected by a loss of vascularity and perfusion [55].

Fracture site stability is the third key element that will profoundly alter the ability of a fracture to heal. This may be the result of fracture treatments that result in either excessive motion (i.e. a conservative fracture managed in a conservatively) or excessive stability (i.e. a fracture that has not been adequately reduced allowing for too large a fracture gap to persist, and there is a loss of normal mechanical stimulus) [55]. Fractures that have excessive motion are more likely to result in hypertrophic non-unions. Atrophic non-unions are more likely to be associated with excessive stability due to the loss of mechanical stimulus that results in secondary bone healing if a fracture gap is too large for primary bone healing [55]. According to Perren's strain theory, fractures with excessive motion do not progress beyond the early stages of soft tissue healing while those with excessive stability do not progress through the stages of secondary bone healing [55]. Further information regarding the types of fracture repair and various stabilizing methodologies are biomechanical in nature and beyond the scope of this review.

The second part of the third key element is fracture site vascularity. If vascularity is decreased then there will be fewer cells available for repair, signaling and production of substrates [55]. This may lead to potential bone necrosis further reduction in the potential for healing and enhancing the local environment for infection [55]. Vascularity may be disrupted due to high energy fractures, open injuries, or when there is stripping

and disruption of the local soft tissue supply and periosteum [55]. Finally, open surgical fixation may further disrupt blood supply necessitating the need for respect to fracture biology and evaluation of any potential enhancements that would preserve vascularity [55].

Finally, the osteoconductive scaffold is the final part of fracture healing. If bony apposition is achieved the necrotic bone present within the fracture will act as the osteoconductive scaffold for osteogenic cells [55]. This element of fracture healing deals with the micro-architecture of the fracture environment as it relates to cellular migration and adhesion [55]. In order to stimulate new bone to bridge a gap, osteogenic cells must be able to communicate across some type of scaffolding environment that is conducive to cellular communication that promotes bone growth [55].

Treatment of a delayed or non-union fracture should be focused around restoring the 4 key elements of fracture healing. While mechanical stability and tissue vascularity, and osteogenic cells are beyond the scope of this review, we aim to evaluate potential alternatives for osteoconductive scaffolds and growth factors that may be used when this element of fracture healing is in jeopardy and cannot be fixed by means of traditional therapies that are reviewed next.

Osteoconductive Scaffolds

Osteoconductive scaffolds may take many forms as the sole goal of the scaffold is to provide osteogenic cells the ability to communicate with each other to promote bone growth. The scaffold may be a bone graft material, a ceramic material, a synthetic material, or a combination of the above. Ideally the combination should promote a bone healing response by providing osteogenic, osteoconductive, or osteoinductive activity to a local site [57]. Osteogenic may be defined as a material that contains living cells capable of differentiation into bone, while an osteoinductive material provides a biologic stimulus that induces local or transplanted cells to enter a pathway of differentiation leading to mature osteoblasts [57]. Looking more closely at osteoconductive materials, these promote bone apposition to its surface, functioning in part as a receptive scaffold to facilitate enhanced bone formation [57].

The typical gold standard for bone grafting has traditionally been autografting [7, 57]. This has been followed by allografting and then xenografting. Autografting possess all the properties required for grafting while retaining complete histocompatibility as it is a graft taken from the patient (or donor) themselves [7]. It is osteoinductivece, osteoconductive, and osteogenic [7]. The supply of autogenous graft material however is self-limiting and does not come without cost [7]. Donor site morbidity can lead to major or minor complications and have been reported at rates of up to almost 21% [7]. Allografting is taking a piece of bone from a cadaver or donor rather than from the patient themselves. It is available in either cancellous, cortical, or demineralized bone matrix forms [7]. It is typically osteoconductive, while demineralized bone matrix may processed in a way to retain osteoinductive properties [7]. If the graft is cortical, then it may retain some structural support properties in addition to being osteoconductive [7]. Allografts are at a disadvantage in that they do not retain osteogenic properties; however, they are available large quantities and not associated with donor site morbidity or increased surgical operative time [7]. The large disadvantage of allografts is the potential for transmission of viruses and other infective agents and the potential for an immune

response from the recipient necessitating a match with the donor [7]. Xenografts are are based on natural hydroxyapatite and deorganified bone that is obtained from a species other than the host species [58]. They are strictly osteoconductive [58]. The concern is again for a risk of a host-immune response [58].

Beyond more traditional grafts are the use of substitute materials. Some of the first bone graft materials used are known as bioceramics [7, 58]. Bioceramics are neither osteoinductive nor osteogenic [7]. They work by creating a scaffold to promote osteosynthesis [58]. Bioceramics vary in terms of rate of re-absorption and mechanical properties depending on which ceramic is used [7]. These rates vary widely from as fast as four weeks to as long as 18 months [7]. Based on this, researchers have been attempting to optimize the characteristics of bioceramics by creating composites of various bone graft substitues [7]. There are four main types of bioceramics, calcium sulphate, calcium phosphate, triacalcium phosphate, and coralline hydroxyapatite [7]. They come in multiple forms and combinations each seeking to provide the optimal osteoconduction, osteoinduction, and osteointegration that most closely resembles the autografts [58].

A second class of substitute materials are the polymer-based substitutes. While natural polymers exist, they are rarely used alone [59]. Natural polymers include collagen, alginate, agarose, chitosan, fibrin, and hylaronan [59]. The benefit of synthetic polymers is that they can range from nondegradadable to fully biodegradable and offer more flexibility and processability into different shapes and sizes [59]. Similar to bioceramics, they can be found in different forms and manufactured in a variety of ways [59]. While ceramic materials resemble components of bone, they are brittle, do not match mechanical properties of bone and are unsuitable for growth of soft tissues that enhance different cellular receptors [60]. The most common synthetic polymers are aliphatic polyesters such as polycaprolactone, polactic acid and its copolymers such as polylactide-co-glycolide, and polyglycolic acid [60]. Additional commonly used polymers for bone tissue engineering include poly(vinyl alcohol), poly(propylene fumarate) and polyurethane [61]. Functional groups or side chains can be incorporated into synthetic polymers thus allowing them to be bioactivated in regards to bone tissue [60].

Due to polymers tending to be too flexible and ceramics tending to be too brittle, recently, composite materials have been made of polymers reinforced with ceramic fillers [60]. The goal is to create a reinforced porous scaffold with enhanced bioactivity and controlled resorption rate [60]. One of the most researched polymer composites is a nanohydroxyapatite/polyurethane composite (nHA/PU) [62, 63]. While there has been extensive research into the exact ratio of nHA to PU it has been shown to have excellent cytocompatibility regardless of hydrothermal preparation methods [63-66]. Additionally, it has been shown to have the capability of eluting rhBMP-2 in a rat model [67]. It has shown promising degradation and integration capabilities into long bones in small animal models [68]. Alternatively, this combination is suitable to the addition of other regenerative materials such as bioactive glass [69]. Currently, there is a lack of large animal studies, and commercialization methods that prevent this promising composite material from moving forward.

Osteomyelitis

One of the most devastating and common reasons for either non-union or failure of an osteoconductive scaffold is infection. Bone infection is termed osteomyelitis [70]. Osteomyelitis is an inflammatory bone disease caused by an infecting microorganism [70]. The end result is progressive bone loss and destruction accounting for significant morbidity and expense [70-73]. Opportunistic Gram-positive staphylococci, specifically Staphylococcus aureus (SA) are responsible for up to 75% of clinical osteomyelitis cases [72].

Staphylococcus aureus (SA) is a gram positive bacteria that is both a commensal and a pathogen[75]. It is the most common pathogen in osteomyelitis (OM) [72, 74]. OM is most commonly classified using the Waldvogel classification system [75]. One branch of this system is contiguous-focus OM (infection from trauma or surgery with direct implantation of organisms) which provides key insights into the how SA is able to infect bone as healthy bone is resistant to infection [76]. SA has evolved to overcome this resistance and infect bone in three key ways. The first is through genes that encode microbial surface component recognizing adhesive matrix molecules (MSCAMMs) that allow it to attach to bone cells (osteoblasts) [77]. The second is through biofilm formation that provide a safe haven from both the immune system and antimicrobials [72]. Finally, the last is the ability of SA to invade osteoblasts themselves, and survive in an altered metabolic state [78, 79].

Currently, very little is known about how the SA-osteoblast relationship results in bone formation. It may be that infected osteoblasts release inflammatory cytokines within the first few days of infection, similar to osteoblasts after the first few days of an injury [80]. Thus, infected osteoblasts may play a role in the initial inflammatory phases of bone production prior to shifting activity to osteoclastic bone resorption and overall bone loss [72]. Additionally, it may be that the exact strain of infectious SA plays an important role. It has been shown that SA strains lacking genes that encode certain MSCRAMMs are less likely to cause OM infections in animal models [81, 82]. A key development in attempting to elucidate the SA-osteoblast relationship has been ability to determine difference in strains of bacteria, and the presence of these genes, has been the use of multilocus sequencing [83, 83]. One relatively novel sequence type (ST) of SA is ST 398, which we have shown it to be putatively capable of producing a large amount of bone formation. Additionally, this sequence type has a proven track record of being a one-health problem, representing a newer sequence type from previous studies investigating any potential SA-osteoblast relationships that result in bone formation [85-88].

Investigation of the sequence specific SA-osteoblast relationship may start with physiologic evidence of bone formation. Evidence of such formation may be the result of osteoblast inflammation which has been well studied with in both *in-vitro* and *in-vivo* models of SA infection [89-94]. Osteoblast inflammation *in-vitro* may be characterized as osteoblast invasion by SA and resultant cell death (apoptosis), a release of inflammatory markers (cytokines), and a production of bone formation markers (type I collagen, osteopontin, osteocalcin) [89-93]. This inflammation may be ST dependent with ST 398 capable of producing more periosteal new bone as compared to known laboratory strains. These *in-vitro* studies would then be definitively confirmed in a known animal model of infection providing the necessary link for definitive phenotypic evidence that the amount of bone formation is sequence dependent [95]. Genetic comparisons of sequence types

may additionally elucidate how this little studied ST 398 is capable of physiologically altering the SA-osteoblast relationship towards bone formation.

Next, altering the ability of SA to attach to osteoblasts may provide the necessary evidence to elucidate the mechanism of the SA-osteoblast relationship in the production of bone formation. The MSCRAMMs are protein surface adhesins that provide the ability to attach to osteoblasts [96]. The synthesis of these surface adhesins is activated by global regulatory loci such as *sarA* and *cna*, while environmental signals are generated to activate *agr* [97]. *sarA* has been implicated in SA's ability to form biofilms, while *agr* has been implicated in SA's virulence through production of hemolysins [97]. This leaves *cna* which produces collagen binding protein (*Cna*) to become attached to osteoblasts, and internalized to potentially alter osteoblast activity [97]. It becomes particularly important in terms of direct inoculation (trauma or surgery) as osteoblasts are being primed for bone repair and set to produce type I collagen [73]. Therefore how SA OM results in new bone formation may be tied to the function of *cna* during direct inoculation. This has been a remotely investigated phenomenon in terms of bone formation. At present SA OM has been primarily identified as bone losing disease [70, 72]. Therefore, current treatment and prevention efforts do not consider the potential overall impact of bone formation as a therapeutic advantage in areas devoid of bone formation or as a potential target for treatment to limit its formation (reduce virulence) in areas where it has become excessive.

Conclusion

In summary, a bone substitute should be osteconductive thereby mitigating the loss of cell signaling that occurs with non-unions and returning fractures to proper fracture healing and restoring bone back to its proper anatomical and functional form. If they are capable of either eluting an antimicrobial or altering osteoblast activity towards resisting infection, they are of added benefit as this is the primary and most devastating complication. BMP-2 remains the most investigated growth factor with the most potential towards accelerating fracture healing that may be eluted from osteoconductive scaffolds. Investigation is still necessary for finding the most effective dose and delivery of this potent growth factor. Nanohydroxyapetite and polyurethane composites are some of the most studied bone regenerative scaffold composites which need FDA approval for commercial manufacturing and large animal testing prior to becoming clinically usable bone substitutes. The end goal for any bone substitute should always be to return long bones to their normal functional anatomy.

References

1. Court-Brown, C. M., Rimmer, S., Prakash, U., & McQueen, M. M. (1998). The epidemiology of open long bone fractures. *Injury*, *29*(7), 529-534.
2. Belmont Jr, P. J., McCriskin, B. J., Hsiao, M. S., Burks, R., Nelson, K. J., & Schoenfeld, A. J. (2013). The nature and incidence of musculoskeletal combat wounds in Iraq and Afghanistan (2005–2009). *Journal of orthopaedic trauma*, *27*(5), e107-e113.
3. Belmont, P. J., Schoenfeld, A. J., & Goodman, G. (2010). Epidemiology of combat wounds in Operation Iraqi Freedom and Operation Enduring Freedom: orthopaedic burden of disease. *J Surg Orthop Adv*, *19*(1), 2-7.
4. Smith, B. D., & Grande, D. A. (2015). The current state of scaffolds for musculoskeletal regenerative applications. *Nature Reviews Rheumatology*, *11*(4), 213.
5. Finkemeier, C. G. (2002). Bone-grafting and bone-graft substitutes. *JBJS*, *84*(3), 454-464.
6. Baldwin, P., Li, D. J., Auston, D. A., Mir, H. S., Yoon, R. S., & Koval, K. J. (2019). Autograft, allograft, and bone graft substitutes: clinical evidence and indications for use in the setting of orthopaedic trauma surgery. *Journal of orthopaedic trauma*, *33*(4), 203-213.
7. Fillingham, Y., & Jacobs, J. (2016). Bone grafts and their substitutes. *The bone & joint journal*, *98*(1_Supple_A), 6-9.
8. Fernandez de Grado, G., Keller, L., Idoux-Gillet, Y., Wagner, Q., Musset, A. M., Benkirane-Jessel, N., ... & Offner, D. (2018). Bone substitutes: a review of their characteristics, clinical use, and perspectives for large bone defects management. *Journal of tissue engineering*, *9*, 2041731418776819.
9. Reichert, J. C., Saifzadeh, S., Wullschleger, M. E., Epari, D. R., Schütz, M. A., Duda, G. N., ... & Hutmacher, D. W. (2009). The challenge of establishing preclinical models for segmental bone defect research. *Biomaterials*, *30*(12), 2149-2163.
10. Zura, R., Xiong, Z., Einhorn, T., Watson, J. T., Ostrum, R. F., Prayson, M. J., ... & Steen, R. G. (2016). Epidemiology of fracture nonunion in 18 human bones. *JAMA surgery*, *151*(11), e162775-e162775.
11. Harwood, P. J., Newman, J. B., & Michael, A. L. (2010). (ii) An update on fracture healing and non-union. *Orthopaedics and Trauma*, *24*(1), 9-23.
12. Belmont, P. J., Schoenfeld, A. J., & Goodman, G. (2010). Epidemiology of combat wounds in Operation Iraqi Freedom and Operation Enduring Freedom: orthopaedic burden of disease. *J Surg Orthop Adv*, *19*(1), 2-7.
13. Court-Brown, C. M., Rimmer, S., Prakash, U., & McQueen, M. M. (1998). The epidemiology of open long bone fractures. *Injury*, *29*(7), 529-534.
14. Nandra, R., Grover, L., & Porter, K. (2016). Fracture non-union epidemiology and treatment. *Trauma*, *18*(1), 3-11.
15. Clarke, B. (2008). Normal bone anatomy and physiology. *Clinical journal of the American Society of Nephrology*, *3*(Supplement 3), S131-S139.

16. Mittag, U., Kriechbaumer, A., Bartsch, M., & Rittweger, J. (2015). Form follows function: a computational simulation exercise on bone shape forming and conservation. *Journal of musculoskeletal & neuronal interactions*, *15*(2), 215.
17. Zachary, J. F., & McGavin, M. D. (2013). *Pathologic Basis of Veterinary Disease-Book*. Elsevier Health Sciences.
18. Gasser J.A., Kneissel M. (2017) Bone Physiology and Biology. In: Smith S., Varela A., Samadfam R. (eds) Bone Toxicology. Molecular and Integrative Toxicology. Springer, Cham
19. Safadi, F. F., & Khurana, J. S. (2009). Bone Structure and Function. In *Diagnostic Imaging of Musculoskeletal Diseases* (pp. 1-13). Humana Press.
20. Jee, W., & Weiss, L. (1983). Histology: Cell and tissue biology. *Histology Cell and Tissue Biology*, *5*(9), 200-255.
21. Dyce, K. M., Sack, W. O., & Wensing, C. J. G. (2009). *Textbook of veterinary anatomy-E-Book*. Elsevier Health Sciences.
22. Wang, X., Nyman, J. S., Dong, X., Leng, H., & Reyes, M. (2010). Fundamental biomechanics in bone tissue engineering. *Synthesis Lectures on Tissue Engineering*, *2*(1), 1-225.
23. Elgazzar, A. H. (2017). Basic Sciences of Bone and Joint Diseases. In *Orthopedic Nuclear Medicine* (pp. 1-36). Springer, Cham.
24. Henriksen, K., & Karsdal, M. A. (2016). Type I collagen. In *Biochemistry of collagens, laminins and elastin* (pp. 1-11). Academic Press.
25. Ramírez-Rodríguez, G. B., Delgado-López, J. M., Iafisco, M., Montesi, M., Sandri, M., Sprio, S., & Tampieri, A. (2016). Biomimetic mineralization of recombinant collagen type I derived protein to obtain hybrid matrices for bone regeneration. *Journal of structural biology*, *196*(2), 138-146.
26. Canalis, E., McCarthy, T. L., & Centrella, M. (1991). Growth factors and cytokines in bone cell metabolism. *Annual review of medicine*, *42*(1), 17-24.
27. Young, M. F. (2003). Bone matrix proteins: their function, regulation, and relationship to osteoporosis. *Osteoporosis international*, *14*(3), 35-42.
28. Majidinia, M., Sadeghpour, A., & Yousefi, B. (2018). The roles of signaling pathways in bone repair and regeneration. *Journal of cellular physiology*, *233*(4), 2937-2948.
29. Dallas, S. L., & Bonewald, L. F. (2010). Dynamics of the transition from osteoblast to osteocyte. *Annals of the New York Academy of Sciences*, *1192*, 437.
30. McCawley, L. J., & Matrisian, L. M. (2001). Matrix metalloproteinases: they're not just for matrix anymore!. *Current opinion in cell biology*, *13*(5), 534-540.
31. Suswillo, R. F., Javaheri, B., Rawlinson, S. C., Dowthwaite, G. P., Lanyon, L. E., & Pitsillides, A. A. (2017). Strain uses gap junctions to reverse stimulation of osteoblast proliferation by osteocytes. *Cell biochemistry and function*, *35*(1), 56-65.
32. Groeneveld, E. H., & Burger, E. H. (2000). Bone morphogenetic proteins in human bone regeneration. *European journal of endocrinology*, *142*(1), 9-21.
33. Einhorn, T. A., & Gerstenfeld, L. C. (2015). Fracture healing: mechanisms and interventions. *Nature Reviews Rheumatology*, *11*(1), 45.

34. Nyary, T., & Scammell, B. E. (2018). Principles of bone and joint injuries and their healing. *Surgery (Oxford)*, *36*(1), 7-14.
35. Schindeler, A., McDonald, M. M., Bokko, P., & Little, D. G. (2008, October). Bone remodeling during fracture repair: The cellular picture. In *Seminars in cell & developmental biology* (Vol. 19, No. 5, pp. 459-466). Academic Press.
36. Marsell, R., & Einhorn, T. A. (2011). The biology of fracture healing. *Injury*, *42*(6), 551-555.
37. Chen, D. I., Zhao, M., & Mundy, G. R. (2004). Bone morphogenetic proteins. *Growth factors*, *22*(4), 233-241.
38. Urist, M. R. (1965). Bone: formation by autoinduction. *Science*, *150*(3698), 893-899.
39. Tsuji, K., Bandyopadhyay, A., Harfe, B. D., Cox, K., Kakar, S., Gerstenfeld, L., ... & Rosen, V. (2006). BMP2 activity, although dispensable for bone formation, is required for the initiation of fracture healing. *Nature genetics*, *38*(12), 1424.
40. Chung, C. H., Kim, Y. K., Lee, J. S., Jung, U. W., Pang, E. K., & Choi, S. H. (2015). Rapid bone regeneration by Escherichia coli-derived recombinant human bone morphogenetic protein-2 loaded on a hydroxyapatite carrier in the rabbit calvarial defect model. *Biomaterials research*, *19*(1), 17.
41. Quinlan, E., Thompson, E. M., Matsiko, A., O'Brien, F. J., & López-Noriega, A. (2015). Long-term controlled delivery of rhBMP-2 from collagen–hydroxyapatite scaffolds for superior bone tissue regeneration. *Journal of controlled release*, *207*, 112-119.
42. Poldervaart, M. T., Wang, H., van der Stok, J., Weinans, H., Leeuwenburgh, S. C., Öner, F. C., ... & Alblas, J. (2013). Sustained release of BMP-2 in bioprinted alginate for osteogenicity in mice and rats. *PloS one*, *8*(8), e72610.
43. Jansen, J. A., Vehof, J. W. M., Ruhe, P. Q., Kroeze-Deutman, H., Kuboki, Y., Takita, H., ... & Mikos, A. G. (2005). Growth factor-loaded scaffolds for bone engineering. *Journal of Controlled Release*, *101*(1-3), 127-136.
44. Lee, J. H., Ryu, M. Y., Baek, H. R., Lee, K. M., Seo, J. H., Lee, H. K., & Ryu, H. S. (2013). Effects of porous beta-tricalcium phosphate-based ceramics used as an E. coli-derived rhBMP-2 carrier for bone regeneration. *Journal of Materials Science: Materials in Medicine*, *24*(9), 2117-2127.
45. Bessho, K., Konishi, Y., Kaihara, S., Fujimura, K., Okubo, Y., & Iizuka, T. (2000). Bone induction by Escherichia coli-derived recombinant human bone morphogenetic protein-2 compared with Chinese hamster ovary cell-derived recombinant human bone morphogenetic protein-2. *British Journal of Oral and Maxillofacial Surgery*, *38*(6), 645-649.
46. Geiger, M., Li, R. H., & Friess, W. (2003). Collagen sponges for bone regeneration with rhBMP-2. *Advanced drug delivery reviews*, *55*(12), 1613-1629.
47. Yamamoto, M., Takahashi, Y., & Tabata, Y. (2003). Controlled release by biodegradable hydrogels enhances the ectopic bone formation of bone morphogenetic protein. *Biomaterials*, *24*(24), 4375-4383.

48. Cho, T. J., Gerstenfeld, L. C., & Einhorn, T. A. (2002). Differential temporal expression of members of the transforming growth factor β superfamily during murine fracture healing. *Journal of Bone and Mineral Research*, *17*(3), 513-520.
49. Jane Jr, J. A., Dunford, B. A., Kron, A., Pittman, D. D., Sasaki, T., Li, J. Z., ... & Kallmes, D. F. (2002). Ectopic osteogenesis using adenoviral bone morphogenetic protein (BMP)-4 and BMP-6 gene transfer. *Molecular Therapy*, *6*(4), 464-470.
50. Bandyopadhyay, A., Tsuji, K., Cox, K., Harfe, B. D., Rosen, V., & Tabin, C. J. (2006). Genetic analysis of the roles of BMP2, BMP4, and BMP7 in limb patterning and skeletogenesis. *PLoS genetics*, *2*(12), e216.
51. Kugimiya, F., Kawaguchi, H., Kamekura, S., Chikuda, H., Ohba, S., Yano, F., ... & Nakamura, K. (2005). Involvement of endogenous bone morphogenetic protein (BMP) 2 and BMP6 in bone formation. *Journal of Biological Chemistry*, *280*(42), 35704-35712.
52. Nyary, T., & Scammell, B. E. (2018). Principles of bone and joint injuries and their healing. *Surgery (Oxford)*, *36*(1), 7-14.
53. Ding, Z. C., Lin, Y. K., Gan, Y. K., & Tang, T. T. (2018). Molecular pathogenesis of fracture nonunion. *Journal of orthopaedic translation*, *14*, 45-56.
54. DeCamp, C. E. (2015). *Brinker, Piermattei and Flo's handbook of small animal orthopedics and fracture repair*. Elsevier Health Sciences.
55. Harwood, P. J., Newman, J. B., & Michael, A. L. (2010). (ii) An update on fracture healing and non-union. *Orthopaedics and Trauma*, *24*(1), 9-23.
56. Giannoudis, P. V., Einhorn, T. A., & Marsh, D. (2007). Fracture healing: the diamond concept. *Injury*, *38*, S3-S6.
57. Bauer, T. W., & Muschler, G. F. (2000). Bone graft materials: an overview of the basic science. *Clinical Orthopaedics and Related Research®*, *371*, 10-27.
58. Popescu, E., Forna, D. A., Earar, K., & Forna, N. C. (2017). Bone Substitutes Used in Guided Bone Regeneration Technique. *Materiale plastice*, *54*(2), 390.
59. Fernandez de Grado, G., Keller, L., Idoux-Gillet, Y., Wagner, Q., Musset, A. M., Benkirane-Jessel, N., ... & Offner, D. (2018). Bone substitutes: a review of their characteristics, clinical use, and perspectives for large bone defects management. *Journal of tissue engineering*, *9*, 2041731418776819.
60. . Gloria, A., De Santis, R., & Ambrosio, L. (2010). Polymer-based composite scaffolds for tissue engineering. *Journal of Applied Biomaterials and Biomechanics*, *8*(2), 57-67.
61. Shi, R., Chen, D., Liu, Q., Wu, Y., Xu, X., Zhang, L., & Tian, W. (2009). Recent advances in synthetic bioelastomers. *International journal of molecular sciences*, *10*(10), 4223-4256.olds for tissue engineering. *Journal of Applied Biomaterials and Biomechanics*, *8*(2), 57-67.
62. Sultan, M. (2018). Hydroxyapatite/polyurethane composites as promising biomaterials. *Chemical Papers*, *72*(10), 2375-2395

63. Popescu, L. M., Piticescu, R. M., Antonelli, A., Rusti, C. F., Carboni, E., Sfara, C., ... & Buruiana, T. (2013). Recent advances in synthesis, characterization of hydroxyapatite/polyurethane composites and study of their biocompatible properties. *Journal of Materials Science: Materials in Medicine*, *24*(11), 2491-2503.
64. Popescu LM, Rusti CF, Piticescu RM, Valero T, Kintzios S, Buruiana T. Synthesis and characterization of acid polyurethane hydroxyapatite composites for biomedical applications. J Compos Mater. 2012;. doi:10.1177/0021998312443396.
65. Popescu LM, Piticescu RM, Rusti CF, Maly M, Danani A, Kintzios S, Valero Grinan MT. Preparation and characterization of new hybrid nanostructured thin films for biosensors design. Mater Lett. 2011;65:2032–5. doi:10.1016/j.matlet.2011.04.028.
66. Negroiu G, Piticescu RM, Chitanu GC, Mihailescu IN, Zdrentu L, Miroiu M. Biocompatibility evaluation of a novel hydroxyapatite- polymer coating for medical implants (in vitro tests). J Mater Sci Mater Med. 2008;19:1537–44. doi:10.1007/s10856-007- 3300-6.
67. Dumas, J. E., Prieto, E. M., Zienkiewicz, K. J., Guda, T., Wenke, J. C., Bible, J., ... & Guelcher, S. A. (2013). Balancing the rates of new bone formation and polymer degradation enhances healing of weight-bearing allograft/polyurethane composites in rabbit femoral defects. *Tissue Engineering Part A*, *20*(1-2), 115-129.
68. Dong, Z., Li, Y., & Zou, Q. (2009). Degradation and biocompatibility of porous nano-hydroxyapatite/polyurethane composite scaffold for bone tissue engineering. *Applied Surface Science*, *255*(12), 6087-6091
69. .Ryszkowska, J. L., Auguścik, M., Sheikh, A., & Boccaccini, A. R. (2010). Biodegradable polyurethane composite scaffolds containing Bioglass® for bone tissue engineering. *Composites Science and Technology*, *70*(13), 1894-1908.
70. Kavanagh, N., Ryan, E. J., Widaa, A., Sexton, G., Fennell, J., O'Rourke, S., ... & Kerrigan, S. W. (2018). Staphylococcal osteomyelitis: disease progression, treatment challenges, and future directions. *Clinical microbiology reviews*, *31*(2), e00084-17.
71. Jin, T., liang Zhu, Y., Li, J., Shi, J., qing He, X., Ding, J., & qing Xu, Y. (2013). Staphylococcal protein A, Panton-Valentine leukocidin and coagulase aggravate the bone loss and bone destruction in osteomyelitis. *Cellular Physiology and Biochemistry*, *32*(2), 322-333.
72. Claro, T., Widaa, A., O'Seaghdha, M., Miajlovic, H., Foster, T. J., O'Brien, F. J., & Kerrigan, S. W. (2011). Staphylococcus aureus protein A binds to osteoblasts and triggers signals that weaken bone in osteomyelitis. *PloS one*, *6*(4), e18748.
73. Calhoun, J., Manring, M. M. & Shirtliff, M. Osteomyelitis of the Long Bones. Semin. Plast. Surg. 23, 059–072 (2009).
74. Springer, B., Orendi, U., Much, P., Höger, G., Ruppitsch, W., Krziwanek, K., ... & Mittermayer, H. (2009). Methicillin-resistant Staphylococcus aureus: a new zoonotic agent?. *Wiener klinische Wochenschrift*, *121*(3-4), 86-90.

75. Pan, A., Battisti, A., Zoncada, A., Bernieri, F., Boldini, M., Franco, A., ... & Monaci, M. (2009). Community-acquired methicillin-resistant Staphylococcus aureus ST398 infection, Italy. *Emerging infectious diseases*, *15*(5), 845.
76. Feßler, A., Scott, C., Kadlec, K., Ehricht, R., Monecke, S., & Schwarz, S. (2010). Characterization of methicillin-resistant Staphylococcus aureus ST398 from cases of bovine mastitis. *Journal of Antimicrobial Chemotherapy*, *65*(4), 619-625.
77. Wright, J. A., & Nair, S. P. (2010). Interaction of staphylococci with bone. *International journal of medical microbiology*, *300*(2-3), 193-204.
78. Floras, A., Lawn, K., Slavic, D., Golding, G. R., Mulvey, M. R., & Weese, J. S. (2010). Sequence type 398 meticillin-resistant Staphylococcus aureus infection and colonisation in dogs.
79. Tucker, K. A., Reilly, S. S., Leslie, C. S., & Hudson, M. C. (2000). Intracellular Staphylococcus aureus induces apoptosis in mouse osteoblasts. *FEMS microbiology letters*, *186*(2), 151-156
80. Abouelkhair, M. A., Rifkin, R. E., Grzeskowiak, R. M., Biris, A. S., Anderson, D. E., Bemis, D. A., & Kania, S. A. (2018). Complete Genome Sequences of Four Staphylococcus aureus Sequence Type 398 Isolates from Four Goats with Osteomyelitis. *Microbiol Resour Announc*, *7*(12), e01174-18
81. Cheon, I. S., Woo, S. S., Kang, S. S., Im, J., Yun, C. H., Chung, D. K., ... & Han, S. H. (2008). Peptidoglycan-mediated IL-8 expression in human alveolar type II epithelial cells requires lipid raft formation and MAPK activation. *Molecular immunology*, *45*(6), 1665-1673.
82. Kim, J., Yang, J., Park, O. J., Kang, S. S., Kim, W. S., Kurokawa, K., ... & Han, S. H. (2013). Lipoproteins are an important bacterial component responsible for bone destruction through the induction of osteoclast differentiation and activation. *Journal of Bone and Mineral Research*, *28*(11), 2381-2391.
83. Alexander, E. H., & Hudson, M. (2001). Factors influencing the internalization of Staphylococcus aureus and impacts on the course of infections in humans. *Applied microbiology and biotechnology*, *56*(3-4), 361-366.
84. Sinha, B., & Fraunholz, M. (2010). Staphylococcus aureus host cell invasion and post-invasion events. *International Journal of Medical Microbiology*, *300*(2-3), 170-175.
85. Bow, A. J., Newby, S., Rifkin, R., Jackson, B., Matavosian, A., Griffin, C., ... & Morello, R. (2019). Evaluation of a polyurethane platform for delivery of nanohydroxyapatite and decellularized bone particles in a porous three-dimensional scaffold. *ACS Applied Bio Materials*.
86. Bankevich, A., Nurk, S., Antipov, D., Gurevich, A. A., Dvorkin, M., Kulikov, A. S., … Pevzner, P. A. (2012). SPAdes: A New Genome Assembly Algorithm and Its Applications to Single-Cell Sequencing. *Journal of Computational Biology*, *19*(5), 455–477. https://doi.org/10.1089/cmb.2012.0021
87. Seemann, T. (2014). Prokka: rapid prokaryotic genome annotation. *Bioinformatics (Oxford, England)*, *30*(14), 2068–2069. https://doi.org/10.1093/bioinformatics/btu153

88. Jain, C., Rodriguez-R, L. M., Phillippy, A. M., Konstantinidis, K. T., & Aluru, S. (2018). High throughput ANI analysis of 90K prokaryotic genomes reveals clear species boundaries. *Nature Communications*, *9*(1), 5114. https://doi.org/10.1038/s41467-018-07641-9
89. Contreras-Moreira, B., & Vinuesa, P. (2013). GET_HOMOLOGUES, a Versatile Software Package for Scalable and Robust Microbial Pangenome Analysis. *Applied and Environmental Microbiology*, *79*(24), 7696–7701. https://doi.org/10.1128/AEM.02411-13
90. Kanehisa, M., Furumichi, M., Tanabe, M., Sato, Y., & Morishima, K. (2017). KEGG: new perspectives on genomes, pathways, diseases and drugs. *Nucleic Acids Research*, *45*(D1), D353–D361. https://doi.org/10.1093/nar/gkw1092
91. Tatusov, R. L., Galperin, M. Y., Natale, D. A., & Koonin, E. V. (2000). The COG database: a tool for genome-scale analysis of protein functions and evolution. *Nucleic Acids Research*, *28*(1), 33–36.
92. Finn, R. D., Bateman, A., Clements, J., Coggill, P., Eberhardt, R. Y., Eddy, S. R., … Punta, M. (2014). Pfam: the protein families database. *Nucleic Acids Research*, *42*(D1), D222–D230. https://doi.org/10.1093/nar/gkt1223
93. Liu, B., Zheng, D., Jin, Q., Chen, L., & Yang, J. (2019). VFDB 2019: a comparative pathogenomic platform with an interactive web interface. *Nucleic Acids Research*, *47*(D1), D687–D692. https://doi.org/10.1093/nar/gky1080
94. Yoon, S. H., Park, Y.-K., & Kim, J. F. (2015). PAIDB v2.0: exploration and analysis of pathogenicity and resistance islands. *Nucleic Acids Research*, *43*(Database issue), D624–D630. https://doi.org/10.1093/nar/gku985
95. Abouelkhair, M. A., Bemis, D. A., Giannone, R. J., Frank, L. A., & Kania, S. A. (2018). Characterization of a leukocidin identified in Staphylococcus pseudintermedius. *PloS one*, *13*(9), e0204450.
96. Strobel, M., Pförtner, H., Tuchscherr, L., Völker, U., Schmidt, F., Kramko, N., ... & Niemann, S. (2016). Post-invasion events after infection with Staphylococcus aureus are strongly dependent on both the host cell type and the infecting S. aureus strain. *Clinical Microbiology and Infection*, *22*(9), 799-809.
97. Chen, W., Zhang, Y., Yeo, W. S., Bae, T., & Ji, Q. (2017). Rapid and efficient genome editing in Staphylococcus aureus by using an engineered CRISPR/Cas9 system. *Journal of the American Chemical Society*, *139*(10), 3790-3795.

Appendices

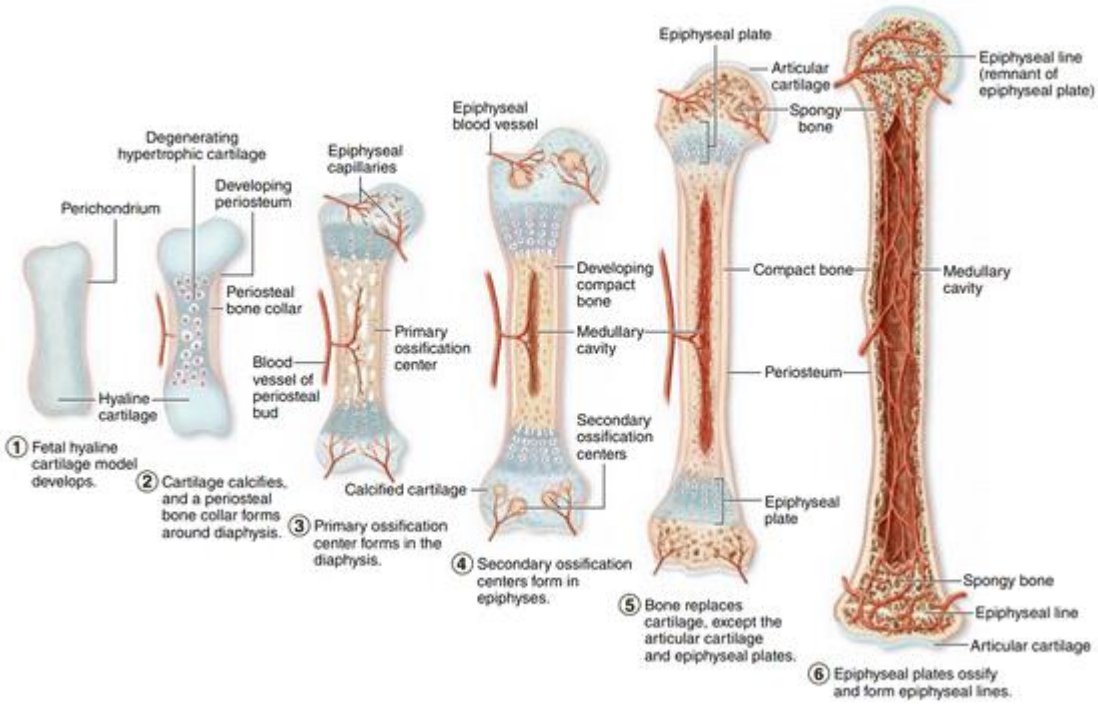


Figure 1-1. Endochondral ossification and long bone blood supply.
Image curtesy of Gasser J.A., Kneissel M. (2017) Bone Physiology and Biology. In: Smith S., Varela A., Samadfam R. (eds) Bone Toxicology. Molecular and Integrative Toxicology. Springer, Cham

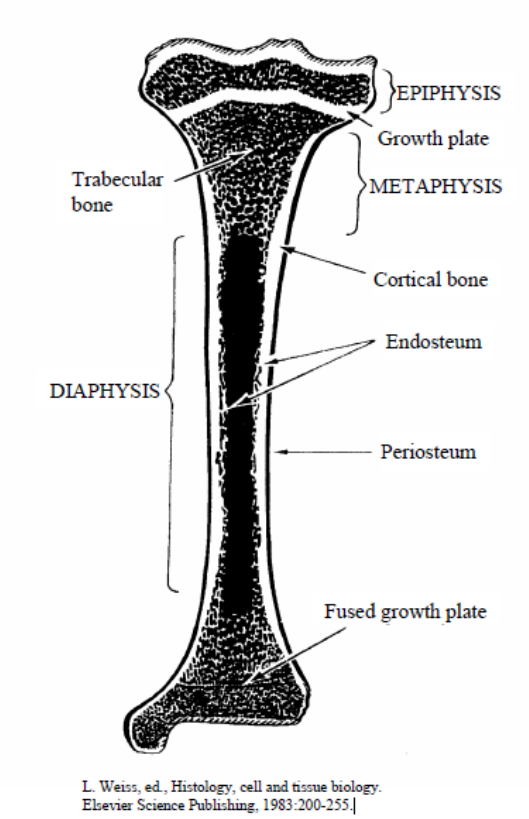


Figure 1-2. Anatomy of a long bone.
Image curtesy of Jee, W., & Weiss, L. (1983). Histology: Cell and tissue biology. *Histology Cell and Tissue Biology*, *5*(9), 200-255.

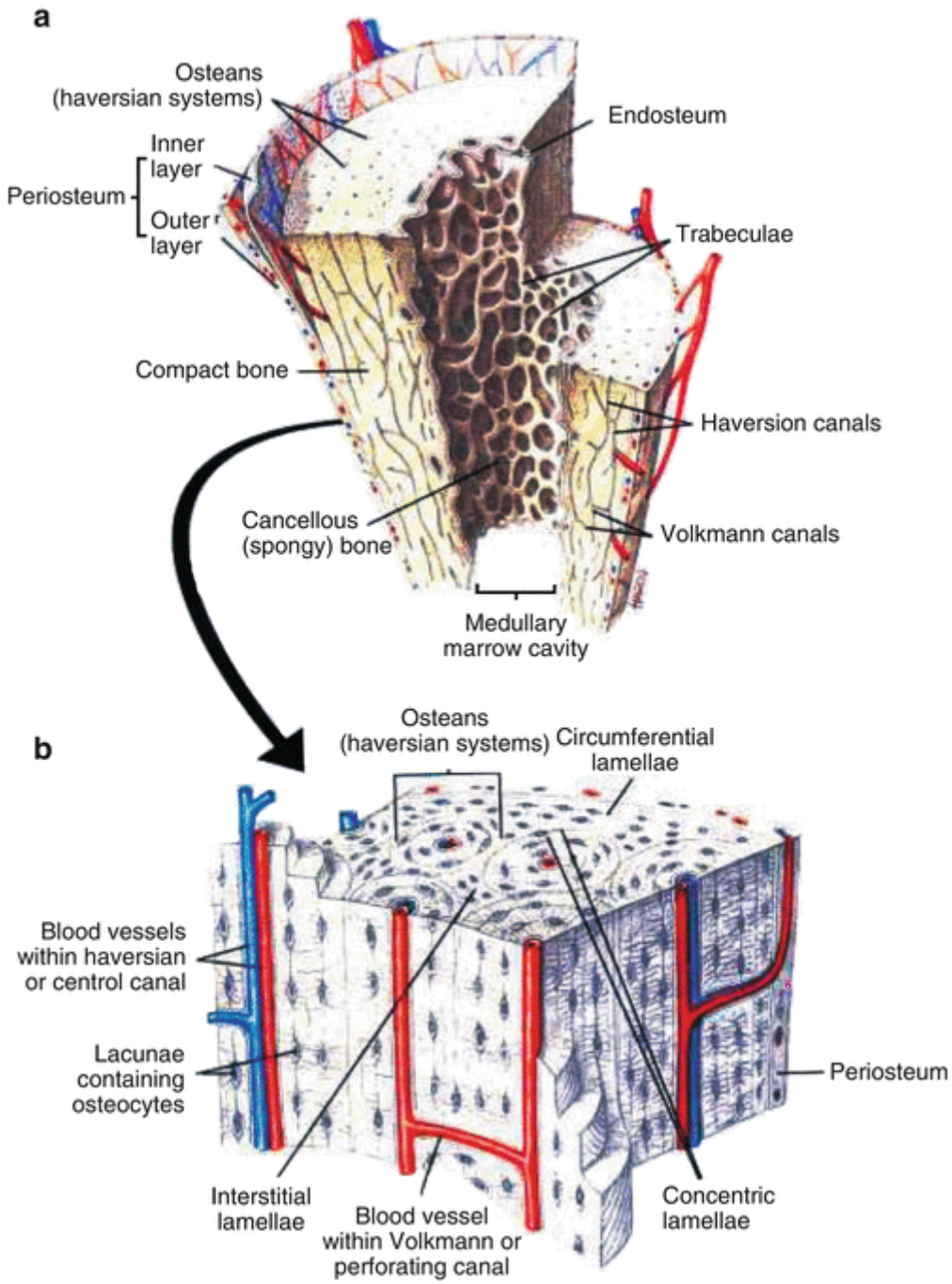


Figure 1-3. Haversian systems.
Image courtesy of Elgazzar, A. H. (2017). Basic Sciences of Bone and Joint Diseases. In *Orthopedic Nuclear Medicine* (pp. 1-36). Springer, Cham.

Table 1-1. Major cytokines, growth factors, non-collagenous proteins and their proposed roles.

Type	Proposed Function	Origin
Cytokines		
Tumor necrosis factor-alpha (TNF- IX)	Stimulates bone resorption, directly inhibits osteoblastic collagen synthesis,	Osteoblasts
Interluekin-1(IL-1)	Increases bone resorption	Osteoblasts, Mononuclear cells
Interleukin-6 (IL-6)	Exact role unknown	Osteoblasts
Growth Factors		
Fibroblast Growth Factor (FGF)	Local regulator of skeletal metabolism	Osteoblasts Stored in the extracellular matrix
Transforming Growth Factor Beta (TGF-B)	Enhance cells replication, collagen synthesis, and matrix formation	Initially platelets Multiple tissues including bone
Insulin like Growth Factor-1 (IGF-1)	Stimulate preostoblastic cell replication	Liver or skeletal tissue
Platelet-Derived Growth Factor (PDGF)	Increases bone collagen and matrix, stimulates bone resorption collagen degradation	Originally platelets, but suspect osteoblasts
Adhesion proteins		
Osteopontin	Bone resorption, regulate mineralization- potent inhibitor	Osteoblasts and osteoclasts
Fibronectin	Binds to integrin receptors located at cell surface Regulates mineralization by binding to other matrix proteins	Fibroblasts
Mineralized Proteins		
Osteocalcin	Metabolic regulation	Osteoblasts and osteocytes
Calcium Binding Proteins		
Osteonectin	"bone connector", strong affinity for collagen and mineral, bind calcium	Secreted by osteoblasts
Bone Sialoprotein	Binds to calcium and hydroxyapatite	Osteoblasts

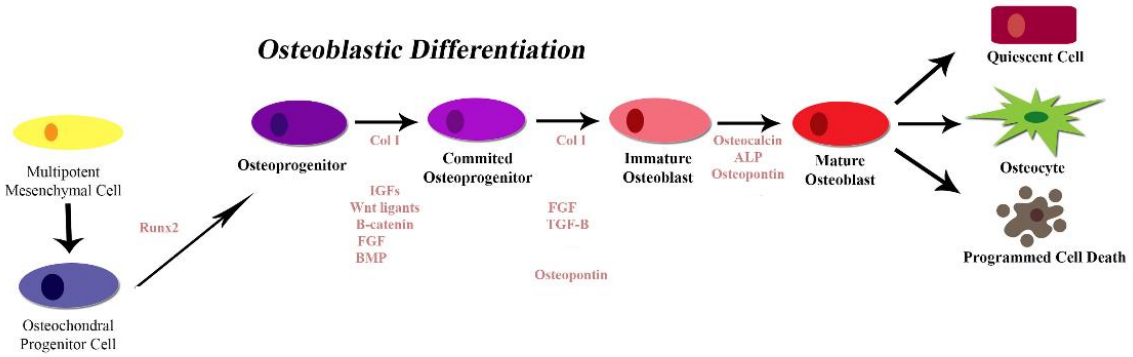


Figure 1-4. Commitment of a mesenchymal stem cell to an osteocyte with important proteins.
Commitment starts with the Runx2/Wnt/B-catenin pathway. The major protein in bone is collagen I (col I) with other non-collagenous proteins outlined in Table 1. Image modified and courtesy of McCawley, L. J., & Matrisian, L. M. (2001). Matrix metalloproteinases: they're not just for matrix anymore!. *Current opinion in cell biology*, *13*(5), 534-540.

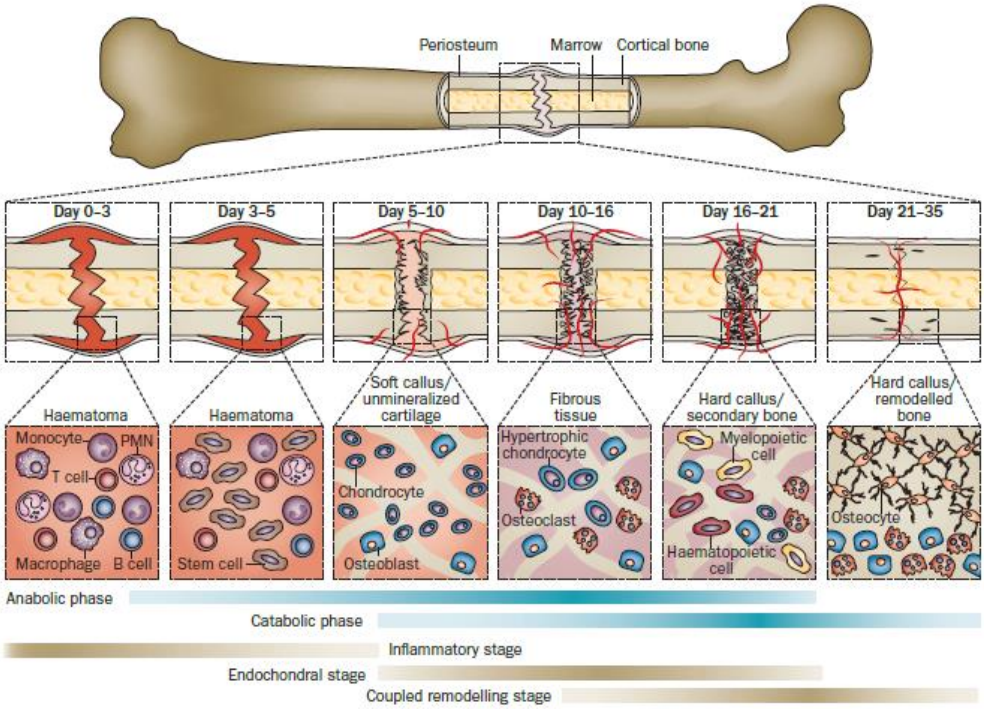


Figure 1-5. An accelerated overview of the four stages of bone healing (inflammation, soft callus formation, hard callus formation, remodeling) as seen in a mouse model of long bone fracture healing.
Image courtesy of Einhorn, T. A., & Gerstenfeld, L. C. (2015). Fracture healing: mechanisms and interventions. *Nature Reviews Rheumatology*, *11*(1), 45

CHAPTER 2.
USE OF A PRESSURE-SENSING WALKWAY SYSTEM FOR BIOMETRIC ASSESSMENT OF GOATS

A version of this chapter was originally published by Rebecca E. Rifkin:

Rifkin, R. E., Grzeskowiak, R. M., Mulon, P. Y., Adair, H. S., Biris, A. S., Dhar, M., & Anderson, D. E. (2019). Use of a pressure-sensing walkway system for biometric assessment of gait characteristics in goats. *PloS one*, *14*(10).

This article was published by PlosOne publications in the journal PlosOne in 2019. It has been reprinted with permission from Rifkin, R.E., Grzeskowiak, R.M., Mulon, P.Y., Adair, H.S., Biris, A.S., Dhar, M., & Anderson. D.E. Use of a pressure-sensing walkway system for biometric assessment of gait characteristics in goats. Plos one, 14 (10): doi:10.1371/journal.pone.0223771. Copyright 2019 PlosOne. Biometric gait assessment, statistical analysis, and all study design was performed at the University of Tennessee in Knoxville. As such this chapter will address all conclusions drawn from the data.

Abstract

The purpose of this study was to quantitatively assess gait characteristics and weight-bearing forces during ambulation in goats free of lameness using a pressure-sensing walkway as a biometric tool for stride, gait, and force analysis. Forty-six non-lame adult goats ranging in age from 5 to 6 years, mixed-breeds, and with a mean body weight of 52 ± 7.1 kgs were used. Goats were trained to walk over a pressure-sensing walkway. Data for analysis was collected on 2 different days, 3 days apart. On each day, 2 to 5 walking passes, in the same direction, were captured for each goat. Data from 2 valid passes meeting the criteria for consistent walking gait on each day were averaged then used for analysis. Analysis was performed, including the day-effect, for stride, gait, and force characteristics. Of the 46 goats enrolled in the study, complete data sets were achieved in 33 (72%) goats. Gait biometrics were similar among the assessment days; therefore, all data was pooled for the purpose of characterizing data for individual limb and biometric parameter comparisons at the individual goat level. Statistical analysis revealed that no difference within the paired limbs, and that there were significant differences between the front limbs and hind limbs. Maximum force and maximum peak pressure were significantly greater for the front limbs as compared with the hind limbs ($p < 0.001$). Based on the results, gait and force characteristics can be consistently measured in goats using a pressure-sensing walkway during a consistent walking gait. Goats apply greater force to the forelimbs during the weight-bearing phase of stride as compared with the hind limbs. The use of objective assessment tools is expected to improve the ability of researchers and clinicians to monitor changes in weight bearing and gait and will contribute to improved animal welfare.

Introduction

Goats are often chosen as a model for orthopedic research [1-4]. Advantages in the use of goats in research include ease of handling, ease of training, size, weight, and ambulatory characteristics relevant to translational research in humans [3, 4]. More detailed information concerning gait in goats is needed, especially when translation of data to implants and materials for use in people are needed, as goats have suitable metabolic and bone remodeling rates for translation to people [4]. Currently, subjective visual assessment of gait (Visual Lameness Score; VLS) is the standard of care in practice to assess lameness [5-12]. It is limited to use of a visual analog scoring, or numeric rating, with the gait of each animal being assigned a score [7]. There appears to be no validated standards for objective gait analysis in goats. Limitations associated with subjective gait analysis are numerous and include inter-observer variability, lack of a validated standard scoring system, and limitations associated with analysis of categorical data [8-12]. In other livestock species, such as cattle and horses, subjective visual assessment is shifting to objective assessment [13-16].

Objective lameness assessment currently relies on sensor technology, such as pressure sensing systems, force plates, accelerometers, and kinematic studies with 3D motion capture technology [16]. Devices used to monitor lameness are important tools that need to be precise and accurate [17]. Studies have shown that certain kinetic measurements may differ based on the device that is implemented, or even the method by which it is calibrated [18]. Weight bearing provides an important tool for assessing the functional use of the limbs. Most studies using objective gait assessment are aimed at gaining information related to lameness [14]. Lameness assessment research often is focused on the detection of severely lame animals, with less precision given to mild lameness [14]. Even minor dairy species, such as Mediterranean buffalo, are beginning to be looked at objectively for lameness, but problems arise with sensors that short, as continuous strides may be missed with a limited algorithm [19].

Difficulties associated with objective lameness technology become particularly relevant in orthopedic research, when new material or devices may rely on lameness assessment as an outcome parameter in terms of animal welfare [3, 4]. Many studies rely on subjective lameness scoring systems, only mention monitoring lameness post-operatively, and/or rarely report findings of lameness in study conclusions [20-22]. While several studies exist describing objective lameness outcomes in relation to orthopedic research, few are done from a basis of described normal variables available for that specific species [23, 24].

Advantages to pressure-sensing systems with walkways are that they are time efficient, can evaluate multiple sequential steps, and have the ability to evaluate the contralateral limbs within the same walking pass and in the same trial [18]. Although originally used in biped gait analysis, pressure-sensing mats have been used to study gait in multiple species, such as horses, cattle, turkeys, sheep, pigs, dogs, and cats [17, 18, 23-30]. However, few studies validate these measurements or describe normal biometric variables [17, 31]. In one study, normal intact Santa Ines sheep were evaluated using a pressure-sensitive walkway and a 3-camera kinematic system, which allowed for normal parameters to be described for varying age groups [31]. Literature describing pressure sensitive platforms for use in the biometric assessment of lameness has been described, but is lacking for goats initially free of lameness [32, 34]. Sheep and goats are important

models for orthopedic research and share many similarities [4]. Some aspects of gait analysis in sheep require more comprehensive assessment tools because of their flight zone and flocking behavior. These limitations can be addressed with training [4].

The purpose of this study was to quantitatively assess biometric variables of gait and associated forces during ambulation in goats free of lameness. We hypothesized that goats could be trained to walk across a pressure-sensing walkway to allow consistent recording of data for variables of stride, gait, and force. The objectives were to describe the characteristics associated with stride and weight-bearing force in goats free of lameness, thereby providing a baseline for future studies using a pressure-sensing mat investigating lameness. This information will not only benefit the veterinary community in providing a baseline for goats free of lameness, which may be applied to herd health lameness monitoring programs, but will provide a valuable set of gait parameters for goats as a reference in the design and conduction of orthopedic research where lameness is induced or is a concern.

Materials and Methods

Goats

All study procedures were approved by the University of Tennessee Animal Care and Use Committee (protocol number 2383). Forty-six mixed breed goats between five and six years old and weighing 52 ± 7.1 kgs (range 40-69 kgs) were purchased from a licensed, commercial vendor. Goats were a mixed breed population, including Boer, Spanish, Nubian, Saanen, Oberhasli, and hybrid goats. Goats were judged to be free of lameness based on a visual lameness score of 0 (normal movement) out of 4 [2]. Hooves and feet were inspected, and hooves were trimmed to ensure all goats had normal and consistent conditioned feet. Goats were housed in groups of five to six in small pens (15 ft^2 per animal) (National Research Council. *Guide for the care and use of laboratory animals*; National Academies Press, 2010). Flooring included a layer of wood shavings (2.5 to 5-cm thick) laid on top of rubber mats placed on top of a concrete floor in a conditioned housing facility for the duration of the study. They were fed a total mixed ration, provided access to hay as an environmental enrichment, and given access to automatic waterers to meet nutritional and metabolic requirements. Goats were weighed at study entry and exit to monitor nutrition and health.

Data Collection

After confirming that all goats entering the study were free of lameness (VLS score of 0), gait parameters were objectively assessed by evaluating measurements obtained from an automated, real-time pressure sensing system (Walkway Pressure Mapping System, Tekscan Inc, South Boston, MA). The sensor matrix was 87.1 cm long by 36.9 cm wide and had a sensor density of 1.4 sensors/cm^2. The mat was calibrated and equilibrated according to the manufacturer's instructions. Triggering was enabled so that recordings would start at the first contact, or a raw sum force of 200 kPa, and end at total of 400 recorded frames at a rate of 15 frames per second. An alleyway was assembled in order to create a fixed walkway for the goats. The pressure mat was placed in the midpoint of the alleyway and covered with a soft, rubber overlay to create a consistent

visual and tactile flooring with good footing for the testing area (**Fig 2-1**).[2] The width of the alleyway was made such that goats could move freely in a straight line, would be discouraged from turning around, and that each goat's footfalls would strike the sensitive area of the mat. Prior to initiation of the trial, goats were individually weighed using a digital scale. Goats were then fitted with a halter and led at a walking pace across the pressure-sensing mat, with an investigator sitting to the right of the mat adjacent to the constructed alleyway. The halter and lead were useful to encourage goats to pass through the walkway without stopping. During the study, no tension or pressure was applied to the halter to ensure that no changes in head movement or gait occurred.

Biometric assessment of gait was collected from the 2 best-fit recording in one direction, on each of 2 separate days (day 0 and 3). Each goat was walked across the mat up to 5 times (5 passes) until at least 2 valid walking passes were obtained. A pass was considered valid if the goat maintained a progressive walking gait, had a VLS of 0 during the pass, walked calmly through the alleyway without stopping or resisting walking forward, walked over the walkway without distraction, and if all four limbs had contact with the pressure sensing surface of the walkway. The data from the first two valid passes on each day were recorded and averaged for each goat, allowing for one set of data to be analyzed for each day.

Data was discarded during the data acquisition phase of the study if any goat hesitated, changed their gait or pace, or reacted to surroundings in a way that altered their gait. Acceptable behavior was limited to a subjectively assessed lameness score of 0, and walking in a forward manner without distraction from the investigator or hesitation from the halter and lead. Each pass was recorded with a digital video camera to record extremity strike and gait as the goat walked over the pressure sensor mat, and data from the mat sensor were transmitted to the system's computer software (Microsoft LifeCam Cinema, Microsoft Corporation, Redmond, WA). The frame rate of the video camera was adjusted to 15 frames per second to match the pressure-sensing mat. Once data was transmitted to the software it was then exported to Microsoft Excel, backed up, and stored within an external hard-drive (Microsoft Excel for Windows 10, Seagate Portable 1TB External Hard Drive USB 3.0, USA). Due to significant range in the mixed breeds of the goats (Boer, Spanish, Nubian, Saanen, Oberhasli, and true mixes) and various limb lengths, it was necessary to average two valid passes to obtain consecutive footfalls, allowing for a complete data set for one valid run per day. Data sets were included in statistical analysis if they were complete for all variables.

Gait Variables

Gait variables included the number of stance (or footfalls), gait time-front (sec), gait distance-front (cm), gait velocity-front (cm/sec), and cycles per minute. Stance and stride variables measured included stance time (sec), swing time (sec), stride time (sec), stride length (cm), stride velocity (cm/sec; **Table 2-1**). With goats that had long swing times, stride times, and/or stride lengths, multiple passes were required to obtain one

[2] All figures and tables for this chapter are presented in the appendix.

valid run; therefore, the first two valid passes that allowed a complete data set were used in the analysis.

Force Variables

Measurements of force variables included maximum force (Kg), maximum force normalized to body weight (%BW), impulse (Kg*sec), impulse normalized to body weight (%BW*sec), and maximum peak pressure (KPa). Maximum force (Kg) was the maximum force recorded during the stance phase of each extremity. Maximum force (%BW) was defined during the stance phase of the given extremity (normalized to the animal's body weight). When there were multiple stances within the same pass, the maximum force values for that extremity were averaged. Impulse (Kg*sec) was the average of all foot strikes for the given extremity. Impulse (%BW*sec) was the average impulse of all foot strikes for a given extremity and normalized to body weight. Finally, maximum peak pressure (kPa) was defined as the peak force per unit area for a given extremity. To our knowledge, this device has not been validated for mixed breed goats with a significant range of weights; we present descriptive data for this population.

Statistical Analysis

Descriptive statistics for each parameter were generated, including the mean, standard deviation, and minimum and maximum values (IBM SPSS 25, Armonk, NY). Each gait parameter was analyzed with a Shapiro Wilk test to evaluate for normality of distribution (p-value > 0.05). An appropriate parametric student t-test or nonparametric Wilcoxon rank sum was performed for each variable between days to evaluate for repeatability between days. A one-way ANOVA followed by Tukey's post-hoc test was performed to compare gait parameters between limbs. For variables that were not normally distributed, a one-way Kruskal-Wallis test followed by a pairwise comparison between limbs with a Dunn-Bonferroni correction to compare gait parameters was performed. A sample size estimate to detect the effect of time and extremity with 80% power was performed. For all statistical tests, a p-value of < 0.05 was considered significant.

Results

Out of 46 goats, 33 (72%) met the inclusion criterion for analysis. Goats readily walked through the alleyway and across the pressure-sensing mat system without difficulty. Thirteen goats were removed from statistical analysis because of having incomplete data sets (lack of 2 valid passes within a maximum of 5 attempts). Due to the range in stance time (sec), swing time (sec), stride time (sec), and stride length (cm), it was necessary to average two valid passes to obtain consecutive footfalls for a complete data set for each test day. After the repeatability assessment, data was then pooled. Pooled data for stance-stride variables were tabulated **(Tables 2-2 and 2-3**). Descriptive statistics for gait variables are reported as the means ± standard deviation and range (minimum, maximum) for 33 goats having complete datasets. The mean number of stances was 9.03±1.81 (6.00, 14.00). The gait-time front (sec) was 1.73±0.72 (0.51, 4.10), the gait distance-front (cm) was 132.38±13.92 (96.90, 153.00), and the gait velocity-front (cm/sec) was 92.64±36.30 (34.40, 279.60). The mean gait cycle time (sec) for 33 goats

was 1.00±0.25 (0.44, 2.00), while the mean cycles/minute was 64.67±15.62 (30.00, 139.00).

Data that were normally distributed included maximum force (%BW), maximum force (Kg), stride length (cm), and maximum peak force (KPa; $p > 0.05$). Of those parameters, maximum force (%BW), maximum force (Kg), and maximum peak force (KPa) were significantly different among the limbs ($p < 0.001$).There was no significant difference in stride length (cm) among the limbs ($p > 0.05$). As the gait parameters maximum force (%BW), maximum force (Kg), and maximum peak force (KPa) may be most associated with future orthopedic or animal welfare studies, they were selected for the sample size estimate analysis to detect the effect of time and extremity. Based on these variables, only 12 animals were needed to detect the effect of time and extremity.

When evaluating day 1 versus day 3, there were no significant differences for the variables maximum force (%BW), maximum force (Kg), impulse (%BW *sec), impulse (Kg*sec), or maximum peak pressure (KPa; $p > 0.05$) for any of the extremities. There was a day-effect for the variables stance time, stride time, stride length, and stride velocity. For the variable stance time (sec), there was a significant decrease in time for the majority of goats ($n = 21$, left front; $n = 23$, right front; $n = 23$, right hind) on day 3 as compared to day 1 ($p < 0.05$). For the variable stride time (sec), there was a significant decrease in time for the majority of goats ($n = 19$) on day 3 as compared to day 1 for the right hind limb ($p < 0.05$). For the variable stride length (cm) there was a significant difference for the left front and right front means with the left front being greater on day 3 versus day 1 and the right front mean being greater on day 3 versus day 1 (**Table 2-3**; $p < 0.05$). For the variable stride velocity (cm/sec) there was a significant difference for all extremities on day 1 versus day 3, with the means for the left front being greater on day 3, the means for the left hind being greater on day 3, the right front means being greater on day 3, and the right hind means being greater on day 3 ($p < 0.05$; **Table 2-4**). The mean stride length (cm) was greater on day 3 as compared with day 1 for the left front limb and right front limb ($p < 0.05$). The left hind and right hind limb means are reported with * as they were not significantly different between days. The mean stride velocity (cm/sec) was greater on day 3 as compared to day 1 for all extremities ($p < 0.05$).

Within paired limbs, there were no significant differences between the means of the left front and right front limbs, nor the left hind and right hind limbs, respectively ($p > 0.05$). Significant differences were found for maximum force (Kg) between the limbs. There was a significant difference between the left front and hind limbs with the left front mean being greater than the left hind and right hind limb ($p < 0.001$). There was a significant difference between the right front limb and the hind limbs with the right front limb being greater than the left hind and right hind limb ($p < 0.001$; **Fig 2-2B**). Significant differences were found for maximum force (normalized to %BW; $p < 0.001$) between the limbs. There was a significant difference between the left front and left hind and the hind limbs with the left front mean being greater than the left hind and right hind limb ($p < 0.001$). There was a significant difference between the right front and the hind limbs' weight, the right front mean being greater than the left hind and right hind limb ($p < 0.001$; **Fig 2-2A**). A significant difference was found between the limbs for maximum peak pressure (kPa). The left front limb was significantly greater than the left hind and right hind limb ($p<0.001$). The right front limb was greater than the left hind and right hind limb ($p < 0.001$; **Fig 2-2C**).

No significant differences were found between the extremities for the gait parameters stance time (sec), swing time (sec), stride time (sec), and stride velocity (cm/sec; $p > 0.05$). Significant differences were found among between the extremities for the gait parameters impulse (%BW*sec) and impulse (kg*sec; $p < 0.001$). Impulse was significantly less for the paired hind limbs compared with the paired forelimbs ($p < 0.001$; **Fig 2-3B**). The impulse normalized to percent body weight was significantly less for the paired hind limbs compared with the paired forelimbs ($p < 0.001$; **Fig 2-3A**).

Discussion

In the present study, we were able to quantitatively assess biometric variables of gait and associated forces during ambulation in goats free of lameness. We found that goats could be quickly trained to walk across a pressure-sensing walkway, allowing consistent recordings of data for variables of stride, gait, and force. Based on the results of this study, we found that data derived for stride variables is more susceptible to variations when assessments are done at multiple time points. Also, front limb and rear limb assessments should be evaluated separately when using force variables to serially evaluate goat ambulation. We were able to describe the characteristics associated with stride and weight-bearing forces in goats free of lameness. Thus, the consequences of this study are important in that they provide a baseline for future studies using a pressure-sensing mat investigating lameness.

Detailed knowledge of gait characteristics in goats may benefit the veterinary community in that lameness evaluation of small ruminants may now be more easily done at an objective level, allowing this technology to potentially be used in herd health situations. Our results suggest that biometric pressure sensing may be a useful tool for gait assessment in goats regardless of breed. Using a pressure sensing system, we were able to quantitatively assess gait and biometric forces during ambulation in goats free of lameness using a pressure-sensing mat as a biometric tool for gait analysis. It is important to note that baseline clinical health examinations were not included as confounding variables in this study. Due to our interests in orthopedic research, which typically do not include infirmed, immature, or geriatric animals, we limited our population to young, skeletally mature goats free of lameness [1]. It was assumed that this population included mainly healthy goats. Currently, we do not have baseline values for goats that are clinically evaluated to be ill or outside the skeletal range we have evaluated. Future studies would need to include a correlation between visual lameness scores and alterations from the baseline values reported here

Pressure sensing systems evaluate ground reaction forces where pressure causes activation of the sensors [34]. Quantitative measurements may be useful to determine functional weight bearing and to assess changes in acute weight bearing or for serial evaluation of pain [35] The number of walking passes needed to obtain valid data sets may vary; we were able to obtain data using the pressure sensing walkway set-up within an alleyway with relatively few repeated walking trials [36]. We were successful in being able to collect complete data sets with relatively few passes in the majority of goats tested. The pressure-sensing mat was useful to measure functional gait characteristics even in the face of a nonhomogeneous population. With minor variations, the biometric data acquired was useful for statistical analysis within walking trials and between trial days allowing for pooled analysis. The walkway system provided a means of collecting

valuable data with limited training while using a more realistic animal model population. Additionally, when weight bearing is used as an outcome variable, this accurate quantitative tool may help in power calculations of treatment group size when designing animal experiments.

Some caution may be warranted when evaluating the parameters stance time (sec), stride time (sec), stride length (cm), and stride velocity (cm/sec) between days, as these variables were not always repeatable between days among the extremities. This is particularly true for stride velocity (cm/sec), which was not repeatable for any limb between days. A solution to this in the future would be to standardize for stride velocity (cm/sec) as has been reported for other walkway assessment tools [31]. As we used a nonhomogeneous population, this standard was not met. A previously published study in which dogs of various sizes were allowed to walk with their preferred velocity, reliable gait assessment was obtained, indicating that perhaps standard velocity may not be necessary when assessing gait parameters for lameness [33]. Despite this limitation, we were able to obtain valid results that should be acceptable as quantitative data for gait analysis even when performed serially over time. One potential confounding variable is that the investigator was placed on the right side of the mat. Goats tended to walk closer to the left side of the mat, opposite from the data acquisition station. Similar to sheep, goats are prey species animals and tend to shy away from human contact [5, 11, 36]. This contributed to 13 goats being eliminated from the data set, as their behavior was unacceptable in that they were unable to walk forward without distraction or hesitation. This is consistent with dogs being walked on a leash and leash side influencing gait symmetry [33]. In these goats, multiple passes were discounted because of walking more quickly than desired or stopping halfway across the pressure mat. Additional training, such as walking in either direction, acclimatization, or a different alleyway system for acquiring ambulatory data, may help normalize this data. Despite goats being removed from study, significant results were able to be retained, similar to a pressure sensing study with turkeys [27]. While not all birds were available at all time points, significant results were able to be obtained indicating that data may be pooled for herd populations and gait parameters may be evaluated over time [27]. Finally, goats have relatively small hooves; therefore, using a pressure mat with a greater sensor density may improve precision and accuracy of weight bearing data.

Similar to other studies, we found that maximum force (Kg), maximum force normalized to body weight (%BW), and maximum peak pressure (kPa) was greater in the forelimbs than the hind limbs when measured using a pressure-sensitive walkway [31]. This is valuable for orthopedic research when using small ruminant models to establish methods for objective, quantitative assessment of weight bearing and gait [17, 31]. Providing a tool to supplement subjective VLS evaluations with objective data will allow more robust monitoring and assessment of gait in research subjects. The importance of providing an objective standard for lameness assessment in orthopedic models cannot be understated. Measuring weight bearing in fracture models is an expected standard of care; however, there remains a deficiency of literature on the topic [37]. Current animal use protocols, in general, use subjective measurements because of ease of application and lack of access to objective alternatives [38-41]. Moving towards nonbiased objective data is expected to benefit animal welfare and improve the quality of quantitative data in the use of small ruminants as models for orthopedic disease.

No validated visual or objective lameness assessment system exists for goats. Categorical assessment tools are subject to bias interpretation and must be analyzed using statistical tests for categorical data, making them less sensitive at identifying differences [5-12]. Difficulties with subjective data include inter-observer differences, limitations of categorical data, and lack of a standard scoring system for the species. Inter-observer differences have long been noted in lameness research in horses [41]. Objective assessment tools offer the possibility of validating subjective tools for use in research, which is currently limiting [41]. Analysis of categorical data, such as VLS scores, are challenging even after transformation to proportional (categorical) data and can yield spurious results [41]. Categorical data, therefore, requires different methods for analysis that may be less sensitive than objective, continuous data obtained with tools, such as pressure mat sensing systems [42]. Variability in subjective scoring systems, comparing lameness scores across any type of research model of lameness, becomes inherently problematic at a time where there is a call for large animal models to become more standardized [43, 44]. Other alternatives include the use of accelerometers to measure activity and define 3D gait characteristics, such as height of excursion of the limb/foot. These technologies are less adaptable to real-time analysis and assessment [37].

In the present study, we quantitatively assessed gait and biometric forces during ambulation in goats subjectively free of lameness using a pressure-sensing mat as a biometric tool for gait analysis. The pressure-sensing mat is an objective tool, free of inter-observer differences, and easy-to use. In an era where scientific procedures involving the use of animals is at an all-time low, the importance of providing stress free, accurate results when doing potentially painful procedures cannot be overstated [45]

References

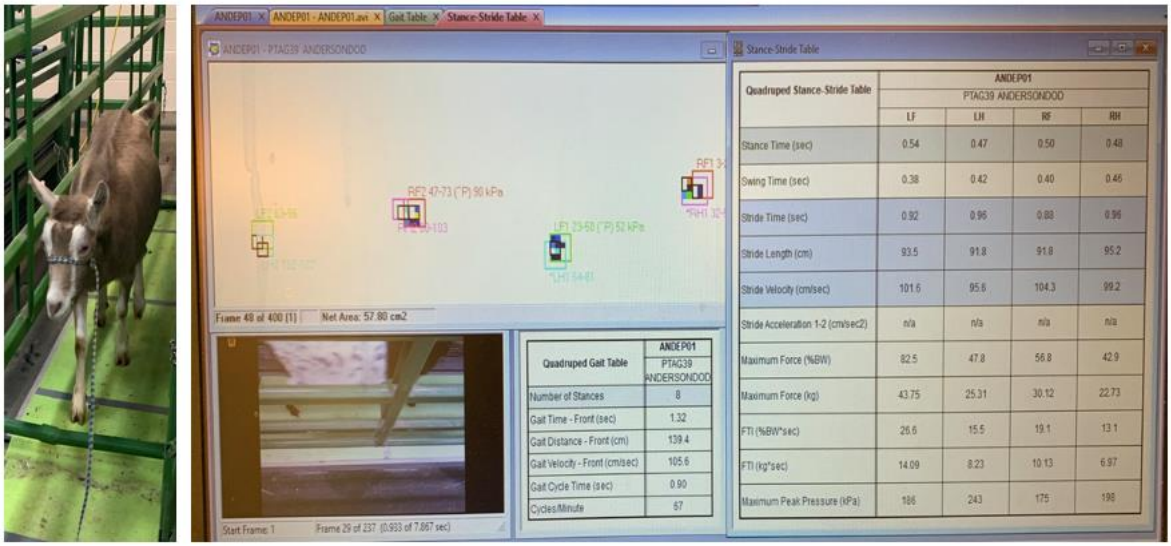
1. Harvey EJ, Giannoudis PV, Martineau PA, Lansdowne JL, Dimitriou R, Moriarty TF, et al. Preclinical animal models in trauma research. J Orthop Trauma. 2011;25(8):488-493. doi: 10.1097/BOT.0b013e3182251421.
2. Reichert JC, Saifzadeh S, Wullschleger ME, Epari DR, Schütz MA, Duda GN, et al. The challenge of establishing preclinical models for segmental bone defect research. Biomaterials. 2009;30(12):2149-2163. doi: 10.1016/j.biomaterials.2008.12.050.
3. Pearce AI, Richards RG, Milz S, Schneider E, Pearce SG. Animal models for implant biomaterial research in bone: a review. Eur Cell Mater. 2007;13(1):1-10.
4. Fulton LK, Clarke MS, Farris Jr HE. The goat as a model for biomedical research and teaching. Ilar J. 1994;1;36(2):21-29.
5. Muri K, Stubsjøen SM, Valle PS. Development and testing of an on-farm welfare assessment protocol for dairy goats. Anim Welfare. 2013;22(3):385-400.
6. Browning Jr R, Leite-Browning ML, Byars Jr M. Reproductive and health traits among Boer, Kiko, and Spanish meat goat does under humid, subtropical pasture conditions of the southeastern United States. J Anim Sci. 2011;89(3):648-660. doi: 10.2527/jas.2010-2930.
7. Deeming LE, Beausoleil NJ, Stafford KJ, Webster JR, Zobel G. The development of a reliable 5-point gait scoring system for use in dairy goats. J Dairy Sci. 2018;101(5):4491-4497. doi: 10.3168/jds.2017-13950.
8. Gigliuto C, De Gregori M, Malafoglia V, Raffaeli W, Compagnone C, Visai L, et al. Pain assessment in animal models: do we need further studies?. J Pain Res. 2014;7:227-236. doi: 10.2147/JPR.S59161.
9. Hill NP, Murphy PE, Nelson AJ, Mouttotou N, Green LE, Morgan KL. Lameness and foot lesions in adult British dairy goats. Vet Rec. 1997;141(16):412-416.
10. Olechnowicz J, Jaśkowski JM. Lameness in small ruminants. Med Weter. 2011;67(11):715-719.
11. Vieira A, Oliveira MD, Nunes T, Stilwell G. Making the case for developing alternative lameness scoring systems for dairy goats. Appl Anim Behav Sci. 2015;171:94-100.
12. Anzuino K, Bell NJ, Bazeley KJ, Nicol CJ. Assessment of welfare on 24 commercial UK dairy goat farms based on direct observations. Vet Rec. 2010;167(20):774-780. doi: 10.1136/vr.c5892.
13. Flower FC, Sanderson DJ, Weary DM. Hoof pathologies influence kinematic measures of dairy cow gait. J Dairy Sci. 2005;88(9):3166-3173. doi: 10.3168/jds.S0022-0302(05)73000-9.
14. Flower FC, Weary DM. Gait assessment in dairy cattle. Animal. 2009;3(1):87-95.
15. Keegan KG, Kramer J, Yonezawa Y, Maki H, Pai PF, Dent EV, et al. Assessment of repeatability of a wireless, inertial sensor–based lameness evaluation system for horses. Am J Vet Res. 2011;72(9):1156-1163. doi: 10.2460/ajvr.72.9.1156.

16. Van Nuffel A, Zwertvaegher I, Van Weyenberg S, Pastell M, Thorup V, Bahr C, et al. Lameness Detection in Dairy Cows: Part 2. Use of Sensors to Automatically Register Changes in Locomotion or Behavior. Animals. 2015;5(3):861-885. doi: 10.3390/ani5030388.
17. Kim J, Breur GJ. Temporospatial and kinetic characteristics of sheep walking on a pressure sensing walkway. Can J Vet Res. 2008;72(1):50-55.
18. Oosterlinck M, Pille F, Sonneveld DC, Oomen AM, Gasthuys F, Back W. Contribution of dynamic calibration to the measurement accuracy of a pressure plate system throughout the stance phase in sound horses. Vet J. 2012;193(2):471-474. doi: 10.1016/j.tvjl.2012.01.029.
19. D'Andrea L, Guccione J, Alsaaod M, Deiss R, Di Loria A, Steiner A, et al. Validation of a pedometer algorithm as a tool for evaluation of locomotor behaviour in dairy Mediterranean buffalo. J Dairy Res. 2017;84(4):391-394. doi: 10.1017/S0022029917000668.
20. Black LL, Gaynor J, Gahring D, Adams C, Aron D, Harman S, et al. Effect of adipose-derived mesenchymal stem and regenerative cells on lameness in dogs with chronic osteoarthritis of the coxofemoral joints: a randomized, double-blinded, multicenter controlled trial. Vet Ther. 2007;8(4):272-284.
21. Hill RJ, Mason HM, Yeip G, Merchant SS, Olsen AL, Stott RD, et al. The Influence of Oblique Angle Forced Exercise in Surgically Destabilized Stifle Joints Is Synergistic with Bone, but Antagonistic with Cartilage in an Ovine Model of Osteoarthritis. Arthritis. 2017;2017:7481619. doi: 10.1155/2017/7481619.
22. Easley J, Puttlitz CM, Seim 3rd H, Ramo N, Abjornson C, Cammisa Jr FP, et al. Biomechanical and histologic assessment of a novel screw retention technology in an ovine lumbar fusion model. Spine J. 2018;18(12):2302-2315. doi: 10.1016/j.spinee.2018.07.021.
23. Meijer E, Bertholle CP, Oosterlinck M, van der Staay FJ, Back W, van Nes A. Pressure mat analysis of the longitudinal development of pig locomotion in growing pigs after weaning. BMC Vet Res. 2014;10(1):37. doi: 10.1186/1746-6148-10-37.
24. Meijer E, Oosterlinck M, van Nes A, Back W, van der Staay FJ. Pressure mat analysis of naturally occurring lameness in young pigs after weaning. BMC Vet Res. 2014 Dec;10(1):193. doi: 10.1186/s12917-014-0193-8.
25. Zammit GV, Menz HB, Munteanu SE. Reliability of the TekScan MatScan® system for the measurement of plantar forces and pressures during barefoot level walking in healthy adults. J Foot Ankle Res. 2010;3(1):11. doi: 10.1186/1757-1146-3-11.
26. Wheeler CA, White BJ, Anderson DE, Amrine DE, Larson RL. Assessment of biometric tools for quantitative gait analysis in Holstein calves. Am J Vet Res. 2013;74(11):1443-1449. doi: 10.2460/ajvr.74.11.1443.

27. Kremer JA, Robison CI, Karcher DM. Growth Dependent Changes in Pressure Sensing Walkway Data for Turkeys. Front Vet Sci. 2018;5:241. doi: 10.3389/fvets.2018.00241.
28. Kim J, Kazmierczak KA, Breur GJ. Comparison of temporospatial and kinetic variables of walking in small and large dogs on a pressure-sensing walkway. Am J Vet Res. 2011;72(9):1171-1177. doi: 10.2460/ajvr.72.9.1171.
29. Light VA, Steiss JE, Montgomery RD, Rumph PF, Wright JC. Temporal-spatial gait analysis by use of a portable walkway system in healthy Labrador Retrievers at a walk. Am J Vet Res. 2010;71(9):997-1002. doi: 10.2460/ajvr.71.9.997.
30. Verdugo MR, Rahal SC, Agostinho FS, Govoni VM, Mamprim MJ, Monteiro FO. Kinetic and temporospatial parameters in male and female cats walking over a pressure sensing walkway. BMC Vet Res. 2013;9(1):129. doi: 10.1186/1746-6148-9-129.
31. Agostinho FS, Rahal SC, Araújo FA, Conceição RT, Hussni CA, El-Warrak AO, et al. Gait analysis in clinically healthy sheep from three different age groups using a pressure-sensitive walkway. BMC Vet Res. 2012;8(1):87. doi: 10.1186/1746-6148-8-87.
32. Lequang T, Maitre P, Roger T, Viguier E. Is a pressure walkway system able to highlight a lameness in dog?. In6th World Congress of Biomechanics (WCB 2010). August 1-6, 2010 Singapore 2010 (pp. 190-193). Springer, Berlin, Heidelberg.
33. Fahie M, Cortez J, Ledesma M, Su Y. Pressure mat analysis of walk and trot gait characteristics in 66 normal small, medium, large and giant breed dogs. Front Vet Sci. 2018;5:256. doi: 10.3389/fvets.2018.00256.
34. Whittle MS. Gait analysis: an introduction. Edinburgh: Elsevier; 2007. pp. 47-193.
35. Martini L, Lorenzini RN, Cinotti S, Fini M, Giavaresi G, Giardino R. Evaluation of pain and stress levels of animals used in experimental research. J Surg Res. 2000;88(2):114-119. doi: 10.1006/jsre.1999.5789.
36. Agostinho FS, Rahal SC, Geraldo B, Justolin PL, Teixeira CR, Lins FL, et al. Influence of calibration protocols for a pressure-sensing walkway on kinetic and temporospatial parameters. Vet Comp Orthop Traumatol. 2015;28(1):25-29. doi: 10.3415/VCOT-14-05-0081.
37. Aranzulla PJ, Muckle DS, Cunningham JL. A portable monitoring system for measuring weight-bearing during tibial fracture healing. Med Eng Phys. 1998;20(7):543-548.
38. Fitzpatrick J, Scott M, Nolan A. Assessment of pain and welfare in sheep. Small Ruminant Res. 2006;62:55-61. doi: 10.1016/j.smallrumres.2005.07.028.
39. Stasiak KL, Maul DO, French E, Hellyer PW, Vandewoude S. Species-specific assessment of pain in laboratory animals. Contemp Top Lab Anim Sci. 2003;42(4):13-20.

40. Martini L, Fini M, Giavaresi G, Giardino R. Sheep model in orthopedic research: a literature review. Compar Med. 2001;51(4):292-299.
41. Keegan KG, Dent EV, Wilson DA, Janicek J, Kramer J, Lacarrubba A, et al. Repeatability of subjective evaluation of lameness in horses. Equine Vet J. 2010;42(2):92-97. doi: 10.2746/042516409X479568.
42. Barendregt JJ, Veerman JL. Categorical versus continuous risk factors and the calculation of potential impact fractions. J Epidemiol Community Health. 2010;64(3):209-212. doi: 10.1136/jech.2009.090274.
43. Jaeger TF. Categorical data analysis: Away from ANOVAs (transformation or not) and towards logit mixed models. J Mem Lang. 2008;59(4):434-446. doi: 10.1016/j.jml.2007.11.007.
44. Sah RL, Ratcliffe A. Translational models for musculoskeletal tissue engineering and regenerative medicine. Tissue Eng Part B Rev. 2010;16(1):1-3. doi: 10.1089/ten.TEB.2009.0726.
45. Annual Statistics of Scientific Procedures on Living Animals Great Britain 2017: Presented to Parliament pursuant to section 21(7) and 21A(1) of the Animals (Scientific Procedures) Act 1986. National Statistics. 2018. Available from: https://assets.publishing.service.gov.uk/government/uploads/system/uploads/attachment_data/file/724611/annual-statistics-scientific-procedures-living-animals-2017.pdf

Appendices



(A) (B)

Figure 2-1. Examples of halter-lead training and sample gait analysis.
(A) Pressure-sensing walkway placed in an alleyway system with soft mats and loose halter and lead for training. (B) Example of gait analysis with goat walking across pressure- sensing matrix placed in the alleyway system in the lower left-hand corner. The video recording with strike boxes is present in the upper left-hand corner, the stride stable is visible on the right, and the gait table is visible in the lower middle.

Table 2-1. Working definitions used for gait variables.

Gait Variable	**Definition**
Number of stances	The total number of stances (footfalls) taken by the animal.
Gait time-front (sec)	The time of first contact of the given front extremity stance to the time of first contact of the last given extremity stance as registered on the sensor.
Gait distance-front (cm), or length unit,	The gait distance measured along the line of progression, from posterior of the given front extremity stance to posterior of the last given extremity front stance.
Gait velocity-front (cm/sec)	The gait distance divided by the gait time.
Gait cycle time (sec)	Began with the first contact time of the given front extremity fall to be valid on the sensor. Time was measured to the first contact of the next instance of that given extremity striking the sensor.
Cycles per minute	The number of complete gait cycles per minute, or gait cycle time divided by sixty.
Stand-Stride Variable	**Definition**
Stance Time (sec)	The weight-bearing period, was defined as the time from first contact to last contact of a given extremity in seconds.
Swing Time (sec),	The non-weight bearing period, was defined as the elapsed time between the last contact of a preceding and the first contact of the next of two consecutive footfalls of a given extremity. When there were no consecutive footfalls, no data was recorded.
Stride Time (sec)	The elapsed time between the first contacts of two consecutive footfalls of a given extremity. If there were no consecutive footfalls, no data was recorded. If there were multiple strides within the same pass, times were averaged.
Stride Length (cm)	The distance measured parallel to the line of progression between the posterior heel points of two consecutive footfalls of a given extremity. When there were multiple strides, the lengths were averaged.
Stride Velocity (cm/sec)	The stride length divided by the stride time for the given extremity. When there were multiple strides, the velocities were averaged.

Table 2-2. Descriptive statistics for the stance gait parameters.
Results are displayed as mean ± standard deviation (SD) followed by a range (minimum, maximum).

Extremity (N=33)	**Stance Time (sec)**	**Swing Time (sec)**	**Stride Time (sec)**	**Stride Length (cm)**	**Stride Velocity (cm/sec)**
Limb	Mean ± SD (min., max.)	Mean ± SD (min.,max.)	Mean ± SD (min.,max.)	Mean ± SD (min., max.)	Mean ± SD (min., max.)
Left Front	0.68±0.23 (0.20, 1.23)	0.37±0.14 (0.17, 0.98)	1.00±0.26 (0.30, 2.05)	81.95±14.60 (45.50, 111.40)	90.13±40.63 (34.40, 334.30)
Left Hind	0.67±0.25 (0.28, 1.49)	0.36±0.17 (0.09, 1.19)	1.03±0.30 (0.43, 1.87)	77.23±20.51 (18.70, 122.40)	85.20±41.93 (15.70, 294.50)
Right Front	0.66±0.23 (0.25, 1.48)	0.37±0.12 (0.21, 0.85)	1.02±0.28 (0.48, 1.90)	83.82±14.41 (57.80, 119.00)	92.30±35.25 (35.20, 247.90)
Right Hind	0.68±0.27 (0.28, 1.81)	0.35±0.12 (0.13, 0.82)	1.00±0.24 (0.50, 1.61)	78.17±17.86 (32.90, 114.80)	84.96±33.17 (24.70, 218.90)

Table 2-3. Descriptive statistics for the stride gait parameters.
Results are displayed as mean ± standard deviation (SD) followed by a range (minimum, maximum).

Extremity (N=33)	**Maximum Force (%BW)**	**Maximum Force (Kg)**	**Impulse (%BW*sec)**	**Impulse (kg*sec)**	**Maximum Peak Pressure (KPa)**
Limb	Mean ± SD (min., max.)	Mean ± SD (min., max.)	Mean ± SD (min., max.)	Mean ± SD (min., max.)	Mean ± SD (min., max.)
Left Front	46.89±10.92 (24.80, 71.70)	24.38±5.22 (10.18, 35.86)	22.97±8.82 (9.20, 57.90)	12.23±5.09 (3.75, 28.94)	109.44±25.28 (42.00, 212.00)
Left Hind	34.61±7.58 (17.70, 50.50)	18.01±4.56 (7.26, 28.29)	16.30±7.02 (5.80, 39.00)	8.64±4.25 (2.39, 20.53)	92.55±20.49 (37.00, 144.00)
Right Front	47.21±9.10 (27.50, 65.10)	24.49±4.68 (11.88, 35.14)	22.89±8.14 (7.30, 47.70)	11.87±4.57 (3.66, 27.71)	107.97±23.05 (49.00, 176.00)
Right Hind	35.98±8.77 (20.50, 54.40)	18.89±4.76 (8.39, 34.77)	16.92±6.23 (6.6, 35.70)	9.07±3.84 (2.73, 18.57)	92.89±22.53 (39.00, 157.00)

Table 2-4.Student's t-test evaluating day 1 versus day 3.

Extremity (N=33)	**LF**			**RF**			**LH**			**RH**		
Runs	Day 1	Day 3	Mean +/- SD	Day 1	Day 3	Mean +/- SD	Day 1	Day 3	Mean +/- SD	Day 1	Day 3	Mean +/- SD
Stride Length (cm)	78.07	85.83	7.76 +/-	78.82	88.81	9.99 +/-	75.97	78.48	2.51 +/- *	74.58	81.75	7.17 +/-*
Stride Velocity (cm/sec)	79.91	100.35	20.44+/-	81.34	103.25	21.91 +/-	75.79	94.62	18.83 +/-	74.72	95.21	20.48 +/-

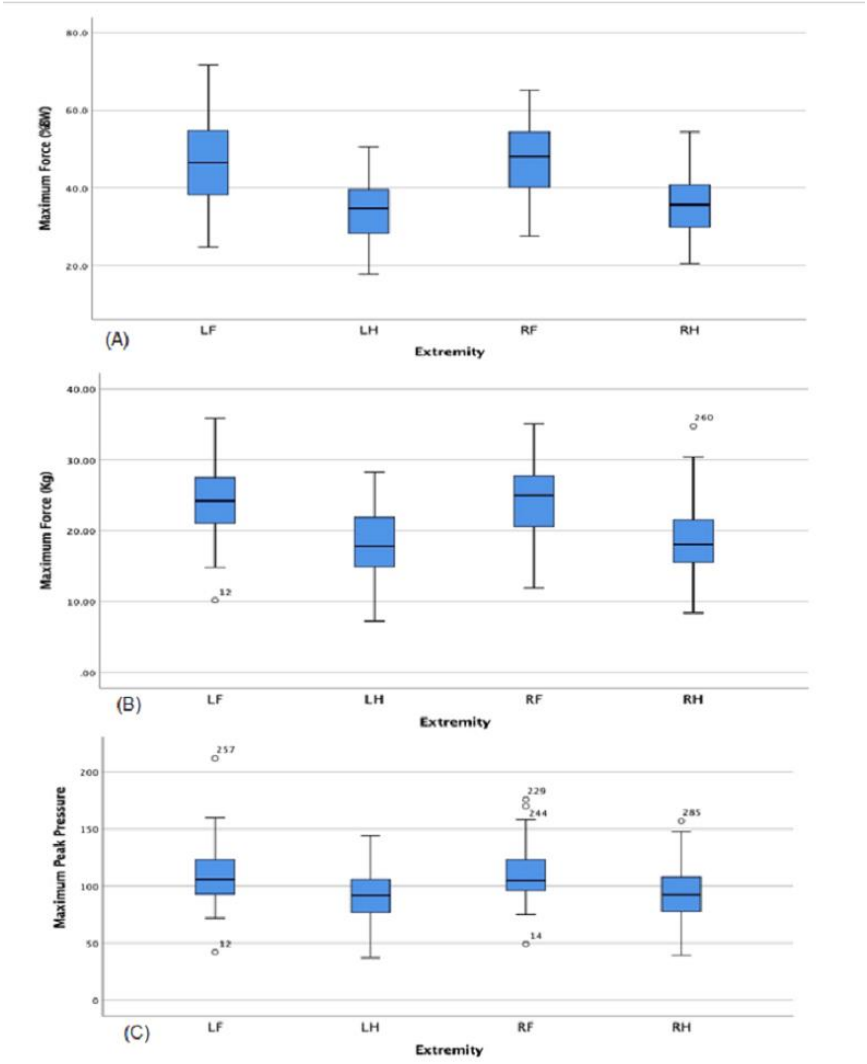


Figure 2-2. Box plots for Maximum Force (%BW), Maximum Force (Kg), and Maximum Peak Pressure (KPa).
The line in the middle of each box represents the median value for each extremity for each variable. Outliers are represented as circles. (A) Maximum force (%BW) shows that the paired left front and right front means are greater than the left hind and right hind means ($p < 0.001$). (B) Maximum force (Kg) shows evidence that paired left front and right front means are again greater than paired left hind and right hind means($p < 0.001$). Finally, in panel (C), Maximum Peak Pressure (kPa) is shown to be significantly different among the extremities with the paired forelimbs being greater than the paired hindlimbs ($p < 0.001$).

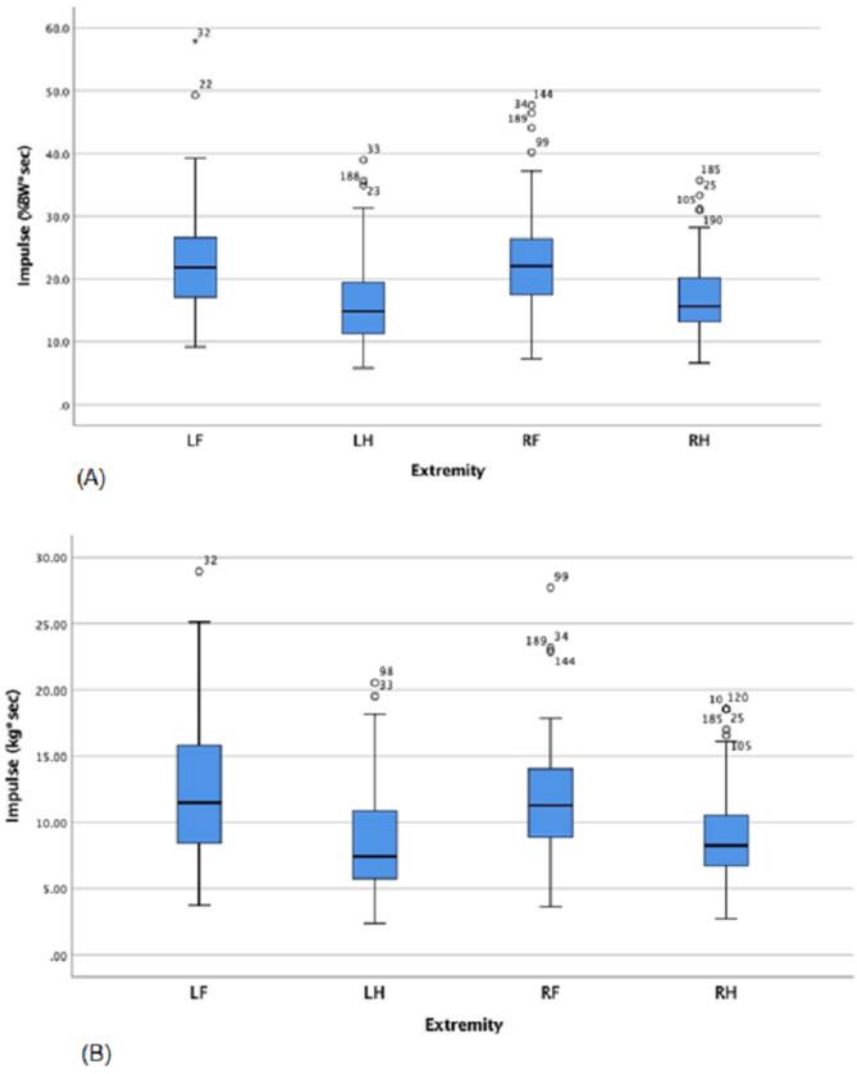


Figure 2-3. Box plots for Impulse (%BW*sec) and Impulse (Kg*sec).
The line represents the median value for each extremity for each variable. Upper and lower quartile ranges are shown and the entire range is represented by lines (whiskers) with outliers being represented as circles either above or below the whiskers. (A) Impulse (%BW*sec) is significantly greater for the paired forelimbs than the paired hind limbs ($p < 0.001$). (B) Impulse (kg*sec) is significantly greater for the paired forelimbs than the paired hind limbs ($p < 0.001$).

CHAPTER 3.
ASSESSMENT OF OSSEOINTEGRATION OF A NOVEL SYNTHETIC BONE SCAFFOLD IN A TIBIA SEGMENTAL DEFECT MODEL

Abstract

Treatment of debilitating long bone fractures have yet to find a suitable synthetic scaffold replacement to the gold standard bone autograft. In this study, the long term ability of a multi-layered polyurethane-nanohydroxyapatite-decellularized (nHA/PU/DBP) bone particle scaffold to repair long bone ostectomy defects is investigated in a large animal model. Data presented is in a clinically relevant large animal bone healing model over a 12 month period of time. Based on radiographic, computed tomographic, and load-to-failure analysis, all treatment groups healed over time. Dual energy x-ray absorptiometry showed greater bone mineral density for goats treated with scaffold and scaffold plus bone morphogenetic protein-2 (BMP-2) groups. Histomorphometric analysis showed greater osteoid formation for scaffold and BMP-2 goats, while mineralization and osteoclast numbers were consistent with bone remodeling over time. Low morbidity and mortality associated with the preclinical large animal model presented here show the potential for this model to become standardized for ostectomy gap healing. The use of a nHA/PU/DBP scaffold with the addition of BMP-2 showed potential for treatment of patients with severe long bone defects.

Introduction

The use of regenerative therapies for human musculoskeletal defect injuries is on the verge of becoming standard practice. [1] Traditionally, catastrophic fractures have required the use of bone grafts when a decision has been made to salvage a limb [2, 3]. The gold standard for bone grafting materials has been the autograft (bone taken from the patient's own body) or the allograft (cadaveric bone from a bone bank) [4, 5]. The procedure is not without complication. Approximately 30-60% of grafting procedures result in one or more complications, ranging from infection to incomplete integration and donor site pain [6]. In humans, the incidence of non-union fractures is approximately 5-10% [7]. The consensus for the definition of delayed healing or fracture non-union is inconsistent and subjective [8]. Musculoskeletal injuries have been reported to compromise approximately 50% of all combat wounds and are becoming an orthopedic burden of disease highlighting the need for approval of new regenerative therapies that will lower the incidence of these costly injuries [9-11].

Development of a wide variety of synthetic materials has been undertaken in an effort to improve healing of debilitating factures [4]. An ideal regenerative material would be both osteo-inductive (provide a biologic stimulus for cells to differentiate into mature osteoblasts) and osteo-conductive (promote bone apposition or function as a receptive scaffold to enhance bone formation) [4]. Bio-ceramics such as calcium sulphate, tricalcium phosphate and hydroxyapatite are early products developed for use as synthetic grafting materials with extensive history of safety data [4, 5]. The combination of decellularized bone particles in combined with nano-hydroxyapatite impregnated polymer has been shown to be cyto-compatible and causes a substantial increase in osteoblast proliferation in vitro [12]. To date, an effective material to promote bone healing in large defects has yet to be constructed and in- vivo studies, especially in large animal preclinical models are lacking [6, 13].

Few studies have looked at bone regeneration and healing in animal study models exceeding ninety days [14]. Even fewer studies have used large animals, which are more translatable to humans [15-17]. The reasons for lack of large animal studies vary with the most common being expense [18]. The ability to generate validated data to meet Food and Drug Administration and International Organization for Standardization [ISO] 10993 for new medical devices, such as a bone regenerative material or scaffold, require a relevant preclinical segmental bone defect in a large animal model to ensure the safety and efficacy of the material [6, 19]. When selecting a large animal model, the cost to acquire the animal, the care for the animal, the availability of the animal, society's acceptance of the animal model, the animal's tolerance to captivity and the ease of housing must all be considered [13, 14, 20]. In light of these hurdles, goats are an ideal animal for the study of bone regeneration. Furthermore, the sequence of cellular events during osseointegration of grafting material has been shown to be similar in goats and humans [6, 14]. Historically in the evaluation of a new biomaterial, tibial fracture gap sizes have been made with a length of 2.0-2.5 times that of the shaft diameter, and are typically 20 to30 mm in length [6, 18, 19]. These segmental bone defects have been stabilized during the study period with a variety of acceptable fixation methods, ranging

from external fixator pins, bone plating, and intramedullary nailing, each with its own unique set of complications [6].

Recently, a 3D bio-scaffold composed of polyurethane(PU)-nano-hydroxyapatite(nHA) manufactured with 80% PU/nHA interspersed with decellularized bone particles exhibited promising new bone formation in vitro and in rat models [12, 21]. The combination of nHA/PU has been explored in-vitro and in small animal models [22, 23]. Selection of hydrophilic polyurethane as a candidate for scaffold fabrication offers suitable characteristics including biocompatibility, mechanical flexibility, and its bioresorbability [24-26]. Nano-hydroxyapatite has been combined with a variety of synthetic polymers to better mimic the mineral component and the microstructure of natural bone [27]. The ideal for the nHA/PU composite is to serve as a 3D substrate for cell attachment and migration, and in our lab we have demonstrated that the addition of decellularized bone particles further stimulates this integration with native tissue [21, 27].

Hypothetically, the addition of a growth factor such as recombinant human bone morphogenetic protein-2 (rhBMP2) classically produced by *E. coli* or by hamster oocyte cell cultures, to the 3D scaffold could further stimulate bone formation. Bone morphogenetic protein-2 is a growth factor in the transforming growth factor beta superfamily with activity that was first identified in the 1960s [28, 29]. It is known for its osteoinductive capacity [29]. Large amounts of BMP-2 are difficult to produce and extremely costly [30]. Also, there is increasing evidence of deleterious side effects of associated with off-label use of hamster oocyte derived rhBMP-2 products despite its ability to elicit a consistent osteogenic effect [31]. Exaggerated bone response may be associated with the large initial release of the protein from various BMP-2 carrier devices [32, 33]. While the majority of recombinant human BMP-2 (rhBMP-2) is traditionally derived from Chinese hamster ovary cells, *E. coli* derived rhBMP-2 has been shown to show compatible fusion rates [30, 34-36]. *E. coli* derived rhBMP-2 is more cost effective and has shown potential as a growth factor capable of elution from scaffolds with a pore size of 100-300 um [34]. In typical fractures, BMP-2 is upregulated for up to 4 weeks following injury, supporting the idea that an alternative strategy is to have a sustained release of physiologically appropriate BMP-2 allowing for enhanced osteogenic differentiation while mitigating untoward side effects [32, 37-39].

The aim of this project was to evaluate the long-term effect (up to twelve months) of a 3D synthetic bone regeneration scaffold, with and without the addition of *E. coli* derived rhBMP-2, implanted into a large segmental bone defect to assess the inherent and enhanced capability to promote bone formation [21]. For this purpose, we used a 2.5cm mid-diaphyseal tibia segmental osteotomy gap previously developed in our laboratory. In this model, we create and stabilize the defect using a custom designed and manufactured 4.0-mm locking plate construct. We hypothesized that the scaffold would promote bone formation without adverse effects, effectively deliver BMP2, and integrated and degraded over time. Our objectives were to assess the fracture model and the effect of the scaffold on the goats' biometrics, bone healing, and scaffold degradation over a period of up to 1 year.

Materials and Methods

Scaffold Fabrication

Multi-layered scaffolds were fabricated as previously described (**Fig 3-1a**) [12, 21].[3] Cylindrical scaffolds were manufactured to serve as a transmedullary implant (spanning the gap from proximal to distal medullary canals). As such they were manufactured to a length of 2.5 cm and a diameter of 8 mm to provide a secure fit into the intramedullary cavity of both the distal and proximal segments of the cut tibia. Scaffolds were sterilized using ethylene oxide prior to surgery.

Study Design

All experimental procedures and protocols were approved by the appropriate animal care and use committees (University of Tennessee IACUC 2383). Eighty-three mixed breed goats [2 to 6 years old, average weight 52.49±0.25 kgs (35-78 kgs)] were purchased from a USDA licensed vendor. Goats were group housed in pens with free access to grass hay, water, trace minerals and fed a daily total mixed ration [40]. Animals were acclimatized for a minimum of 10 days before surgery. The study design consisted of three groups: Control group: goats had the segmental defect without any treatment of the defect; Scaffold group goats had the native scaffold inserted in the gap; BMP-2 impregnanted scaffold group goats had an rhBMP-2 impregnated scaffold inserted into the gap. In BMP-2 animals (scaffold + rhBMP-2), 1.5 mg of lyophyilized *E. coli* derived rhBMP-2 (BioVision, Milpitas, CA., USA) was impregnated into the scaffold for a minimum of 30 minutes prior to implantation Dosage of BMP2 was extrapolotaed from previous studies and clinical use products. Each group of goats were used to study regeneration and scaffold efficacy for 3, 6, 9, and 12 months. Each group at each time point included 8 goats (3 groups x 4 time points x 8 goats = 96 goats in total) with up to 2 replacement goats per group per time point (n=24).

Surgical procedure and scaffold implantation in caprine tibias

Goats were withheld from feed for 24 hours, and water for 12 hours prior to surgery. Each goat was sedated with xylazine (0.05 mg/kg IV) and induced into general anesthesia using midazolam (0.25 mg/kg) and ketamine (5 mg/kg). Goats were then intubated and placed into dorsal recumbency under general anesthesia and maintained using isoflurane gas vaporized in 100% oxygen. Balanced anesthesia was carried out using monitoring parameters (heart rate, respiratory rate, temperature, response to stimulus) and isotonic fluids were provided at 10 ml/kg/hr. The right hind limb was suspended, clipped, and aseptically prepared for surgery. An approximately 20-cm linear incision was made over the medial aspect of the tibia. The periosteum was incised and reflected from the surface of the tibia. A custom designed, 8-hole, 4.0-mm thick, locking

[3] All figures and tables for this chapter are presented in the appendix.

plate was applied to the cranial medial aspect of the tibia. This custom designed locking plate (Veterinary Orthopedic Implants, St. Augustine, Fl., USA) had each of the locking screw holes placed at the ends of the plate (4 at each end) so as to ensure the section of the plate spanning the defect was solid and would prevent bending failure. Four 4.0-mm diameter locking bone screws were placed into each of the proximal and distal segments of the tibia spanning the region of the segmental ostectomy (**Fig 3-1b**). A 2.5-cm length full thickness segment was cut using an osteotomy saw and the bone segment removed from the tibia. The scaffold material was trimmed, using surgical scissors and/or a #10 scalpel blade, to the appropriate length for the ostectomy (**Fig 3-1c and d**). The ostectomy gap was left unfilled in the Control group goats, was filled with scaffold material in the Scaffold group goats, or filled with an rhBMP-2 impregnated scaffold in the BMP-2 group goats. The subcutaneous tissues were closed with 2-0 polydiaxanone in a continuous pattern. The skin was closed using 0 polypropylene in a continuous pattern.

A Robert-Jones splint bandage (Tarsal Real Leg Quick Splint, Large, Jorgensen Laboratories, Loveland, Co., USA) was placed on the limb to protect the surgery site during recovery and for 60 days after surgery. The goats received flunixin meglumine (1 mg/kg IV; non-steroidal anti-inflammatory twice daily) for pain control for the first three days after surgery and received Ceftiofur sodium (2.2 mg/kg IV) for three days for antibiotic prophylaxis. Additional pain control was provided via a fentanyl transdermal patch (72 mcg/kg/hr) which was placed on the dorsal lateral thorax 18 hours prior to surgery and continued for 3 days post-operatively. When needed based on attitude, activity and lameness, additional analgesic were given (meloxicam 1 mg/kg orally one daily and/or fentanyl transdermal patches 75 mcg/kg/hr) as needed. The goats had free access to food and water post-operatively, and were monitored for morbidity daily. Splint bandages were changed daily for the first 5 days, then every other day for two weeks, then weekly for two months. Splint bandages were removed at two months. Goats were housed in individual pens for the first 7 days post-operatively, then group housed in pens thereafter. Based on treatment group assignments, goats were euthanized at 3, 6, 9, or 12 months post-operatively by intravenous overdose of a barbiturate (pentobarbital 1 cc/10lbs).

Lameness evaluation post-operatively

Gait parameters, specifically right hind maximum force as a percent of body weight, were quantitatively assessed using a real-time pressure sensing system (Walkway Pressure Mapping System, Tekscan Inc, South Boston, MA). The sensory matrix was 87.1 cm long by 36.9 cm wide and had a sensor density of 1.4 sensors/cm^2. The mat was calibrated and equilibrated according to the manufacturer's instructions. Triggering was enabled so that recordings would start at the first contact, or a raw sum force of 200 kPa and end at a total of 400 recorded frames at a rate of 15 frames per second. An alleyway was assembled to create a fixed walkway for the goats. The width of the alleyway was made such that the goats could move freely in a straight line, would be discouraged from turning around, and that each goat's foot falls would strike the sensitive area of the mat. Right hind maximum force as a percent of body weight data was collected prior to the creation of the ostectomy gap, then at day 7 post-operatively and at monthly intervals until end points.

Imaging assessment of ostectomy gaps and scaffold integration

High definition thermal imaging

High definition thermal images were acquired post-operatively at days 2, 4, 6, 8, 10, 12, 14, 21, 28, 35, 42, 39, 56, and then monthly until end points (Fluke Thermal Imaging, MSC Corporation, USA). The camera was held one meter away from the goat after the bandage had been removed and the limb had been allowed to acclimate to room temperature when a bandage was still in place. The thermal reading nearest to the ostectomy gap on the lateral aspect or craniocaudal aspect of the images were kept to the nearest Farenheight degree.

Radiographic assessment

Radiographs were performed immediately post-operatively and then monthly until end points (NEXT Equine DR, Sound, Carlsbad, CA., USA). Radiographs were scored by a board certified radiologist to assess ostectomy gap filling **Table 3-1**. For statistical analysis, a score of 5 was equal to that of a healed fracture (ostectomy gap completely filled with new bone and/or bridging callus present on all cortices).

Dual energy x-ray absorptiometry (DEXA)

A dual energy x-ray absorptiometry (DEXA) was performed immediately post-operatively then monthly until end points (Hologic QDR 4500, Horizon DXA Systems, Marlborough, MA., USA). Briefly, the goat was sedated (xylazine 0.05 mg/kg IV) and placed in sternal recumbency, the hind limbs were extended, and the right hind limb was scanned using the lumbar spine settings. A region of interest (ROI) was drawn over the osteotomy gap and bone mineral content (g) and bone mineral density (BMD; g/cm2) were calculated.

Computed tomography

After humane euthanasia, the locking plate was removed from the right tibia. The goat was placed in dorsal recumbency and a computed tomography (CT) scan performed (Philips brilliance-40, Philips International B.V., Amsterdam, Netherlands). Transverse images were reconstructed in 2 mm slice thickness using high definition resolution, and sagittal and dorsal multiplanar (MPR) images were generated. ROI's were drawn over either new bone, or density of the graft and calculated in Hounsfield units (HU).

Biomechanical testing

Once CT imaging was complete, the tibia were harvested, isolated, and prepared for a 4-point bending test. Testing was carried out using an Instron 5965 electromechanical universal testing system coupling with a 5 kN maximum actuator (Instron 5965, Norwood, MA., USA). Testing was done in a single load-to-failure fashion. The tibia and load points were optimally positioned such that the ostectomy site was at midpoint between both the inner and outer arms. Tibias were mounted on the holding grip with span set at 170 mm while the loading points were set at a span of 70 mm. The testing was performed at a rate of 60 mm/min until the specimen failed. The mode of failure was recorded as bone fracture. The testing parameters were specified to

maximum load, expressed in kilograms of force (kgf), and it was defined as the maximum load applied by the actuator to the specimen during the test right before specimen failure. The displacement of the actuator was measured as a relative distance (mm) of the actuator to its' original location at the start of the test. Tissue specimens lacking sufficient integrity to be mounted and tested were considered to have a value of "0" for the purpose of statistical analysis.

Microscopic assessment of ostectomy gap and scaffold integration

After 4-point bending tests were completed, tibia segments were trimmed and placed in 95% ethanol. Using an automated tissue processor (ASP300S, Leica, Germany) tissues were dehydrated in a series of ethanol solutions of increasing concentration (70%, 80%, 95% x2, 100% x3) over a period of several days at ambient temperature and a programmed auto-cycle of pressure, vacuum, and gentle agitation. Specimens were next transferred to three separate exchanges of 100% Methyl Salicylate (Sigma-Aldrich, St. Louis, MO) over the course of 48-72 hours, manually cycled between gentle agitation (modified stir bar setup) and vacuum at -15-20 in Hg (Fisherbrand, Vacuum Chamber), and observed for complete dehydration. Specimens were transferred to 100% xylenes (Sigma-Aldrich, Histological Grade, St. Louis, MO) for a quick rinse before being placed back onto the automated tissue processor (ASP300S, Leica, Germany) for three changes of 100% xylenes to complete the tissue clearing and prepared for methyl methacrylate resin infiltration. Specimens were then manually managed through three separate and fresh in-house prepared Infiltration Solution (IS I, IS II, IS III) exchanges of methyl methacrylate (Sigma-Aldrich, St. Louis, MO) and dibutyl phthalate (Sigma-Aldrich, St. Louis, MO), under ambient temperature over the course of 1.5 - 2 weeks, and with a manually cycled switch between gentle agitation (modified stir bar setup) and vacuum @ -15-20 in Hg (Fisherbrand, Vacuum Chamber).

After a satisfied period of resin infiltration, specimens were transferred to prelabelled polypropylene containers and pre-polymerized base molds, where a fourth and in-house prepared final resin solution was then added along with a benzoyl peroxide based catalyst (Perkadox-16, AKZO Nobel Chemicals, Chicago, IL) to initiate a polymerization reaction to cure each specimen into a bubble free, clear, hardened, methyl methacrylate (MMA) block over a period of approximately 5-8 days. Each specimen block was then trimmed using a wet bandsaw (MarMed Bone Wet Band Saw) so that resulting microtomed sections would fit onto pre-cleaned 50mm x 75mm glass microscope slides (Fisherbrand). Specimen blocks were shaped for microtomy and sections cut at five microns using a motorized SM2500 sledge microtome (Leica, Germany) and d-profile (sledge) tungsten-carbide knives (Delaware Diamond Knives). Each section cut was mounted to an individual 50mm x 75mm precleaned glass microscope slide (Fisherbrand) that was coated with an in-house gelatin based solution recipe (Haupt's Solution) and covered with a plastic protective strip.

Prior to staining, slide-sections from each specimen were sorted for VonKossa, Goldner's Trichrome, Tartrate Resistant Acid Phosphatase (TRAP) staining, and fluorescence microscopy. The VonKossa stain was a silver stain that bound silver ions to the presence of calcium in boney tissue (undemineralized bone). It was developed chemically and visualized as a "jet-black" color identifying native/mature bone. The

process of osteoid, newly formed dense collagen, transitioning into mineralized bone was visualized as a black "peppering" throughout the greyish-blue osteoid layer on the surface of native/mature undemineralized bone. Goldner's Trichrome staining and modified general bone and cartilage stain similar to Masson's Trichrome staining, was used for a contrast between bone soft tissue morphology and the identification of dense collagen/osteoid (red) as compared to mineralized bone (green). Finally, Tartrate Resistant Acid Phosphatase (TRAP) staining (kit #387A, Sigma-Aldrich, St. Louis, MO) was employed to demonstrate the active presence of osteoclastic activity with actively resorbing osteoclasts being identified in red against a hematoxylin counterstained boney matrix. Prior to staining, all sections were deplasticized in a similar fashion that traditional paraffin sections would be deparaffinized so that all tissue components can be uninhibited during staining molecule interactions.

To quantitatively assess the percentage of mineralization (VonKossa), osteoid formation (Goldner's Trichrome), or osteoclast number (TRAP staining) images from each slide were grossly acquired and digitized using a Panasonic HC-V770 (8M, 3264x2448, aspect ratio 4:3, extra optical zoom 20x)then processed in ImageJ (Rasband, W.S., Image J, U.S. National Institutes of Health, Bethesda Maryland, USA, https://imagej.nih.gov/ij/, 1997-2018.). For percentage mineralization, images were made binary such that mineralized bone was the parameter quantitatively assessed. For osteoid formation, images were made binary such that osteoid was the quantitatively assessed parameter. Finally, for the osteoclast number, osteoclasts per mm of bone surface were counted [41]. Unstained sections were evaluated by fluorescence microscopy with an excitation filter and two stop filters allowing radiation with a wavelength between 490 and 520 nm that permitted the identification and morphometric analysis of the mineralizing surface of bone.

Statistical analysis

Statistical analyses were performed using separate mixed-model repeated-measures analysis of variance within the GLIMMIX procedures of SAS to determine whether each outcome variable differed significantly by treatment group over time, with goat considered a random effect (SAS v 9.4, Cary, NC). Multiple comparison adjustments were made using Tukey's post-hoc comparisons to assess the effects of group, time point, and group x time point interaction. For categorical variables, ordinal multinomial logistical regression doing a cumulative logit was performed by monthly analysis to determine if there were differences between treatments. Significance was set at $P<0.05$. Least square means are reported ± standard error.

Results

Clinical observations

Goats were removed from study and replaced when necessary based on infection. Morbidity experienced with this model included osteomyelitis (n=13), plate bending (n=2), wound dehiscence (n=1), broken screws (n=2), anesthetic death (n=2), and sudden death of unrelated causes (n=2). A total of 83 goats (79%) were available for inclusion into statistical analysis (**Table 3-2**).

Lameness evaluation

When evaluating maximum force as a percent of body weight for the right hind operated limb, there was no difference between groups. There was an effect of time in that goats were able to bear more weight through the operated limb (fracture healed and goats become "sound") over time. The increase in pressure (kilograms force as a percent of body weight) exerted in the operated limb over time (19.16±1.26%BW) at 7 days post-operatively) returned to baseline values pre-operatively (34.98±1.23%BW) showed an increased comfort during ambulation regardless of treatment group.

Imaging assessment of ostectomy gap and scaffold osseointegration

High definition thermal imaging

The surface temperature at the site of surgery and scaffold implantation (ostectomy site on lateral or craniocaudal images) was not different between treatment groups regardless of time point. There was an effect of time in that surface temperature decreased (from 98 degrees Farenheit to 83 degrees Farenheit) over time, or that surgical site inflammation decreased and no additional inflammation was noted from fracture healing regardless of group. Alternatively, as the scaffold group and scaffold+BMP-2 was not different from the control group, the addition of the biomaterial caused no additional detectable inflammation.

Radiographs

Radiographs for each goat were reviewed by a board certified radiologist (HS) blinded to the study groups assignments and scored for each month of study. The radiographic score of ostectomy gap filling was compared between groups and over time. A complete bridging callus was eventually formed in 73% of control goats, 66% Scaffold goats, and 79% of BMP-2 goats. Across all groups, there was a significant effect of time in that scores increased (ostectomy gaps healed) over time for all groups ($P<0.05$). There was no effect of treatment group on the ordinal probabilities for ostectomy gap filling at months 1-6, and months 10-12 ($P>0.05$). At month 7, there was an effect of treatment group on the ordinal probabilities for ostectomy gap filling ($P<0.05$). There were reduced odds in the Control group compared to the Scaffold group for lower ordered ostectomy gap filling scores (OR=0.159, CI 95%, 0.04-0.69), meaning that the Control goats showed greater gap filling scores (more healing) compared to Scaffold goats and BMP-2 goats. At month 8, there were reduced odds in the Control group compared to the Scaffold group for lower ordered ostectomy gap filling scores (OR=0.133, CI 95%, 0.03-0.60), and again at month 9 (OR=0.10, CI 95%, 0.02-0.49). Numerically, the odds ratio was 0.45 comparing BMP-2 goats to Scaffold goats for lower ordered ostectomy gap filling scores; however, the confidence interval ranged up to 1.67 and therefore was not statistically significant.

Bone mineral density (BMD)

Bone mineral density within the ostectomy gap was calculated for each goat at monthly intervals. Across all groups, there was a significant effect of time in that BMD within the ostectomy gap increased (ostectomy gaps healed) over time for all groups (**Fig**

3-3A; P<0.05). On average, BMD within the ostectomy gap was greater in Scaffold goats (0.93g/cm^2 ±0.05) and BMP-2 goats (0.97g/cm^2±0.05) as compared to Control goats (0.85g/cm^2 ±0.05). A difference between groups over time approached significance showing that the BMD within the ostectomy gap was changing at a rate dependent on group (Table 3, *P*=0.057; **Fig 3-3B**). On average, the overall rate of change for BMD within the ostectomy gap showed similarities to a quadratic rate for bone healing.

Computed tomography

When evaluating new bone density over time, there was a significant effect of time (*P*<0.05) with 3 month time-point goats, regardless of group, having less new bone density (1126.04HU ±47.71; *P*<0.05) than any other time-point [(6)-1331.27HU± 47.26, (9)-1262.97HU ± 72.83, (12)-1358.43HU ±44.06]. There was no significant difference between groups. When evaluating the density of the material, only Scaffold goats and BMP-2 goats were evaluated. On average, the density of the material was less (increased osseo-integration) in BMP-2 goats (612.17HU ±50.44) as compared to Scaffold goats (854.61HU ± 47.45; *P*<0.05, **Fig 3-4**). On average, both Scaffold goats and BMP-2 goats at twelve months had less density of the material, or more osseo-integration (550.66HU ± 66.76), than all other time points [(3)-823.26HU ± 66.76, (6)-774.97HU ±75.63, (9)-784.66HU ± 67.45; *P*<0.05].

Biomechanical testing

4-point bending load-to-failure testing was performed in nineteen of twenty-six (73%) Control goats, nineteen of twenty-nine (66%) Scaffold goats, and twenty-two of twenty-eight (79%) BMP-2 goats (**Table 3-2**). Tissue specimens lacking sufficient integrity to be mounted and tested were considered to have a value of "0" for the purpose of statistical analysis. Across groups, there was a significant effect of time (*P*<0.05). There was no difference between adjacent time points; however, consistent differences between the means for every 6 months of time in load-to-failure was apparent with load increasing over time in all groups [(3)-57.53kgf±36.32^{c}, (6)-118.05kgf±28.49^{bc}, (9)-192.56kgf±26.10^{ab}, and (12)-207.62kgf±23.87^{a}]. There were no statically significant differences in load-to-failure between groups when bridging callus was achieved and mechanical testing was possible. On average, Control goats failed at 142.10kgf ± 25.19, Scaffold goats failed at 141.62kgf ± 26.94, and Scaffold+BMP-2 goats failed at 148.09kgf ± 23.28.

Microscopic assessment of ostectomy gap and scaffold integration

Undecalcified bone segments slides were successfully processed for histology slides for analysis using stains for Von Kossa (n=78), Goldner's Trichrome (n=79), and TRAP (n=69) staining evaluation. Additionally when available, slides for fluorescence microscopy were evaluated.

Histomorphometry assessment of Von Kossa staining (percent area mineralized in the ostectomy gap), there was no significant difference between group, time point, and group by time point interaction (P>0.05). On average, the percent mineralization for Control goats was 41±1.92%, for Scaffold goats was 43±1.84%, and for BMP-2 goats was 45±1.88. On average, the percent mineralization was 40±2.20% at 3 months,

44±2.20% at 6 months, 44±2.14% at 9 months and 45±2.14% at twelve months (**Fig 3-5**). While no significant difference was apparent over time, the average percent mineralization over time appeared to follow a bone remodeling curve in that mineralization initially increased (new bone was laid down), decreased as the ostectomy gap remodeled and then proceeded to increase again. This was regardless of group.

Histomorphometry assessment of Goldner's Trichrome staining found that the percent osteoid formation was significantly different between groups and across time points; however, there was no group by time point interaction ($P<0.05$). On average, Scaffold goats and BMP-2 goats had greater percent osteoid formation (6.96±0.46% and 6.97±0.46%) as compared to Control goats (3.67±0.48%). On average, the osteoid percentage of area in the ostectomy gap decreased over time, with a slight increase at 9 months then final decrease at 12 months regardless of group [(3-6.79±0.55%^{a}, (6)-5.67±0.55^{ab}, (9)-6.36±0.53%^{a}, (12)-4.63±0.54^{b} ; **Fig 3-6**]. This significant difference over time supports an active ostectomy remodeling gap regardless of group that mimics the percent mineralization in an equal and opposite direction in that new bone (osteoid) is initially laid down, mineralized, and then remodeled and decreases over time.

Osteoclast count per mm of bone surface found a significant difference between group, time point, and a group by time point interaction existed ($P<.05$). The average osteoclast count decreased over time for Scaffold goats and BMP-2 goats, while the average osteoclast count remained static for Control goats (**Fig 3-7, Table 3-4**).

Assesment of fluorescent microscopy (percent bone formation) revealed that there was no significant difference between group, time point, and group by time point interaction ($P>0.05$). Oxytetracycline is an antibiotic that complexes with metal ions such as calcium and becomes incorporated into bone enabling it to be used as a marker of bone formation. It can be detected for months post-injection as bone turn-over can take years. This may explain why there was no difference over time. Goats in the study were double labeled (once prior to surgery and again prior to euthanasia) in the hopes of being able to detect a bone formation rate. Due to healing of most of the gaps by 3 months, this detection was no longer possible. The average percent bone formation for Control goats was 0.12%±0.10, for Scaffold goats was 0.46%±0.10, and for BMP-2 goats was 0.38%±0.10.

Discussion

The use of a long-term bone-healing model to evaluate scaffolds that resembles closely the normal fracture healing process is of great interest for bone regeneration. Long-term bone regeneration studies are lacking, especially for the study of synthetic biomimetic materials [6]. A cost effective large animal preclinical model is of the utmost importance for meeting FDA and ISO 10993 standards are critical [6]. An efficacious model may speed development of medical devices for bone tissue engineering reducing the rates of non-unions, need for amputation, or costly secondary revision surgeries.

A significant outcome for this study was that 80% of the goats survived to their expected time point. The most significant short-term complication was osteomyelitis within one-month post-operatively. The second most common complication was associated with orthopedic complications related to the locking plate itself (9%). The

most common complication was bending of the locking plate, or screw pull out. These complications have been noted previously in large animal segmental defect models [19]. In contrast to an earlier ovine study that noted a lower stiffness of a limited contact locking compression plate as compared to a dynamic compression plate, our study was able to successfully use a custom made 8-hole locking plate for up to 12 months [19]. One significant difference is that our custom- made 8-hole plate did not have screw holes in the middle of the plate which was centered on the gap created by the segmental defect. Anchorage into the main fragments proximal and distal to the ostectomy gap are important and our plate design allowed for screws to be placed farther from the ostectomy gap in a buttress fashion [42, 43]. This in combination with the application of the use of padded splint bandage for 60 days may account for fewer orthopedic complications seen in this study. Additionally, as we aimed to study bone healing and osseointegration of the implant, our control defects were allowed to heal and therefore a non-union was not ensured [19].

Serial imaging was performed with radiographs and dual energy x-ray absorptiometry (DEXA). While conventional radiographs have long been the standard for assessment of fracture healing, they have limited use for evaluation of biomaterials and fracture healing[44]. The use of DEXA has long been a means of assessing osteoportic bone and used in animal models [45, 46]. We successfully used DEXA as a means of studying osseointegration. While, radiographically, it appeared that scaffold goats had lower healing scores, by use of DEXA, there was greater bone mineral density within the ostectomy gap, which may be attributable to the presence of the decellularized bone particles in the scaffold and guided bone formation with less pronounced woven bone during the regenerative phase. Computed tomography bone density appeared to follow a standard bone-remodeling curve, regardless of treatment group, showing an initial increase in bone density after 3 months with a minor drop after 6 months and increase again to 12 months. Computed tomography has been shown to be a parameter for macroscopic assessment of osseo-integration, and BMP-2 goats appeared to have greater osseo-integration as compared to Scaffold goats [47].

One salient observation was the percentage of group two (scaffold) goats that made it to a bridging callus and biomechanical testing. Of the twenty-six goats in group two, nineteen were able to form a sufficient bridging callus regardless of time point. While not statistically different with regard to load-to-failure, more BMP-2 goats were able to form a bridging callus as opposed to group two goats. Once a bridging callus was formed, the load-to-failure was equivocal among groups. It previously has been recognized that polyurethanes used in orthopedic biomaterials have been chosen for some of their mechanical and degradation properties [48, 49]. This synthetic polymer has been previously combined with nanohydroxyapatite allowing the biomaterial to bind to living bone tissue providing osteo-conductivity and biocompatibility [48, 49]. To these author's knowledge, few studies have studied this polymer biomaterial combination in a large animal model beyond a relatively short time period, or against a bone healing model, to further investigate its potential osseo-integrative properties [50].

Of chief importance was this study's ability to provide long-term follow up with a negative control group that served as a bone-healing model for comparison. On

microscopic evaluation, group one (control) goats showed a mean percent area of mineralization that increased in a manner that would be expected for bone formation [51]. Bone healing should progress from soft callus formation, to hard callus formation, and then proceed to bone remodeling [51]. During the remodeling process, irregular woven bone is converted to lamellar bone and the original cortical structure is returned [51]. The greatest disadvantage of this model was the stress shielding that occurred due to the locking plate placed in a buttress fashion. This stress shielding resulted in the cis cortex, or that closest to the plate often becoming thinned [6, 19]. As expected, there was an initial increase in mineralization, followed by a decrease as bone was remodeled, coupled with a second period of increase as bone was returned to its original structure [51]. In line with this concept, percent osteoid formation was opposite to that of mineralization such that there was initially a large amount of immature bone that was initially great and then fell accordingly as bone, or the fracture, remodeled and healed. Scaffold goats and BMP-2 goats had greater percent osteoid formation as compared to Control goats [52]. Finally, it appeared as though there was little osteoclastic activity associated with group one goats once the bridging callus was formed with the average osteoclast count being less than one per mm of bone surface. This may be due to the observation that most group one goats had formed a bridging callus based on radiographic scores by sixty days, and remodeling was based on stress biomechanics rather than true bone remodeling [6, 42]. This would leave osteoclastic activity limited to degredation of the biomaterial thus explaining why there was an increased osteoclast count in the group two and group three goats that decreased to that of the group one goats over time.

Overall results demonstrate that scaffold + rhBMP-2 treatment resulted in more goats reaching a bridging callus that was able to withstand load-to-failure testing. Treatment with rhBMP-2 also resulted in scaffolds that were better integrated based on macroscopic assessment. Based on microscopic assessment, rhBMP2 treatment resulted in goats that were equivocal to the bone healing model control at 12 months in terms of percent area mineralization and osteoclastic resorption. These results highlight the ability of our scaffold to deliver growth factors. While rhBMP2 continues to be a growth factor of controversy, as of this moment, for large bone defects, there are few alternatives [53-57]. Of note, bone formation was not present in muscle or any other ectopic locations as all goats underwent full post-mortem examination. This highlights the capability of the scaffold to serve as an eluting device for growth factors though further kinetic studies are necessary to define the optimal dose and elution rates.

Future studies to improve this model would be to remove the locking plate once the bridging callus is present. One disadvantage of this model was the stress shielding that occurred due to the locking plate placed in a buttress fashion. This stress shielding resulted in the cis-cortex, or that closest to the plate often becoming thinned [6, 42]. Earlier removal of the plate may overcome the limitation of the thinning of the cis cortex and may improve radiographic scoring over time. Previous studies have shown that some iterations of this scaffold have the ability to deliver mesenchymal stem cells [57]. We now have the basis to show that our material scaffold elutes growth factors, and with the addition of growth factors shows superior osseo-integragraion compared to the material alone. Speculatively, in areas of potential non-union the addition of mesenchymal stem

cells could enhance the bone tissue regeneration using our material as a delivery platform. Finally, after the first sixty days, goats were free to return to group housing and required minimal maintenance beyond housing requirements. This allowed for a long-term efficacious model that may bridge the need to provide a large animal preclinical model that is both cost effective and repeatable [6].

Conclusions

Overall the results presented here demonstrate the effectiveness of a multi-layered-nanohydroxyapatite-polyurethane-decellularized bone particle based scaffold in the treatment of long bone segmental defects which is enhanced when used as a delivery device for rhBMP2. The results of this study have shown a successful, repeatable large animal preclinical model of segmental defect long bone healing that provides a bone-healing model for comparison of osseo-integration of synthetic based materials. Evaluation of our multi-layered material showed superior integration at 3, 6, 9, and 12 months with the addition of rhBMP2 as compared to the material alone. Strengths of this study include validation of the importance of a non-treatment control and the long-term evaluation of twelve months.

References

1. Smith, B. D., & Grande, D. A. (2015). The current state of scaffolds for musculoskeletal regenerative applications. *Nature Reviews Rheumatology*, *11*(4), 213.
2. Finkemeier, C. G. (2002). Bone-grafting and bone-graft substitutes. *JBJS*, *84*(3), 454-464.
3. Baldwin, P., Li, D. J., Auston, D. A., Mir, H. S., Yoon, R. S., & Koval, K. J. (2019). Autograft, allograft, and bone graft substitutes: clinical evidence and indications for use in the setting of orthopaedic trauma surgery. *Journal of orthopaedic trauma*, *33*(4), 203-213.
4. Fillingham, Y., & Jacobs, J. (2016). Bone grafts and their substitutes. *The bone & joint journal*, *98*(1_Supple_A), 6-9.
5. Fernandez de Grado, G., Keller, L., Idoux-Gillet, Y., Wagner, Q., Musset, A. M., Benkirane-Jessel, N., ... & Offner, D. (2018). Bone substitutes: a review of their characteristics, clinical use, and perspectives for large bone defects management. *Journal of tissue engineering*, *9*, 2041731418776819.
6. Reichert, J. C., Saifzadeh, S., Wullschleger, M. E., Epari, D. R., Schütz, M. A., Duda, G. N., ... & Hutmacher, D. W. (2009). The challenge of establishing preclinical models for segmental bone defect research. *Biomaterials*, *30*(12), 2149-2163.
7. Zura, R., Xiong, Z., Einhorn, T., Watson, J. T., Ostrum, R. F., Prayson, M. J., ... & Steen, R. G. (2016). Epidemiology of fracture nonunion in 18 human bones. *JAMA surgery*, *151*(11), e162775-e162775.
8. Harwood, P. J., Newman, J. B., & Michael, A. L. (2010). (ii) An update on fracture healing and non-union. *Orthopaedics and Trauma*, *24*(1), 9-23.
9. Belmont, P. J., Schoenfeld, A. J., & Goodman, G. (2010). Epidemiology of combat wounds in Operation Iraqi Freedom and Operation Enduring Freedom: orthopaedic burden of disease. *J Surg Orthop Adv*, *19*(1), 2-7.
10. Court-Brown, C. M., Rimmer, S., Prakash, U., & McQueen, M. M. (1998). The epidemiology of open long bone fractures. *Injury*, *29*(7), 529-534.
11. Nandra, R., Grover, L., & Porter, K. (2016). Fracture non-union epidemiology and treatment. *Trauma*, *18*(1), 3-11.
12. Jackson, B. K., Bow, A. J., Kannarpady, G., Biris, A. S., Anderson, D. E., Dhar, M., & Bourdo, S. E. (2018). Polyurethane/nano-hydroxyapatite composite films as osteogenic platforms. *Journal of Biomaterials Science, Polymer Edition*, *29*(12), 1426-1443.
13. Black, C. R., Goriainov, V., Gibbs, D., Kanczler, J., Tare, R. S., & Oreffo, R. O. (2015). Bone tissue engineering. *Current molecular biology reports*, *1*(3), 132-140.
14. Pearce, A. I., Richards, R. G., Milz, S., Schneider, E., & Pearce, S. G. (2007). Animal models for implant biomaterial research in bone: a review. *Eur Cell Mater*, *13*(1), 1-10.

15. McGonigle, P., & Ruggeri, B. (2014). Animal models of human disease: challenges in enabling translation. *Biochemical pharmacology*, *87*(1), 162-171.
16. Van der Worp, H. B., Howells, D. W., Sena, E. S., Porritt, M. J., Rewell, S., O'Collins, V., & Macleod, M. R. (2010). Can animal models of disease reliably inform human studies?. *PLoS medicine*, *7*(3), e1000245.
17. Hackam, D. G., & Redelmeier, D. A. (2006). Translation of research evidence from animals to humans. *Jama*, *296*(14), 1727-1732.
18. Woodruff, M. A., Lange, C., Reichert, J., Berner, A., Chen, F., Fratzl, P., ... & Hutmacher, D. W. (2012). Bone tissue engineering: from bench to bedside. *Materials Today*, *15*(10), 430-435.
19. Reichert, J. C., Epari, D. R., Wullschleger, M. E., Saifzadeh, S., Steck, R., Lienau, J., ... & Hutmacher, D. W. (2010). Establishment of a preclinical ovine model for tibial segmental bone defect repair by applying bone tissue engineering strategies. *Tissue Engineering Part B: Reviews*, *16*(1), 93-104.
20. Schimandle, J. H., & Boden, S. D. (1994). Spine update. The use of animal models to study spinal fusion. *Spine*, *19*(17), 1998-2006.
21. Bow, A., Newby, S., Rifkin, R., Jackson, B. K., Matavosian, A., Griffin, C., ... & Morello, R. (2019). Evaluation of a polyurethane platform for delivery of nanohydroxyapatite and decellularized bone particles in a porous three-dimensional scaffold. *ACS Applied Bio Materials*, *2*(5), 1815-1829.
22. Meskinfam, M., Bertoldi, S., Albanese, N., Cerri, A., Tanzi, M. C., Imani, R., ... & Fare, S. (2018). Polyurethane foam/nano hydroxyapatite composite as a suitable scaffold for bone tissue regeneration. *Materials Science and Engineering: C*, *82*, 130-140.
23. Tetteh, G., Khan, A. S., Delaine-Smith, R. M., Reilly, G. C., & Rehman, I. U. (2014). Electrospun polyurethane/hydroxyapatite bioactive Scaffolds for bone tissue engineering: The role of solvent and hydroxyapatite particles. *journal of the mechanical behavior of biomedical materials*, *39*, 95-110.
24. Janik, H., & Marzec, M. (2015). A review: Fabrication of porous polyurethane scaffolds. *Materials Science and Engineering: C*, *48*, 586-591.
25. Gibas, I., & Janik, H. (2009). Medical polyurethanes with different hard segments content obtained from polycaprolactone diol, aliphatic diisocyanates and butanediol. *Polish Journal of Applied Chemistry*, *53*(1), 9-14.
26. Chen, Q., Liang, S., & Thouas, G. A. (2013). Elastomeric biomaterials for tissue engineering. *Progress in polymer science*, *38*(3-4), 584-671.
27. Wei, G., & Ma, P. X. (2004). Structure and properties of nano-hydroxyapatite/polymer composite scaffolds for bone tissue engineering. *Biomaterials*, *25*(19), 4749-4757.
28. Urist, M. R. (1965). Bone: formation by autoinduction. *Science*, *150*(3698), 893-899.

29. Chen, D. I., Zhao, M., & Mundy, G. R. (2004). Bone morphogenetic proteins. *Growth factors*, *22*(4), 233-241.
30. Chung, C. H., Kim, Y. K., Lee, J. S., Jung, U. W., Pang, E. K., & Choi, S. H. (2015). Rapid bone regeneration by Escherichia coli-derived recombinant human bone morphogenetic protein-2 loaded on a hydroxyapatite carrier in the rabbit calvarial defect model. *Biomaterials research*, *19*(1), 17.
31. Quinlan, E., Thompson, E. M., Matsiko, A., O'Brien, F. J., & López-Noriega, A. (2015). Long-term controlled delivery of rhBMP-2 from collagen–hydroxyapatite scaffolds for superior bone tissue regeneration. *Journal of controlled release*, *207*, 112-119.
32. Poldervaart, M. T., Wang, H., van der Stok, J., Weinans, H., Leeuwenburgh, S. C., Öner, F. C., ... & Alblas, J. (2013). Sustained release of BMP-2 in bioprinted alginate for osteogenicity in mice and rats. *PloS one*, *8*(8), e72610.
33. Jansen, J. A., Vehof, J. W. M., Ruhe, P. Q., Kroeze-Deutman, H., Kuboki, Y., Takita, H., ... & Mikos, A. G. (2005). Growth factor-loaded scaffolds for bone engineering. *Journal of Controlled Release*, *101*(1-3), 127-136.
34. Lee, J. H., Ryu, M. Y., Baek, H. R., Lee, K. M., Seo, J. H., Lee, H. K., & Ryu, H. S. (2013). Effects of porous beta-tricalcium phosphate-based ceramics used as an E. coli-derived rhBMP-2 carrier for bone regeneration. *Journal of Materials Science: Materials in Medicine*, *24*(9), 2117-2127.
35. Bessho, K., Konishi, Y., Kaihara, S., Fujimura, K., Okubo, Y., & Iizuka, T. (2000). Bone induction by Escherichia coli-derived recombinant human bone morphogenetic protein-2 compared with Chinese hamster ovary cell-derived recombinant human bone morphogenetic protein-2. *British Journal of Oral and Maxillofacial Surgery*, *38*(6), 645-649.
36. Geiger, M., Li, R. H., & Friess, W. (2003). Collagen sponges for bone regeneration with rhBMP-2. *Advanced drug delivery reviews*, *55*(12), 1613-1629.
37. Groeneveld, E. H., & Burger, E. H. (2000). Bone morphogenetic proteins in human bone regeneration. *European journal of endocrinology*, *142*(1), 9-21.
38. Yamamoto, M., Takahashi, Y., & Tabata, Y. (2003). Controlled release by biodegradable hydrogels enhances the ectopic bone formation of bone morphogenetic protein. *Biomaterials*, *24*(24), 4375-4383.
39. Cho, T. J., Gerstenfeld, L. C., & Einhorn, T. A. (2002). Differential temporal expression of members of the transforming growth factor β superfamily during murine fracture healing. *Journal of Bone and Mineral Research*, *17*(3), 513-520.
40. National Research Council. (2010). *Guide for the care and use of laboratory animals*. National Academies Press.
41. Ruiz, P., Martin-Millan, M., Gonzalez-Martin, M. C., Almeida, M., González-Macias, J., & Ros, M. A. (2016). CathepsinKCre mediated deletion of βcatenin results in dramatic loss of bone mass by targeting both osteoclasts and osteoblastic cells. *Scientific reports*, *6*, 36201.

42. Niemeyer, P., & Sudkamp, N. P. (2006). Principles and clinical application of the locking compression plate (LCP). *Acta Chir Orthop Traumatol Cech*, *73*(4), 221-228.
43. Mueller, C. A., Eingartner, C., Schreitmueller, E., Rupp, S., Goldhahn, J., Schuler, F., ... & Suedkamp, N. P. (2005). Primary stability of various forms of osteosynthesis in the treatment of fractures of the proximal tibia. *The Journal of bone and joint surgery. British volume*, *87*(3), 426-432.
44. Blokhuis, T. J., De Bruine, J. H. D., Bramer, J. A. M., Den Boer, F. C., Bakker, F. C., Patka, P., ... & Manoliu, R. A. (2001). The reliability of plain radiography in experimental fracture healing. *Skeletal radiology*, *30*(3), 151-156.
45. Egermann, M., Goldhahn, J., & Schneider, E. (2005). Animal models for fracture treatment in osteoporosis. *Osteoporosis international*, *16*(2), S129-S138.
46. Mosheiff, R., Klein, B. Y., Leichter, I., Chaimsky, G., Nyska, A., Peyser, A., & Segal, D. (1992). Use of dual-energy x-ray absorptiometry (DEXA) to follow mineral content changes in small ceramic implants in rats. *Biomaterials*, *13*(7), 462-466.
47. Assad, M., Likibi, F., Jarzem, P., Leroux, M. A., Coillard, C., & Rivard, C. H. (2004). Porous nitinol vs. titanium intervertebral fusion implants: computer tomography, radiological and histological study of osseointegration capacity. *Materialwissenschaft und Werkstofftechnik: Entwicklung, Fertigung, Prüfung, Eigenschaften und Anwendungen technischer Werkstoffe*, *35*(4), 219-223.
48. Dong, Z., Li, Y., & Zou, Q. (2009). Degradation and biocompatibility of porous nano-hydroxyapatite/polyurethane composite scaffold for bone tissue engineering. *Applied Surface Science*, *255*(12), 6087-6091.
49. Barone, D. J., Raquez, J. M., & Dubois, P. (2011). Bone-guided regeneration: from inert biomaterials to bioactive polymer (nano) composites. *Polymers for Advanced Technologies*, *22*(5), 463-475.
50. Gogolewski, S., Gorna, K., & Turner, A. S. (2006). Regeneration of bicortical defects in the iliac crest of estrogen-deficient sheep, using new biodegradable polyurethane bone graft substitutes. *Journal of Biomedical Materials Research Part A: An Official Journal of The Society for Biomaterials, The Japanese Society for Biomaterials, and The Australian Society for Biomaterials and the Korean Society for Biomaterials*, *77*(4), 802-810.
51. Schindeler, A., McDonald, M. M., Bokko, P., & Little, D. G. (2008, October). Bone remodeling during fracture repair: The cellular picture. In *Seminars in cell & developmental biology* (Vol. 19, No. 5, pp. 459-466). Academic Press.
52. Gruber, H. E. (1992). Adaptations of Goldner's Masson trichrome stain for the study of undecalcified plastic embedded bone. *Biotechnic & histochemistry*, *67*(1), 30-34.

53. Cook, S. D., Salkeld, S. L., Brinker, M. R., Wolfe, M. W., & Rueger, D. C. (1998). Use of an osteoinductive biomaterial (rhOP-1) in healing large segmental bone defects. *Journal of orthopaedic trauma*, *12*(6), 407-412.
54. Conway, J. D., Shabtai, L., Bauernschub, A., & Specht, S. C. (2014). BMP-7 versus BMP-2 for the treatment of long bone nonunion. *Orthopedics*, *37*(12), e1049-e1057.
55. Tseng, S. S., Lee, M. A., & Reddi, A. H. (2008). Nonunions and the potential of stem cells in fracture-healing. *JBJS*, *90*, 92-98.
56. Geiger, F., Bertram, H., Berger, I., Lorenz, H., Wall, O., Eckhardt, C., ... & Richter, W. (2005). Vascular endothelial growth factor gene-activated matrix (VEGF165-GAM) enhances osteogenesis and angiogenesis in large segmental bone defects. *Journal of Bone and Mineral Research*, *20*(11), 2028-2035.
57. Salmasi, S., Nayyer, L., Seifalian, A. M., & Blunn, G. W. (2016). Suppl-3, M8: Nanohydroxyapatite Effect on the Degradation, Osteoconduction and Mechanical Properties of Polymeric Bone Tissue Engineered Scaffolds. *The open orthopaedics journal*, *10*, 900.

Appendices

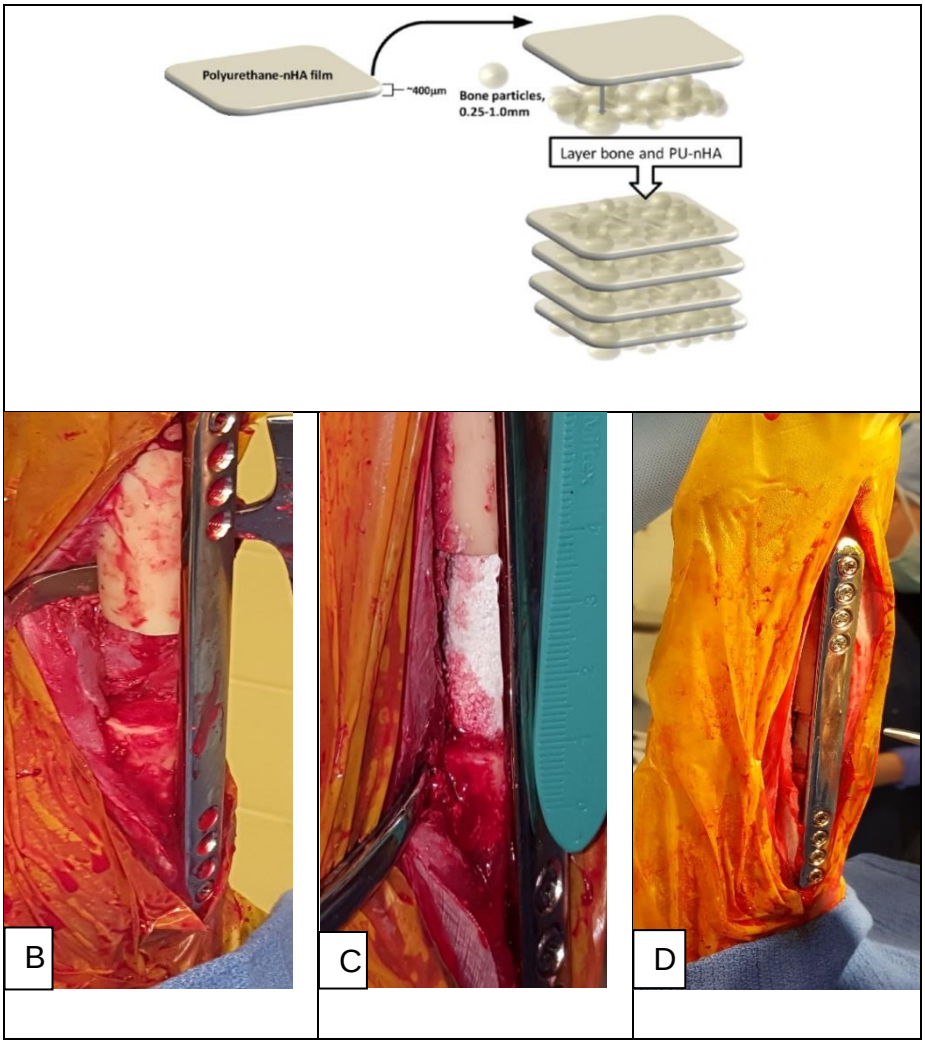


Figure 3-1. Multi-layered nHA-PU-DBP based scaffolds implanted into 2.5 cm segmental defects in the goat tibia.
A) Representation of the PU-nHA film and adding decellularized bone particles in a layer-by-layer method. B) A custom made 8-hole locking plate was placed in a buttress fashion and 2.5 cm full thickness segment of the tibia was removed with an osteotomy saw. C) In scaffold or scaffold+BMP2 treatment groups, the scaffold was trimmed to the appropriate length such that it fit snugly into the proximal and distal segments. D) The remaining screws were placed and tightened.

Table 3-1. Radiographic scoring for assessment of ostectomy gap filling.
Views were taken monthly, assessed, and scored.

Ostectomy Gap Filling	Score
No interval change compared to immediate post-operative radiographs	0
New bone filling <25% of ostectomy gap	1
New bone filling 26-50% of ostectomy gap	2
New bone filling 51-75% of ostectomy gap	3
New bone filling >75% of ostectomy gap but not completely healed	4
Ostectomy gap completely filled and/or bridging callus present on all cortices	5

Table 3-2. Final group break down showing the number of defects in each group that healed (formed a bridging callus) versus those showing insufficient healing (lack of bridging callus).

Time Point	Group	No. of Bridging Callus/Complete Healing	No. Insufficient Healing	Totals
3 Months	Control	3	4	7
	Scaffold	2	5	7
	Sc+BMP-2	4	3	7
		9	***12***	***21***
6 Months	Control	4	2	6
	Scaffold	6	1	7
	Sc+BMP-2	4	2	6
		14	***5***	***19***
9 Months	Control	7	*	7
	Scaffold	4	4	8
	Sc+BMP-2	6	1	7
		17	***5***	***22***
12 Months	Control	5	1	6
	Scaffold	7	*	7
	Sc+BMP-2	8	*	8
		20	***1***	***21***



Figure 3-2. Radiographs were acquired monthly.
This figure represents radiographs from significant time points in bone healing and group progression. Radiographic scores increased over time for all groups ($P<0.05$). Group one (control; 5.47±0.24) and group three (scaffold+ *E.Coli* rhBMP-2; 5.17±0.24) goats had significantly higher scores as compared to group two (scaffold) treated goats (4.6±0.24; $P<0.05$)



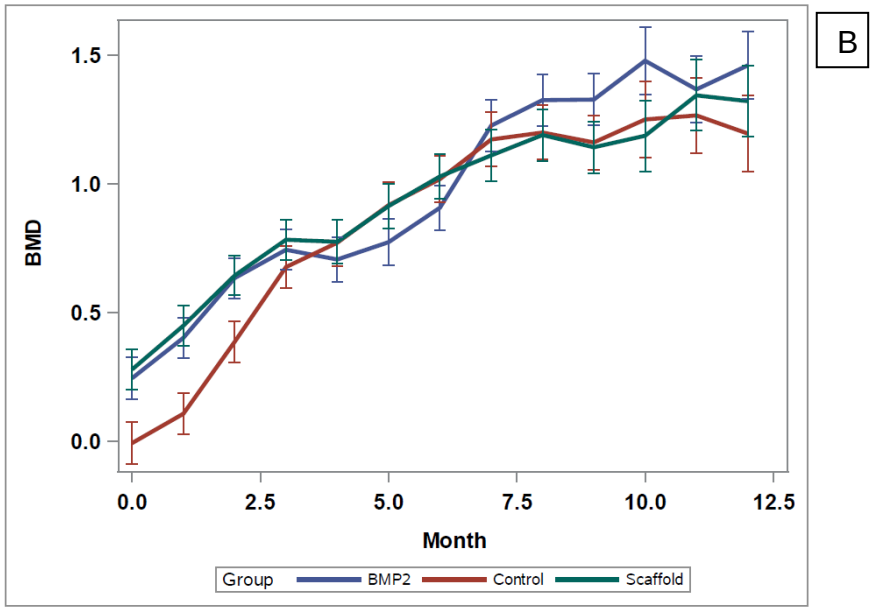


Figure 3-3. DEXA Imaging and Analysis.
A) A goat positioned in sternal recumbency allowing for DEXA imaging. Imaging was easily repeated at monthly intervals. B) Bone mineral density (BMD) increased in all groups over time and approached a group by month interaction (*P*=0.057).

Table 3-3. Group x Month interactions for bone mineral density as measured by DEXA (P=0.057).

Month	Group	Mean ± SE
1	Control	0.107±0.080[b]
	Scaffold	0.450±0.078[a]
	Scaffold+BMP-2	0.403±0.078[a]
2	Control	0.387±0.387[b]
	Scaffold	0.645±0.645[a]
	Scaffold+ BMP-2	0.635±0.635[a]
3	Control	0.678±0.080[a]
	Scaffold	0.784±0.077[a]
	Scaffold+BMP-2	0.745±0.078[a]
4	Control	0.773±0.090[a]
	Scaffold	0.776±0.086[a]
	Scaffold+BMP-2	0.707±0.087[a]
5	Control	0.978±0.090[a]
	Scaffold	0.915±0.086[a]
	Scaffold+BMP-2	0.775±0.088[a]
6	Control	1.020±0.090[a]
	Scaffold	1.030±0.086[a]
	Scaffold+BMP-2	0.908±0.087[a]
7	Control	1.173±0.105[a]
	Scaffold	1.112±0.010[a]
	Scaffold+BMP-2	1.228±0.010[a]
8	Control	1.201±0.105[a]
	Scaffold	1.120±0.010[a]
	Scaffold+BMP-2	1.327±0.010[a]
9	Control	1.162±0.105[a]
	Scaffold	1.143±0.010[a]
	Scaffold+BMP-2	1.329±0.010[a]
10	Control	1.251±0.147[a]
	Scaffold	1.188 0.138[b]
	Scaffold+BMP-2	1.480±0.130[ab]
11	Control	1.267 0.147[a]
	Scaffold	1.345 0.137[a]
	Scaffold+BMP-2	1.368 0.130[a]
12	Control	1.197 0.147a
	Scaffold	1.323±0.137[a]
	Scaffold+BMP-2	1.461 0.130a

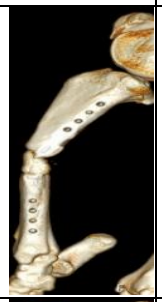
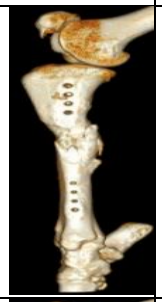
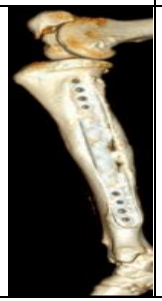
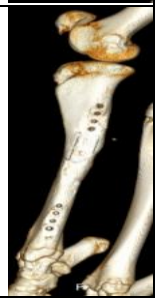
Group	3 Months		6 Months		9 Months		12 Months	
3D	AP	Medial	AP	Medial	AP	Medial	AP	Medial
Scaffold								
Scaffold +BMP-2								

Figure 3-4. Computed tomography (CT).
Performed after humane euthanasia at each time end point once the locking plate had been removed. 3D reconstructed anterior posterior and medial to lateral projections are provided at each time end point. A region of interest was drawn over the scaffold material (with or without BMP-2) and density was calculated in Hounsfield units. On average the density of the scaffold was less in group BMP-2 goats (612.17HU ±50.44) as compared to Scaffold goats (854.61HU ± 47.45) proving better osseo-integration of the material with the addition of BMP-2.

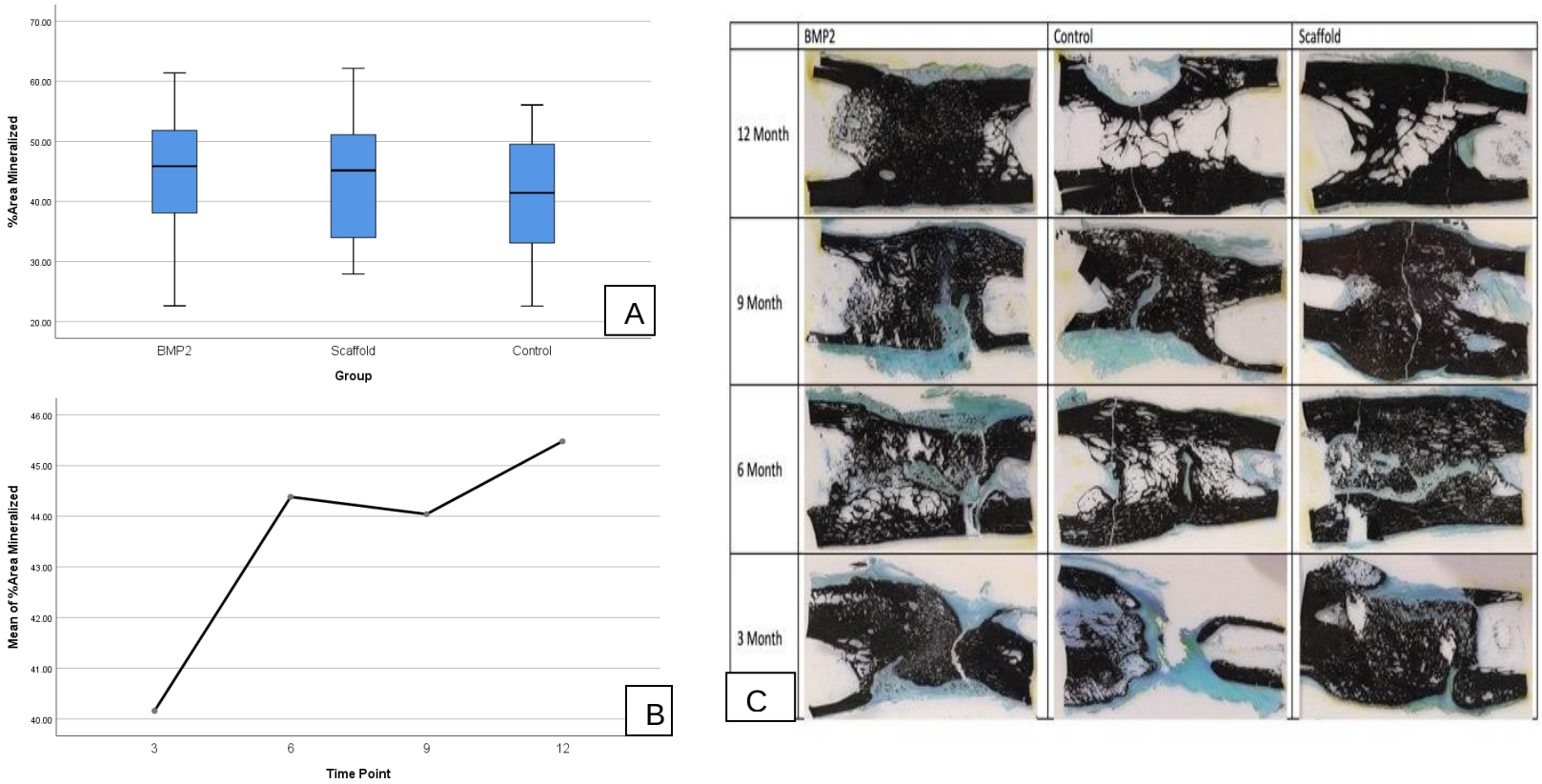


Figure 3-5. Von Kossa (percent mineralization) staining.
A) There was no significant difference in the percent mineralization between groups. B) Although there was no significant difference in percent mineralization over time, the amount of mineralization appears to follow a bone remodeling curve in that it initially increases as the ostectomy gap is filled with new bone that is then remodeled. C) Von Kossa stained samples where black represents mineralized bone. In Scaffold and BMP-2 goats, the scaffold took staining indicating the presence of mineralized bone. Scale bar, 1000 μm.

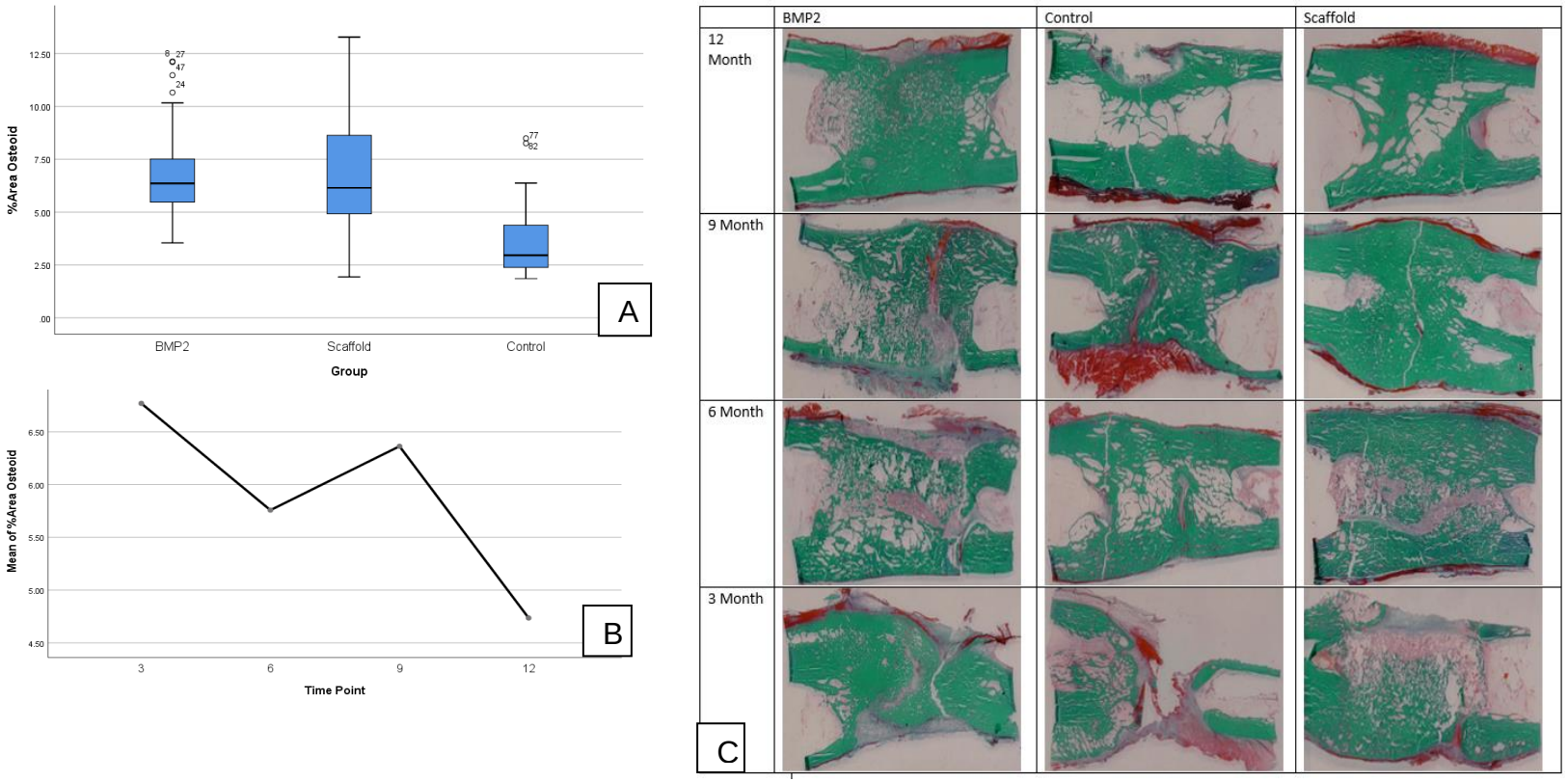


Figure 3-6. Goldner's Trichrome (percent osteoid) staining.
There was a significant difference in the percent mineralization between groups (P<0.05) in that on average Scaffold and BMP-2 goats had greater percent osteoid formation (6.96±0.46% and 6.97±0.46%) as compared to Control goats (3.67±0.48%) B) There was a significant difference in osteoid staining over time, in that the osteoid percentage of area in the ostectomy gap decreased over time, with a slight increase at 9 months then final decrease at 12 months regardless of group [(3-6.79±0.55%^{a}, (6)-5.67±0.55^{ab}, (9)-6.36±0.53%^{a}, (12)-4.63±0.54^{b}]. C) Goldner's Trichrome stained samples where green represents mineralized bone and light pink represents osteoid. Scale bar, 1000 μm.

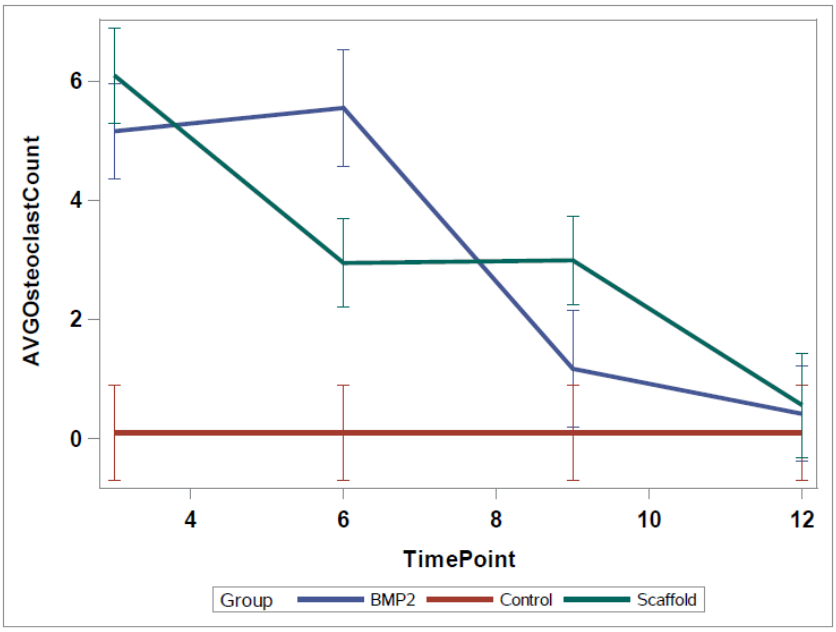


Figure 3-7. The average osteoclast count per mm of bone surface.
There was a group by month interaction in that the average osteoclast count decreased over time for Scaffold and BMP-2 goats, while the average osteoclast count remained static for Control goats ($P<0.05$).

Table 3-4. Group x Time point interactions for average osteoclast count per mm of bone surface.

Month	Group	Mean ± SE
3	Control	0.104±0.800[a]
	Scaffold	8.094±0.800[a]
	Scaffold+ BMP-2	5.156±0.800[a]
6	Control	0.104±0.800[a]
	Scaffold	2.946±0.740[b]
	Scaffold+ BMP-2	5.547±0..979[a]
9	Control	0.104±0.800[a]
	Scaffold	2.991±0.740[b]
	Scaffold+ BMP-2	1.172±0.979[b]
12	Control	0.104±0.800[a]
	Scaffold	0.563±0.875[c]
	Scaffold+ BMP-2	0.417±0.799[b]

CHAPTER 4.
CHARACTERIZATION OF POST-OPERATIVE HYPERTROPHIC OSTEOMYELITIS INDUCED BY *STAPHYLOCOCCUS AUREUS*

Abstract

This study used phenotypic tests and whole genome sequencing to characterize a collection of *Staphylococcus aureus* isolates from goats with clinical evidence of osteomyelitis following tibial ostectomy. *S. aureus* positive goats with clinical evidence of osteomyelitis were evaluated based on radiographic and histomorphometric analysis for phenotypic evidence of proliferative bone production. Isolates were identified using biochemical analysis combined with MLST of *S. aureus* in whole genome sequence-based contigs. All isolates were noted to be ST 398 and *S. aureus* infected goats were noted to have proliferative bone reaction. Further investigation into potential unique virulence factors of ST 398 and its relationship with osteoblast physiology is warranted.

Introduction

Staphylococcus aureus is a gram positive bacteria that is the most common pathogen in bone infection, or osteomyelitis [1-3]. Osteomyelitis itself may be the result of hematogenous spread of bacteria such as seen in the pediatric population [4, 5]. It may be the result of a contiguous focus inoculation such as seen secondary to a fracture or surgical site infection, or osteomyelitis associated with vascular insufficiency such as that seen with diabetic ulcers [4, 5]. The mechanisms by which *S. aureus* successfully invades and thrives in the bone environment are complex and not fully understood [4]. It is now recognized that *S. aureus* is no longer strictly an extracellular pathogen [6, 7]. *S. aureus*, in vitro, has been shown to have the ability to invade osteoblasts and survive in an altered metabolic state [8, 9]. Infected osteoblasts may be subject to altered osteoblast physiology [10, 11]. Currently, very little is known about how the *S. aureus*-osteoblast relationship may result in bone formation.

The gold standard of the study of long bone healing has been through the use of ostectomy gap models [12, 13]. One of the most popular models is the tibial ostectomy gap model in goats [13]. One complication of this model is infection, either of the surgical site or the implant itself [12, 13]. Regardless of the site of infection, the resulting osteomyelitis is classified as contiguous focus. With *S. aureus* being inoculated into healthy bone it may cause bone infection either through genes that encode microbial surface components recognizing adhesive matrix molecules (MMSCRAMMs) that allow it to attach to osteoblasts or through invading osteoblasts and surviving in an altered metabolic state [14]. Radiographs have shown that osteomyelitis cases show proliferative periosteal reaction and exuberant new bone formation in the initial stages of osteomyelitis [15]. Histomorphometric assessment allows for the quantification of osteoid (or the amount of forming bone), mineralization (mature bone), and osteoblastic activity (via tetracycline labelling) [16]. The ostectomy gap model provides the benefit of phenotypic *in-vivo* assessment of potential altered osteoblast proliferation in that bone formation may be quantified and assessed by both radiographic and histomorphometric analysis.

Whole genomic sequencing of *S. aureus* isolates causing clinical osteomyelitis may provide insight as to whether the phenotypic affects are the result of unique factors present within the population of clinical isolation. It is known that some strains of *S. aureus* are more virulent than others [17]. There is little knowledge about strain dependent differences in the ability of *S. aureus* to alter osteoblastic activity towards bone production. One way to differentiate strains is the use of multi-locus sequence typing (MLST [18]. MLST weas first developed in the late 90's to identify internal nucleotide sequences of approximately 400 to 500 bp in typically seven housekeeping genes [18, 19]. For *S. aureus* these genes are typically *acrC, aroE, glp, gmpm, pta, tpi* and *yqiL*, respectively coding for specific proteins [20]. The different sequences are assigned as distinct alleles and defined by the alleles at each of the seven housekeeping loci [19]. There are many alleles at each of the seven loci making it highly unlikely to have identical allelic profiles by chance [19]. It is considered the "gold standard" of typing bacteria. MLST allele sequences and ST profile tables are becoming more accessible with updated databases and software [18].

While MLST has typically been used to classify strains of *S. aureus* in community acquired cases of methicillin resistant staphylococcus aureus, it can also be used to classifty isolates in an understandable and comparable global context [18]. Work has yet to be done that defines MLST of strains *S. aureus* as they relate to potential proliferative bone formation cases of osteomyelitis. The aims of this study was to investigate whether clinical cases of osteomyelitis from goats with a tibial ostectomy gap showed phenotypic evidence of proliferative osteoblastic bone production and if the *S. aureus* isolated from these cases were unique in terms of multilocus sequence typing.

Materials and Methods

Case Population

All experimental procedures and protocols were approved by the animal care and use committee (University of Tennessee IACUC 2383). From a larger study of 105 goats (Chapter III) that had undergone a 2.5 cm tibial ostectomy that was repaired with a 4.0mm locking plate, a total of thirteen goats developed clinical evidence of osteomyelitis (dehiscence and/or infection of the surgical site with initial proliferative bone formation) and were pre-emptively available for inclusion. Of these thirteen, eleven cultured *S. aureus* based on biochemical identification.

Radiographs were performed immediately post-operatively and then monthly until end points (NEXT Equine DR, Sound, Carlsbad, CA., USA). Radiographs were scored by a board certified radiologist to assess ostectomy gap filling and the presence of hypermineralization (excessive periosteal reaction; **Table 4-1**).[4]

Upon diagnosis of osteomyelitis, goats were subjected to humane euthanasia. Tibia segments were trimmed and placed in 95% ethanol. Using an automated tissue processor (ASP300S, Leica, Germany) tissues were dehydrated in a series of ethanol solutions of increasing concentration (70%, 80%, 95% x2, 100% x3) over a period of several days at ambient temperature and a programmed auto-cycle of pressure, vacuum, and gentle agitation. Specimens were next transferred to three separate exchanges of 100% Methyl Salicylate (Sigma-Aldrich, St. Louis, MO) over the course of 48-72 hours, manually cycled between gentle agitation (modified stir bar setup) and vacuum at -15-20 in Hg (Fisherbrand, Vacuum Chamber), and observed for complete dehydration. Specimens were transferred to 100% xylenes (Sigma-Aldrich, Histological Grade, St. Louis, MO) for a quick rinse before being placed back onto the automated tissue processor (ASP300S, Leica, Germany) for three changes of 100% xylenes to complete the tissue clearing and prepared for methyl methacrylate resin infiltration. Specimens were then manually managed through three separate and fresh in-house prepared Infiltration Solution (IS I, IS II, IS III) exchanges of methyl methacrylate (Sigma-Aldrich, St. Louis, MO) and dibutyl phthalate (Sigma-Aldrich, St. Louis, MO), under ambient temperature over the course of 1.5 - 2 weeks, and with a manually cycled switch

[4] All figures and tables for this chapter are presented in the appendix.

between gentle agitation (modified stir bar setup) and vacuum @ -15-20 in Hg (Fisherbrand, Vacuum Chamber).

After a satisfied period of resin infiltration, specimens were transferred to prelabelled polypropylene containers and pre-polymerized base molds, where a fourth and in-house prepared final resin solution was then added along with a benzoyl peroxide based catalyst (Perkadox-16, AKZO Nobel Chemicals, Chicago, IL) to initiate a polymerization reaction to cure each specimen into a bubble free, clear, hardened, methyl methacrylate (MMA) block over a period of approximately 5-8 days. Each specimen block was then trimmed using a wet bandsaw (MarMed Bone Wet Band Saw) so that resulting microtomed sections would fit onto pre-cleaned 50mm x 75mm glass microscope slides (Fisherbrand). Specimen blocks were shaped for microtomy and sections cut at five microns using a motorized SM2500 sledge microtome (Leica, Germany) and d-profile (sledge) tungsten-carbide knives (Delaware Diamond Knives). Each section cut was mounted to an individual 50mm x 75mm precleaned glass microscope slide (Fisherbrand) that was coated with an in-house gelatin based solution recipe (Haupt's Solution) and covered with a plastic protective strip. Prior to staining, slide-sections from each specimen were sorted for fluorescence microscopy, VonKossa staining or Goldner's Trichrome staining. Prior to staining, all sections were deplasticized in a similar fashion that traditional paraffin sections would be deparaffinized so that all tissue components can be uninhibited during staining molecule interactions.

To quantitatively assess the percentage of mineralization (VonKossa), osteoid formation (Goldner's Trichrome), gross images from each slide were grossly acquired and digitized using a Panasonic HC-V770 (picture size 8M, 3264x2448, aspect ratio 4:3, extra optical zoom 20x) and processed in ImageJ (Rasband, W.S., Image J, U.S. National Institutes of Health, Bethesda Maryland, USA, https://imagej.nih.gov/ij/, 1997-2018.). For percentage mineralization, images were made binary such that mineralized bone was the parameter quantitatively assessed. For osteoid formation, images were made binary such that osteoid was the quantitatively assessed parameter. Unstained sections were evaluated by fluorescence microscopy with an excitation filter and two stop filters allowing radiation with a wavelength between 490 and 520 nm that permitted the identification and morphometric analysis of the mineralizing surface of bone.

Bacterial Isolates and Culture Methods

All experimental procedures and protocols were approved by the animal care and use committee (University of Tennessee IACUC 2383). From October 2017 to December 2018 a total of 12 nonduplicate bacterial isolates were collected from tibial ostectomy sites from 10 goats in a project unrelated to this study. All strains were collected aseptically, transferred into Amies gel without charcoal (BBL CultureSwab Plus 220116, USA) and directly plated.

Isolation and Phenotypic Identification of Staphylococcus aureus

Each isolated bacterial sample from Amies media was initial evaluated on Columbia blood (5% sheep blood) agar (Reme, R01217, USA) and CNA (colistin/naladixic acid with 5% sheep blood) agar (Remel, R01322, USA), incubated at 35 degrees Celcius in 5% CO_2. Additionally samples were evaluated on MacConkey II

(Remel, R01552, USA) and thioglycollate broth (Remel, R453452, USA), incubated at 35 degrees Celsius in ambient room temperature for 24 hours.

Tube coagulase (rabbit plasma), phenol red broth with trehalose, phenol red broth with lactose, and Vogues Proskaur (VP) broth were performed on all beta-hemolytic gram positive cocci. All biochemical were incubated at 35 degrees Celsius in ambient room temperature and read at 14 hours with the exception of VP which was read at 48 hours. For S. aureus, all biochemical had a positive reaction. Susceptibility testing was performed on 18-24 hours isolates via disc diffusion (Remel discs, USA).

Genomic analysis

Of the 11 goats that cultured *S. aureus*, one was unavailable for whole genome sequencing. In two goats, two unique strains of *S. aureus* were cultured and each strain was sequenced separately. This left a total of 12 strains of *S. aureus* available for whole genomic analysis from 10 goats with clinical evidence of osteomyelitis.

A single bacterial colony of each strain, grown on blood agar plates, was inoculated into 5 mL of sterile Trypticase soy broth (TSB) and incubated overnight at 37 C with shaking at 225 rpm using an Excella E24 incubator shaker (New Brunswick Scientific, USA). DNA was extracted using the MasterPure DNA purification kit (Epicentre, USA) according to the manufacturer's instructions.

Sequencing libraries were constructed using the Nextera DNA sample prep kit (Illumina, Inc., USA) according to the manufacturer's instructions for all strains. Initially four sequences were sequenced using a MiSeq platform (Illumina, Inc) with a single-end read length of 150 bp at the University of Tennessee Genomics Core facility, the results of which were published (Abouelkhair, 2018). Following this, the remaining sequences were sequenced using a HiSeq platform with paired-end read length of 150 bp at Novogene (Sacramento, CA, USA). All sequences were trimmed with Trimmomatic v.039, assembled using SPAdes (v3.14.0) and annotated using the Kbase version of Prokka (v1.12). For MLST the data base at the University of Oxford (https://pubmlst.org/saureus) for whole-genome multilocus sequence typing was used.

Statistical analysis

The case matching population was not large enough to make statistical comparisons therefore results are limited to descriptive terms only and reported as means ± standard deviation (STD). Raw descriptive data of each strain of osteomyelitis is provided in **Table 4-2**.

Results

Radiographic Analysis

One goat was removed from analysis due to an incomplete data set (lack of whole genomic sequencing data). This left 10 goats available for radiographic analysis. In regards to ostectomy gap filling, eight of the ten (80%) *S. aureus* goats had an ostectomy gap healing score of less than 2 (or new bone filling of less than 25% of the ostectomy gap). Only two out of ten (20%) showed a healing score of greater than 2. If the influence of the biomaterial was removed, and only goats with a negative control gap were evaluated, five out of seven (71%) of goats showed healing scores of less than 2, while

two out of 7 (29%) showed healing scores greater than 2. When compared back to the general population of goats as a whole, if the influence of the biomaterial was removed, S. aureus goats were able to show comparable scores to their uninfected counterparts (Chapter III). Based on descriptive radiographic analysis, S. aureus goats showed prolific, irregular, and palisading periosteal reactions (**Fig 4-1**).

Histomorphometric Analysis

A total of 5 goats had complete data sets available for histomorphometic analysis with case matched controls. For Goldner's Trichrome staining, or percent osteoid formation, *S. aureus* goats showed a percent osteoid formation of 12.94% ± 2.35. In terms of percent mineralization, or VonKossa staining, *S. aureus* goats showed mineralization of 49.46% ± 16.37. Finally, when evaluating the percent fluorescence or the amount of osteoblastic activity, *S. aureus* goats showed osteoblastic activity of 2.52% ± 3.18. When compared to back to the greater population, this appears to be an increase in osteoid formation, mineralization, and osteoblastic activity (**Fig 4-2**).

Genomic Analysis

The number of contigs, G=C content values, and the total lengths of the draft genome sequences for the clinical isolates of *S. aureus* are listed in **Table 4-3**. For HiSeq reads, a subset of the whole genomic sequence was taken such that there was 40x coverage of the genome. Additionally the number of predicted coding sequences as estimated by KBase are provided. All isolates were identified as sequence type (ST) 398 based on multi-locus sequence typing.

Discussion

We discovered that goats, from an unrelated orthopedic study, infected with *S. aureus* ST 398 were prone to develop a substantial amount of bone formation associated with osteomyelitis. It was observed that ST 398 is putatively capable of causing bone formation. Up until this point, it has been thought that proliferative amount of bone has been due to contiguous-focus osteomyelitis due to the fact that the resulting cases of spontaneous osteomyelitis occurred after surgery (direct trauma). Contiguous focus osteomyelitis may provide a key insight into how *S. aureus* able to infect healthy bone [21]. The exact mechanism that resulted in the exuberant bone formation after SA infection with this ST remains to be determined.

One way to further investigate the potential impact of these clinical isolates is further bioinformatics analysis. S. aureus clinical strains could be compared back to known *S. aureus* inducting strains of osteomyelitis and non-osteomyelitis inducing strains. This would allow functional annotation comparisons and comparisons between virulence databases. Assemblies could be subjected to whole genome alignment to detect any difference between the clinical isolates [22]. Alternatively, functional annotation and virulence databases could be compared on a variety of platforms [23-27]. One phenotypic assessment that maybe due to virulence factors or unknown proteins maybe made in that proliferative bone formation, or hypermineralization was associated with surgical site infection. If no surgical site infection was present, the bone tended follow the more

typical appearance of osteolytic or bone loss associated with osteomyelitis if cases those cases were allow to progress beyond one month of observation [1].

Previous studies have investigated bone formation as a radiographic parameter of osteomyelitis [15]. There results proved that bone formation is a constant and early feature of osteomyelitis, and has the strongest association to microbiological results [15]. However, these studies have not attempted to classify whether the amount of bone formation is sequence-dependent [15]. While not statistically significant, if the effect of the biomaterial was removed the *S. aureus* goats showed equivocal healing to case matched controls. The effect of the biomaterial in the presence of infection is not known. Currently work is being done with the biomaterial as both an antibiotic eluting device and bone regeneration scaffold which may have altered the results of ostectomy gap healing [20]. The bone formation seen radiographically was confirmed with histomorphometry. Tetracycline labelling binds reforming bone [16]. While not significant, the amount of remodeling bone was greater in *S. aureus* goats as compared to controls. Further wok investigating whether this is a direct cause and an effect is needed. It is not known whether the proliferative bone reaction as the result of the immune system attempt to deal with the suspected internalized *S. aureus* or whether this was a direct effect of the *S. aureus*- osteoblast relationship.

Major evolutionary changes in the ST 398 lineage have occurred over time [29]. The first being a widening infection spectra of these bacteria to humans livening in animal-free environments, and second an increase in its intrinsic virulence capacity [30, 31]. One important study has shown that methicillin sensitive *S. aureus* ST 398 is easily transmissible among humans [30]. Additionally, its genome is well adapted to the human host [30]. Unfortunately, this study only compared ST 398 strains found in humans to livestock associated methicillin resistant strains of *S. aureus* ST 398 [30]. There remains a gap in knowledge as to how *S. aureus* ST 398 relates to known contiguous-focus inducing OM strains of SA, and whether increased bone formation is the result of unique factors (ex; genes, pathogenecity islands, virulence factors).

References

1. Tong, S. Y., Davis, J. S., Eichenberger, E., Holland, T. L., & Fowler, V. G. (2015). Staphylococcus aureus infections: epidemiology, pathophysiology, clinical manifestations, and management. *Clinical microbiology reviews*, *28*(3), 603-661.
2. Kavanagh, N., Ryan, E. J., Widaa, A., Sexton, G., Fennell, J., O'Rourke, S., ... & Kerrigan, S. W. (2018). Staphylococcal osteomyelitis: disease progression, treatment challenges, and future directions. *Clinical microbiology reviews*, *31*(2), e00084-17.
3. Sheehy, S. H., Atkins, B. A., Bejon, P., Byren, I., Wyllie, D., Athanasou, N. A., ... & McNally, M. A. (2010). The microbiology of chronic osteomyelitis: prevalence of resistance to common empirical anti-microbial regimens. *Journal of Infection*, *60*(5), 338-343.
4. Muthukrishnan, G., Masters, E. A., Daiss, J. L., & Schwarz, E. M. (2019). Mechanisms of Immune Evasion and Bone Tissue Colonization That Make Staphylococcus aureus the Primary Pathogen in Osteomyelitis. *Current osteoporosis reports*, *17*(6), 395-404.
5. Waldvogel, F. A., Medoff, G., & Swartz, M. N. (1970). Osteomyelitis: a review of clinical features, therapeutic considerations and unusual aspects. *New England Journal of Medicine*, *282*(5), 260-266.
6. Tucker, K. A., Reilly, S. S., Leslie, C. S., & Hudson, M. C. (2000). Intracellular Staphylococcus aureus induces apoptosis in mouse osteoblasts. *FEMS microbiology letters*, *186*(2), 151-156
7. Hudson, M. C., Ramp, W. K., Nicholson, N. C., Williams, A. S., & Nousiainen, M. T. (1995). Internalization ofStaphylococcus aureusby cultured osteoblasts. *Microbial pathogenesis*, *19*(6), 409-419.
8. Shi, S., & Zhang, X. (2012). Interaction of Staphylococcus aureus with osteoblasts. *Experimental and therapeutic medicine*, *3*(3), 367-370.
9. Proctor, R. A., Von Eiff, C., Kahl, B. C., Becker, K., McNamara, P., Herrmann, M., & Peters, G. (2006). Small colony variants: a pathogenic form of bacteria that facilitates persistent and recurrent infections. *Nature Reviews Microbiology*, *4*(4), 295.
10. Wright, J. A., & Nair, S. P. (2010). Interaction of staphylococci with bone. *International journal of medical microbiology*, *300*(2-3), 193-204.
11. Loi, F., Córdova, L. A., Pajarinen, J., Lin, T. H., Yao, Z., & Goodman, S. B. (2016). Inflammation, fracture and bone repair. *Bone*, *86*, 119-130.
12. Reichert, J. C., Saifzadeh, S., Wullschleger, M. E., Epari, D. R., Schütz, M. A., Duda, G. N., ... & Hutmacher, D. W. (2009). The challenge of establishing preclinical models for segmental bone defect research. *Biomaterials*, *30*(12), 2149-2163.

13. Reichert, J. C., Epari, D. R., Wullschleger, M. E., Saifzadeh, S., Steck, R., Lienau, J., ... & Hutmacher, D. W. (2010). Establishment of a preclinical ovine model for tibial segmental bone defect repair by applying bone tissue engineering strategies. *Tissue Engineering Part B: Reviews*, *16*(1), 93-104.
14. Smeltzer, M. S. (2000). Characterization of staphylococcal adhesins for adherence to host tissues. In *Handbook of Bacterial Adhesion* (pp. 411-444). Humana Press, Totowa, NJ.
15. Kraft, C. N., Schlegel, U., Pfluger, D., Eijer, H., Textor, J., Hansis, M., & Arens, S. (2001). Radiological signs of osteitis around extramedullary metal implants. *Archives of orthopaedic and trauma surgery*, *121*(6), 338-342.
16. Compston, J., Skingle, L., & Dempster, D. W. (2018). Bone histomorphometry. In *Vitamin D* (pp. 959-973). Academic Press.
17. Feil, E. J., Cooper, J. E., Grundmann, H., Robinson, D. A., Enright, M. C., Berendt, T., ... & Moore, C. E. (2003). How clonal is Staphylococcus aureus?. *Journal of bacteriology*, *185*(11), 3307-3316.
18. Larsen, M. V., Cosentino, S., Rasmussen, S., Friis, C., Hasman, H., Marvig, R. L., ... & Lund, O. (2012). Multilocus sequence typing of total-genome-sequenced bacteria. *Journal of clinical microbiology*, *50*(4), 1355-1361.
19. Enright, M. C., Day, N. P., Davies, C. E., Peacock, S. J., & Spratt, B. G. (2000). Multilocus sequence typing for characterization of methicillin-resistant and methicillin-susceptible clones ofStaphylococcus aureus. *Journal of clinical microbiology*, *38*(3), 1008-1015.
20. Kuhn, G., Francioli, P., & Blanc, D. S. (2006). Evidence for clonal evolution among highly polymorphic genes in methicillin-resistant Staphylococcus aureus. *Journal of bacteriology*, *188*(1), 169-178.
21. Lew, D. P., & Waldvogel, F. A. (1997). Osteomyelitis. *New England Journal of Medicine*, *336*(14), 999-1007.
22. Chen, I.-M. A., Chu, K., Palaniappan, K., Pillay, M., Ratner, A., Huang, J., … Kyrpides, N. C. (2019). IMG/M v.5.0: an integrated data management and comparative analysis system for microbial genomes and microbiomes. *Nucleic Acids Research*, *47*(D1), D666–D677. https://doi.org/10.1093/nar/gky901
23. Kanehisa, M., Furumichi, M., Tanabe, M., Sato, Y., & Morishima, K. (2017). KEGG: new perspectives on genomes, pathways, diseases and drugs. *Nucleic Acids Research*, *45*(D1), D353–D361. https://doi.org/10.1093/nar/gkw1092
24. Tatusov, R. L., Galperin, M. Y., Natale, D. A., & Koonin, E. V. (2000). The COG database: a tool for genome-scale analysis of protein functions and evolution. *Nucleic Acids Research*, *28*(1), 33–36.
25. Finn, R. D., Bateman, A., Clements, J., Coggill, P., Eberhardt, R. Y., Eddy, S. R., … Punta, M. (2014). Pfam: the protein families database. *Nucleic Acids Research*, *42*(D1), D222–D230. https://doi.org/10.1093/nar/gkt1223

26. Liu, B., Zheng, D., Jin, Q., Chen, L., & Yang, J. (2019). VFDB 2019: a comparative pathogenomic platform with an interactive web interface. *Nucleic Acids Research*, *47*(D1), D687–D692. https://doi.org/10.1093/nar/gky1080
27. Yoon, S. H., Park, Y.-K., & Kim, J. F. (2015). PAIDB v2.0: exploration and analysis of pathogenicity and resistance islands. *Nucleic Acids Research*, *43*(Database issue), D624–D630.
28. Beenken, KE, Alghazali, K., Campbell MJ, Rifkin, RE, Hecht, S., Ramire… "Evaluation of a polyurethane-based bone regenartion scaffold for local antibiotic delivery to prevent Staphyloccocus aureus infection in a contaminated segmental bone defect." Bone Showcase, 2020. University of Arkansas at Little Rock.
29. Busche, T., Hillion, M., Van Loi, V., Berg, D., Walther, B., Semmler, T., ... & Holmes, M. A. (2018). Comparative Secretome Analyses of Human and Zoonotic Staphylococcus aureus Isolates CC8, CC22, and CC398. *Molecular & Cellular Proteomics*, *17*(12), 2412-2433. Fischer, B., Vaudaux, P., Magnin, M., El Mestikawy, Y., Vasey, H., Lew, D. P., & Proctor, R. A. (1996). Novel animal model for studying the molecular mechanisms of bacterial adhesion to bone-implanted metallic devices: Role of fibronectin in Staphylococcus aureus adhesion. *Journal of orthopaedic research*, *14*(6), 914-920.
30. Senneville, E., Brière, M., Neut, C., Messad, N., Lina, G., Richard, J. L., ... & French Study Group on the Diabetic Foot. (2014). First report of the predominance of clonal complex 398 S taphylococcus aureus strains in osteomyelitis complicating diabetic foot ulcers: a national F rench study. *Clinical Microbiology and Infection*, *20*(4), O274-O277.

Appendices

Table 4-1. Radiographic scoring for assessment of ostectomy gap filling.

Ostectomy Gap Filling	Score
No interval change compared to immediate post-operative radiographs	0
New bone filling <25% of ostectomy gap	1
New bone filling 26-50% of ostectomy gap	2
New bone filling 51-75% of ostectomy gap	3
New bone filling >75% of ostectomy gap but not completely healed	4
Ostectomy gap completely filled and/or bridging callus present on all cortices	5

Table 4-2. Descriptive data of each strain of osteomyelitis subjected to whole genomic sequencing.
MLS typing was done with the data base from the University of Oxford

Strain	MLST	Biomaterial	Surgical Site Infection	Hypermineralization
MI 18-33	398	Yes	Yes	Yes
MI 18-34	398	No	Yes	Yes
MI 18-935	398	No	Yes	Yes
MI 18-1974	398	No	Yes	Yes
MI 18-4421	398	Yes	No	No
MI 18-3926a	398	Yes	No	No
MI 18-3225	398	No	No	No
MI 18-2814a	398	No	Yes	Yes
MI 18-2814b	398	No	Yes	Yes
MI 18-3857	398	Yes	No	No
MI 18-2759	398	No	Yes	Yes
MI 18-3926b	398	Yes	No	No

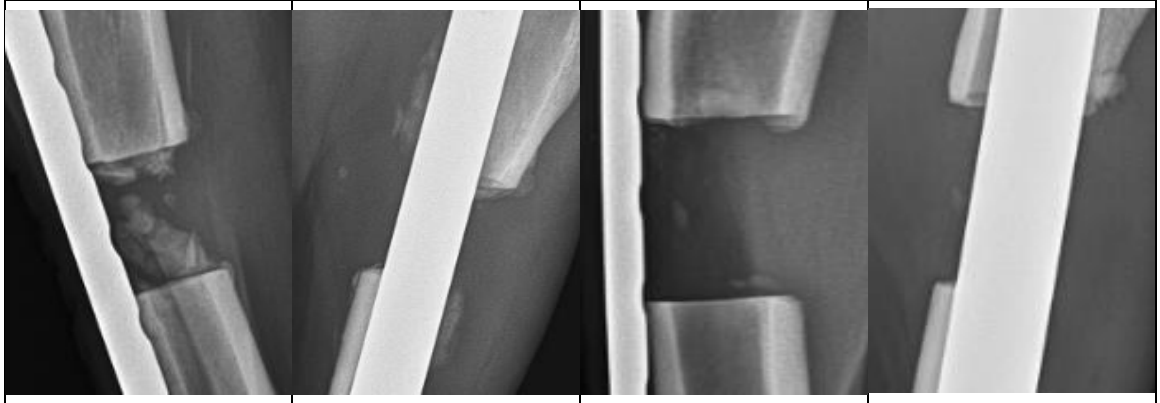
S. aurues 1 Month	*S. aureus* 1 Month	Case Comparison 1 Month	Case Comparison 1 Month
			

Figure 4-1. Radiographic ostectomy gap filling of an *S. aureus* goat and a case comparsion.
S. aureus goats consistently showed prolific, irregular and palisading periosteal reactions.

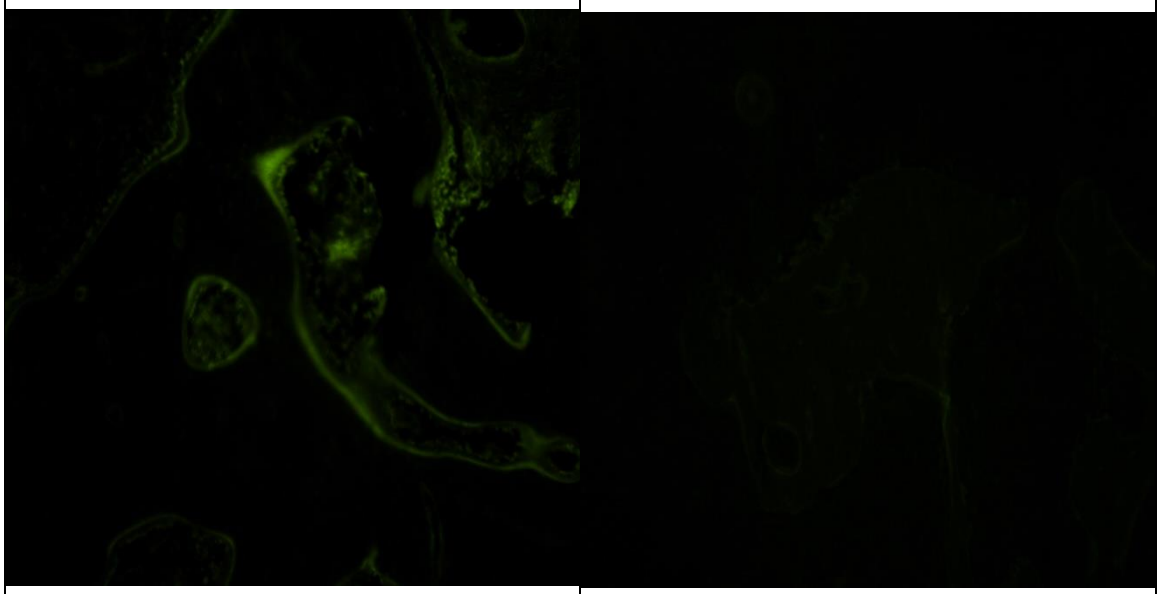
S. aureus	Case Comparison
	

Figure 4-2. Tetracycline labelling of an *S. aureus* goat and a case comparsion.
The amount of fluorsence (% area) was greater in S. aureus goats as compared to case matched controls.

Table 4-3. Bioinformatic data from *S. aureus* isolates subjected to whole genomic sequencing.

Strain	MI18_935	MI18_1974	MI18_33	MI18_34	S1	S2	S3	S4	S5	S6	S7	S8
# of contigs	56	54	60	54	38	41	36	50	43	43	26	38
Genome Length (bp)	2,819,698	2,819,900	2,819,224	2,819,890	2,823,232	2,785,957	2,759,738	2,744,959	2,772,319	2,771,634	2,739,302	2,786,630
G=C content (%)	32.9	32.9	32.9	32.9	32.9	32.9	32.9	32.9	32.9	32.8	32.8	32.8
# of predicted coding sequences	2629	2632	2629	2627	2639	2641	2559	2531	2577	2580	2532	2588

CHAPTER 5.
CONCLUSIONS AND FUTURE RESEARCH

Conclusions

The above work comprised in these chapters represents research conducted to evaluate the long-term effect of a three dimensional synthetic bone regeneration scaffold, with and without the addition of BMP-2. The scaffold was implanted into a large segmental bone defect to assess the inherent and enhanced capability to promote bone formation. Additionally, when complications of osteomyelitis arose, clinical cases were compared to their case matched controls and bacteria subjected to biochemical identification and whole genomic sequencing.

Few large animal preclinical models extend beyond a ninety day time period, have the capacity to look at bone regeneration, and are translatable to humans [1-4]. Challenges associated with long-term preclinical large animal models include the ability to assess animal comfort, an animal's tolerance to captivity, availability of the animal, society's acceptance of the animal model, and the animal's tolerance to captivity and the ease of housing [5-7]. Goats are often chosen for orthopedic research due to their ability to meet all of these needs [8-11].

Currently subjective visual assessment of gait is the standard of care in practice to assess lameness, and there appears to be no validated standards for objective gait analysis in goats [12-19]. The results of chapter II allowed for an objective baseline to be made. Quantitative gait assessment of biometric forces during ambulation in goats free of lameness using a pressure-sensing mat allowed for objective measurements of the animal's comfort during the long-term study.

While a wide variety of synthetic materials have been researched in effort to improve healing of debilitating fractures, no synthetic material has yet to be better than the gold standard autograft [20]. A 3D biomaterial from our lab has undergone extensive in-vitro and small animal in-vivo assessments. A tibial segmental defect model in the goat was chosen for the large animal preclinical model as discussed in chapter III. The results of the study demonstrated the effectiveness of the material when combined with the growth factor BMP-2. Additionally, the "negative" control gap turned into a positive control as controls goats showed ostectomy gap healing. This provided a bone-healing model for cmparison of osseo-integration of the synthetic based material.

Finally, bone infection is a complication of any orthopedic procedure [21, 22]. In our population of *S. aureus* goats, all strains were identified as sequence type 398 based on multilocus sequence typing after whole genomic sequencing. The phenotypic change of proliferative bone was found prompting potential for further investigation as to how *S. aureus* ST 398 may result in increased bone formation associated with osteomyelitis.

Future Research

The need for large animal preclinical models and evaluation of their most common complication, osteomyelitis, is complex. To expand the large animal preclinical model, work needs to be done for rehabilitation not only of the bone but of the whole limb in order to assess full return of function. The preclinical model presented here provides the advantage of potentially being able to remove the locking plate once the bone has healed to further assess osseo-integration.

Finally, the proliferative amount of bone associated with early osteomyelitis has been of particular interest to me. It remains to be seen whether this is associated with strain specific differences of *S.aureus*, and if it is truly an effect of *S. aureus* on osteoblast physiology. The results of such work may identify preventive and therapeutic targets for *S. aureus* prior to its devastating consequences of bone loss osteomyelitis.

References

1. Pearce, A. I., Richards, R. G., Milz, S., Schneider, E., & Pearce, S. G. (2007). Animal models for implant biomaterial research in bone: a review. *Eur Cell Mater*, *13*(1), 1-10.
2. McGonigle, P., & Ruggeri, B. (2014). Animal models of human disease: challenges in enabling translation. *Biochemical pharmacology*, *87*(1), 162-171.
3. Van der Worp, H. B., Howells, D. W., Sena, E. S., Porritt, M. J., Rewell, S., O'Collins, V., & Macleod, M. R. (2010). Can animal models of disease reliably inform human studies?. *PLoS medicine*, *7*(3), e1000245.
4. Hackam, D. G., & Redelmeier, D. A. (2006). Translation of research evidence from animals to humans. *Jama*, *296*(14), 1727-1732
5. Flower FC, Sanderson DJ, Weary DM. Hoof pathologies influence kinematic measures of dairy cow gait. J Dairy Sci. 2005;88(9):3166-3173. doi: 10.3168/jds.S0022-0302(05)73000-9.
6. Flower FC, Weary DM. Gait assessment in dairy cattle. Animal. 2009;3(1):87-95.
7. Black LL, Gaynor J, Gahring D, Adams C, Aron D, Harman S, et al. Effect of adipose-derived mesenchymal stem and regenerative cells on lameness in dogs with chronic osteoarthritis of the coxofemoral joints: a randomized, double-blinded, multicenter controlled trial. Vet Ther. 2007;8(4):272-284.
8. Harvey EJ, Giannoudis PV, Martineau PA, Lansdowne JL, Dimitriou R, Moriarty TF, et al. Preclinical animal models in trauma research. J Orthop Trauma. 2011;25(8):488-493. doi: 10.1097/BOT.0b013e3182251421.
9. Reichert JC, Saifzadeh S, Wullschleger ME, Epari DR, Schütz MA, Duda GN, et al. The challenge of establishing preclinical models for segmental bone defect research. Biomaterials. 2009;30(12):2149-2163. doi: 10.1016/j.biomaterials.2008.12.050.
10. Pearce AI, Richards RG, Milz S, Schneider E, Pearce SG. Animal models for implant biomaterial research in bone: a review. Eur Cell Mater. 2007;13(1):1-10.
11. Fulton LK, Clarke MS, Farris Jr HE. The goat as a model for biomedical research and teaching. Ilar J. 1994;1;36(2):21-29.
12. Muri K, Stubsjøen SM, Valle PS. Development and testing of an on-farm welfare assessment protocol for dairy goats. Anim Welfare. 2013;22(3):385-400.
13. Browning Jr R, Leite-Browning ML, Byars Jr M. Reproductive and health traits among Boer, Kiko, and Spanish meat goat does under humid, subtropical pasture conditions of the southeastern United States. J Anim Sci. 2011;89(3):648-660. doi: 10.2527/jas.2010-2930.
14. Deeming LE, Beausoleil NJ, Stafford KJ, Webster JR, Zobel G. The development of a reliable 5-point gait scoring system for use in dairy goats. J Dairy Sci. 2018;101(5):4491-4497. doi: 10.3168/jds.2017-13950.
15. Gigliuto C, De Gregori M, Malafoglia V, Raffaeli W, Compagnone C, Visai L, et al. Pain assessment in animal models: do we need further studies?. J Pain Res. 2014;7:227-236. doi: 10.2147/JPR.S59161.

16. Hill NP, Murphy PE, Nelson AJ, Mouttotou N, Green LE, Morgan KL. Lameness and foot lesions in adult British dairy goats. Vet Rec. 1997;141(16):412-416.
17. Olechnowicz J, Jaśkowski JM. Lameness in small ruminants. Med Weter. 2011;67(11):715-719.
18. Vieira A, Oliveira MD, Nunes T, Stilwell G. Making the case for developing alternative lameness scoring systems for dairy goats. Appl Anim Behav Sci. 2015;171:94-100.
19. Anzuino K, Bell NJ, Bazeley KJ, Nicol CJ. Assessment of welfare on 24 commercial UK dairy goat farms based on direct observations. Vet Rec. 2010;167(20):774-780. doi: 10.1136/vr.c5892.
20. Fillingham, Y., & Jacobs, J. (2016). Bone grafts and their substitutes. *The bone & joint journal*, *98*(1_Supple_A), 6-9.
21. Muthukrishnan, G., Masters, E. A., Daiss, J. L., & Schwarz, E. M. (2019). Mechanisms of Immune Evasion and Bone Tissue Colonization That Make Staphylococcus aureus the Primary Pathogen in Osteomyelitis. *Current osteoporosis reports*, *17*(6), 395-404.
22. Waldvogel, F. A., Medoff, G., & Swartz, M. N. (1970). Osteomyelitis: a review of clinical features, therapeutic considerations and unusual aspects. *New England Journal of Medicine*, *282*(5), 260-266.

VITA

Rebecca Elaine Rifkin, born in February 1988, received her doctorate in veterinary medicine in May of 2013. She then completed a rotating internship at Pioneer Equine Hospital followed by a second internship at California Equine Orthopedics. She was in private practice as a racetrack veterinary at Zimmer Equine Sports Medicine prior to coming to the University of Tennessee, Knoxville. She was accepted into the comparative and experimental graduate program in 2016 and began to pursue her PhD under the mentorship of David Anderson. Her studies focused on in-vivo assessments of a large animal preclinical model associated with a biomaterial in an ostectomy gap model. She has written and submitted her dissertation for review for a planned graduation for the spring of 2020.

During her time in graduate school, Rebecca has published a manuscript as a first author. This publication constitutes chapter II in this work. In addition to publication, she has presented a collection of poster and oral presentations at symposia and conferences hosted by the CEM department at UTK, and the American College of Veterinary Surgeons (ACVS).